# Analysis of the influence of structures and boundaries on flow and transport processes in fractured porous media

Von der Fakultät Bau- und Umweltingenieurwissenschaften
der Universität Stuttgart
zur Erlangung der Würde eines Doktors der Ingenieurwissenschaften (Dr.-Ing.)
genehmigte Abhandlung

Vorgelegt von

Mia Süß

aus Västanfors, Schweden

| | |
|---|---|
| Hauptberichter: | Prof. Dr.-Ing. R. Helmig |
| Mitberichter: | Prof. Dr.-Ing. W. Zielke |
| Tag der mündlichen Prüfung: | 10. Dezember 2004 |

Institut für Wasserbau der Universität Stuttgart

2005

Heft 135

# Analysis of the influence of structures and boundaries on flow and transport processes in fractured porous media

von Dr.-Ing. Mia Süß

Eigenverlag des Instituts für Wasserbau an der Universität Stuttgart

**D93** **Analysis of the influence of structures and boundaries on flow and transport processes in fractured porous media**

**Süß, Mia:**
Analysis of the influence of structures and boundaries on flow and transport processes in fractured porous media / von Mia Süß. Institut für Wasserbau, Universität Stuttgart. - Stuttgart: Inst. für Wasserbau, 2005

(Mitteilungen / Institut für Wasserbau, Universität Stuttgart ; H. 135)
Zugl.: Stuttgart, Univ., Diss., 2004
ISBN 3-933761-38-7



Herausgegeben 2005 vom Eigenverlag des Instituts für Wasserbau
Druck: Drukkerij Labor Vincit, Leiden, Niederlande

# Acknowledgement

This dissertation was written during my time as a research associate at the Institute of Hydraulic Engineering (IWS) of the Universität Stuttgart in Germany. The presented work was conducted within the framework of the project "Hard Rock Aquifer Analogue: Experiments and Modelling (AQA)", financed by the German Research Foundation.

First of all, I would like to thank my chief examiner Prof. Dr.-Ing. Rainer Helmig for supervising my research work. He was a true source of ideas, inspiration and motivation. I also express my gratitude to my first examiner Prof. Dr.-Ing. Werner Zielke.

Second, my acknowledgement is directed at all partners within the AQA-project. I enjoyed working in such a co-operative and friendly atmosphere.

I would also like to thank all my colleagues at IWS for making my time at the institute something to think back to with pleasure. Of course, there are a few who have earned special thanks. Prudence Lawday was always very co-operative and gave friendly, competent and prompt support whenever needed. Essential, thought-provoking impulses were given by Dr.-Ing. Olaf Cirpka. Hartmut Eichel contributed to my work, not only as a student but also later as a colleague and room mate, through simulations and diligent, constructive critical reading of this thesis. I could also benefit from the work of Martin Imig, who I supervised with great pleasure. Alexandros Papafotiou spent a substantial number of hours on conducting an infinite number of simulations. Lina Neunhäuserer, Steffen Ochs and Volker Reichenberger often helped me in solving MUFTE-UG-relevant problems. Anongnart Assteerawatt was a great room mate and I thank her for taking over my duties when I left the institute. I also want to thank Dorothee Schweizer, David Werner, Ulrich Ölmann and Thomas Breiting for their technical support and answers to sometimes probably rather stupid questions. Sabine Manthey provided accommodation when I needed it. Andreas Bielinski was always a reason to cheer up. It is also important to me to explicitly mention all other colleagues at the Department of Hydromachanics and Modeling of Hydrosystems as well as in WAREM and to thank them for being such nice colleagues.

Finally, I want to thank my family, and especially my parents, for supporting me in everything I did. My very special thanks goes to my husband Martin for his support and encouragement.

Voorhout, Netherlands, February 2005
Mia Süß

*"When you are moving toward an objective, said Petrus, it is very important to pay attention to the road. It is the road that teaches us the best way to get there, and the road enriches us as we walk its length."*

From *The Diary of a Magus* by Paulo Coelho.

# Contents

# List of Figures

# List of Tables

# Nomenclature

In the following table, the symbols used in this thesis are listed. Some symbols are not unique, however, from the context it it always clear which definition is relevant. Symbols that are not found in this table are only used locally and are explained in the text.

| Symbol | Unit | Definition |
|---|---|---|
| $A$ | $m^2$ | Area |
| $A$ | deg | Azimuth |
| $D$ | deg | Dip |
| $D$ | m | Direct distance between two ports |
| $D_{d,ij}$ | $m^2\,s^{-1}$ | Dispersion tensor |
| $D_{ij}$ | $m^2\,s^{-1}$ | Hydrodynamic dispersion tensor |
| $D_l$ | $m^2\,s^{-1}$ | Hydrodynamic dispersion in flow direction |
| $D_m$ | $m^2\,s^{-1}$ | Diffusion coefficient |
| $D_{m,e}$ | $m^2\,s^{-1}$ | Effective diffusion coefficient |
| $J_{a,i}$ | $kg\,m^{-2}\,s^{-1}$ | Advective mass flux |
| $J_{d,i}$ | $kg\,m^{-2}\,s^{-1}$ | Dispersive mass flux |
| $J_{hd,i}$ | $kg\,m^{-2}\,s^{-1}$ | Mass flux due to hydrodynamic dispersion |
| $J_i$ | $kg\,m^{-2}\,s^{-1}$ | Mass flux |
| $J_{m,e,i}$ | $kg\,m^{-2}\,s^{-1}$ | Effective diffusive mass flux |
| $K_{ij}$ | $m\,s^{-1}$ | Hydraulic conductivity tensor |
| $L_b$ | m | Shortest average boundary distance |
| $L_F$ | m | Fracture length |
| $L_p$ | m | Distance between in- and output ports |
| $L_r$ | - | Relative length |
| $P$ | - | Shape ratio |
| $Q$ | $m^3\,s^{-1}$ | Volume discharge |
| $R_i$ | $J\,kg^{-1}\,K^{-1}$ | Individual gas constant |
| $S$ | deg | Strike angle |
| $T$ | K | Temperature |
| $V$ | $m^3$ | Volume |
| $V_r$ | - | Relative volume |
| | | |
| $b$ | m | Fracture aperture |
| $c$ | $kg\,m^{-3}$ | Solute concentration |
| $c_{peak}$ | $kg\,m^{-3}$ | Peak concentration |
| $d$ | m | Distance |
| $d_2$ | $m\,m^{-2}$ | Two-dimensional fracture density |
| $d_3$ | $m^2\,m^{-3}$ | Three-dimensional fracture density |

| Symbol | Unit | Definition |
|---|---|---|
| d50 | m | Mean grain size |
| $d_F$ | m | Fracture distance |
| $g_i$ | $m\,s^{-2}$ | Gravitational accelleration vector |
| $h$ | m | Hydraulic head |
| $k_e$ | $m^2$ | Effective permeability (isotropic) |
| $k_F$ | $m^2$ | Fracture permeability (one-dimensional) |
| $k_{ij}$ | $m^2$ | Permeability tensor |
| $k_M$ | $m^2$ | Matrix permeability (isotropic) |
| $k_r$ | $m^2$ | Permeability ratio (structure/background) |
| $l$ | m | Length |
| $n$ | - | Total porosity |
| $n_e$ | - | Effective porosity |
| $p$ | Pa | Pressure |
| $q_i$ | $m\,s^{-1}$ | DARCY velocity |
| $q_m$ | $kg\,m^{-2}\,s^{-1}$ | Tracer mass source/sink term |
| $q_M$ | $kg\,s^{-1}$ | Tracer mass flux |
| $q_{M,peak}$ | $kg\,s^{-1}$ | Peak tracer mass flux |
| $q_s$ | $m^{-1}$ | Volume source/sink term |
| $t$ | s | Time |
| $t_{1\%}$ | s | Arrival time of 1% of injected tracer mass |
| $t_{eff}$ | s | Mean effective travel time |
| $t_{peak}$ | s | Peak arrival time |
| $v_i$ | $m\,s^{-1}$ | Seepage velocity vector |
| | | |
| $\alpha$ | deg | Angle |
| $\alpha$ | rad | $\Theta$-pole coordinate (Fisher distribution) |
| $\alpha_l$ | m | Longitudinal dispersivity |
| $\alpha_t$ | m | Transversal dispersivity |
| $\beta$ | rad | $\phi$-pole coordinate (Fisher distribution) |
| $\kappa$ | - | Concentration parameter (Fisher distribution) |
| $\lambda$ | - | Exponent of log-normal probability function |
| $\mu$ | $kg\,m^{-1}\,s^{-1}$ | Dynamic viscocity |
| $\sigma_x^2$ | (unit of variable)$^2$ | Variance of variable $x$ |
| $\sigma_x$ | unit of variable | Standard deviation of variable $x$ |
| $\theta$ | deg | Angle of incidence |
| $\rho$ | $kg\,m^3$ | Fluid density |
| | | |
| **Co-ordinates, indices, functions** | | |
| $x, y, z$ | m | Carthesian co-ordinates |
| $\Theta, \phi$ | rad | Polar co-ordinates |
| $x_i$ | unit of variable | Vector $x$ |
| $x_{i,j}$ | unit of variable | Tensor $x$ |
| $P(x)$ | - | Probability distribution function of variable $x$ |

# Abstract

This thesis is focused on the evaluation of tracer-breakthrough curves for the purpose of identifying domain structures and material properties. Examples of such structures are single fractures, fracture systems, layers or lenses. The investigations are based on the analysis of numerically modelled as well as measured data of domains on laboratory-scale. The numerical simulations are conducted using a flexible model set-up allowing variations of domain characteristics as well as of boundary conditions.

First, the *influence of impervious domain boundaries* on flow and transport measurements is investigated. Initially, the general influence of boundaries on selected flow and transport variables is discussed. Subsequently, the significance of the influence of, on the one hand, impervious boundaries, and on the other hand, structures on the variation of selected variables of flow and transport is compared. The analysis is based on simulated tracer-breakthrough curves of one homogeneous system with exclusively boundary influence and of ensembles of heterogeneous systems with structure influence only. It is concluded that the influence of the boundaries is of the same magnitude as the influence of the structures. Finally, the sensitivity of tracer-breakthrough curves to structure variations depending on the existence of boundaries is investigated. For this purpose, simulation results from heterogeneous systems with and without impervious boundaries are compared. It is concluded that, in general, the sensitivity of flow and transport results is increased if the domain is limited by impervious boundaries. The investigations show that general predictions of the influence of boundaries on the flow and transport behaviour can only be made in exceptional cases for domains with very simple structure distributions. For more complex domains, boundary effects must be investigated individually in order to exclude unfavourable experimental or numerical set-ups and in order to interpret measured or simulated data correctly. The work presented demonstrates new ways of analysing different aspects of the boundary influence.

Second, *possibilities and limitations of structure identification* are investigated. Based on three groups of test cases of varying characteristics, typical shapes of tracer-breakthrough curves are discussed and the fundamental mechanisms that lead to a certain curve shape are identified. Using the experience gained, an approach which is based on the shape of tracer-breakthrough curves and the initial arrival times, is developed for locating structures and approximating their permeabilities. The identification result is first assessed by applying the approach to the known test cases. Subsequently, the applicability to unknown artificial as well as real cases is tested. For domains containing block-shaped structures the new approach yields satisfying results for both artificial and real domains. For domains containing a few significant fractures, it is a useful support for approximating the structure distribution. Despite deviations, the fundamental characteristics are approximated correctly. The newly developed approach should be considered as one possible method to be used in combination with all other available data in order to obtain accurate identification results.

# Kurzfassung

Der Schwerpunkt der vorliegenden Arbeit liegt in der Auswertung von „Tracerdurchbruchskurven“ für die Identifikation von Strukturen und Materialeigenschaften. Beispiele solcher Strukturen sind Einzelklüfte, Kluftsysteme, Schichten und Linsen. Die Untersuchungen basieren auf der Analyse von sowohl numerisch modellierten als auch gemessenen Daten, die von Gebieten auf der Laborskala stammen.

Zunächst wird der *Einfluss von undurchlässigen Gebietsrändern* auf Strömungs- und Transportmessungen untersucht. Die Diskussion des generellen Einflusses von Rändern auf ausgewählte Strömungs- und Transportvariablen bildet eine Grundlage für die weiteren Untersuchungen. Darauffolgend wird die Stärke des Einflusses von undurchlässigen Rändern bzw. Strukturen auf die Variation von ausgewählten Strömungs- und Transportvariablen untersucht. Die Untersuchung basiert auf simulierten Duchbruchskurven von zwei Systemen mit jeweils ausschließlich Rand- bzw. Struktureinfluss. Es kann gezeigt werden, dass der Einfluss der Ränder von ungefähr gleicher Größe wie der der Strukturen ist. Schließlich wird die Sensitivität von Durchbruchskurven gegenüber Strukturveränderungen in Abhängigkeit des Vorhandenseins von Rändern untersucht. Hierzu werden Simulationsergebnisse heterogener Systeme ohne bzw. mit undurchlässigen Rändern verglichen. Die Schlussfolgerung ist, dass die Sensitivität der Strömungs- und Transportergebnisse bei einer Begrenzung durch undurchlässige Ränder zunimmt. Insgesamt zeigen die Untersuchungen, dass allgemeingültige Vorhersagen des Einflusses von Rändern nur in einfachen Ausnahmefällen gemacht werden können. Für komplexere Gebiete müssen Randeffekte speziell untersucht werden um einen ungünstigen experimentellen oder numerischen Aufbau zu vermeiden und um gemessene oder simulierte Daten korrekt zu interpretieren. Die vorgelegte Arbeit stellt neue mögliche Wege um verschiedene Aspekte des Randeinflusses zu analysieren vor.

Im zweiten Teil der Arbeit werden *Möglichkeiten und Einschränkungen der Strukturidentifikation* untersucht. Basierend auf drei Gruppen von Testfällen mit unterschiedlichen Struktureigenschaften, werden zunächst typische Formen von Durchbruchskurven diskutiert und die prinzipiellen Mechanismen, die zu bestimmten Kurvenformen führen identifiziert. Anschließend wird ein neuer Ansatz zur Approximation der Lage von Strukturen und deren Permeabilitäten, der auf der Form mehrerer Durchbruchskurven sowie der Erstankunftszeit basiert, entwickelt. Der Ansatz wird zunächst mithilfe der bekannten Testfälle evaluiert. Im folgenden Schritt wird die Anwendbarkeit anhand unbekannter künstlicher und natürlicher Gebiete getestet. Für Gebiete, die blockförmige Strukturen beinhalten, werden zufriedenstellende Ergebnisse erzielt. Beinhaltet ein Gebiet einige Einzelklüfte, so stellt der Ansatz eine hilfreiche Unterstützung für die Approximation der Strukturverteilung dar. Trotz Abweichungen werden grundlegende Charakteristiken korrekt angenähert. Der Entwickelte Ansatz sollte als eine mögliche Methode betrachtet werden, die in Kombination mit anderen zur Verfügung stehenden Informationen zu einer hinreichend genauen Identifikation führen kann.

# 1 Introduction

## 1.1 Motivation and aims

Fractured geological formations, which make up a large part of the earth's surface, are relevant in many hydrogeological issues that are of importance in society, both in an economic and environmental sense. Aquifer exploitation for water supply, exploitation of petroleum reservoirs, use of geothermal energy, and safety of subsurface waste repositories are examples of frequently addressed fields of interest.

The properties of a natural geological domain are the result of natural processes leading to a complex distribution of large- and small-scale structures such as, for example, layers, lenses, fracture zones, single fractures and fissures. The physical processes that take place when a fluid is transported through the medium are strongly determined by these structures and their properties. The solution of problems that arise when dealing with the issues mentioned above requires that the flow and transport processes are well understood and that methods for the determination of the structure geometry and the material properties of the investigation domain exist. Such data can be obtained from two principally different types of information (Figure 1.1):

- *Structure information* is obtained from analysis of exposed walls of outcrops or the inspection of core samples and bore holes (e.g. NELSON, 2001[51]). This type of information is two-dimensional or in the case of core samples one-dimensional. By means of statistical evaluation of structure information, three-dimensional systems are generated, assuming certain statistical distribution functions for characteristic geometrical variables (e.g. SILBERHORN-HEMMINGER, 2002[58]). The resulting realisations represent system geometries with a certain probability of occurrence. There are also geophysical methods, yielding three-dimensional structure information on different scales (e.g. U.S. NATIONAL RESEARCH COUNCIL, 1996[62]).

- *Process information* is the result of indirect measurements, hence it is obtained by interpreting flow and transport experiments. The measurement results are a combination of effects of occurring flow and transport processes within the domain. These processes are controlled by the structure of the natural system and the properties, suggesting that it is possible to determine the characteristics of the inner structure of a system by analysing the measurement results. This information has the same dimensionality as the domain itself, i.e. three dimensions, and is specific to the conditions under which the experiments are conducted, i.e. initial and boundary conditions.

The analysis of a domain should never be limited to a certain type of information, but the incorporation of all available knowledge can only improve the quality of the investigation results.

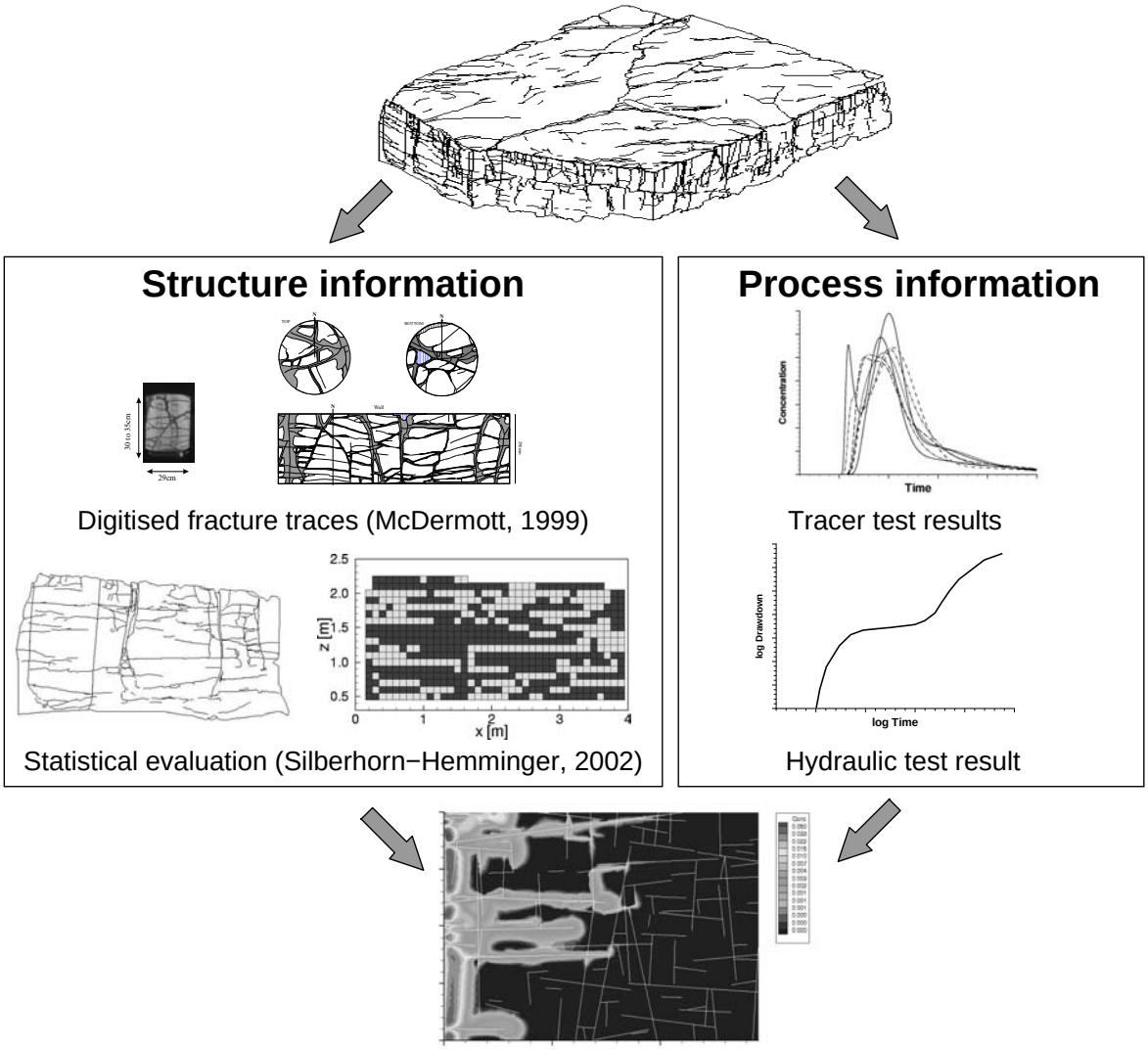


Figure 1.1: The knowledge of structure geometry and material properties, as required for model set-up, can be obtained from structure as well as process information.

This thesis deals with the interpretation of tracer measurements, which yield the latter type of information. Whereas the evaluation methods for tracer-test results from quasi-homogeneous domains are well developed (e.g. KÄSS, 1992[32]), the interpretation of tracer-breakthrough curves from strongly heterogeneous systems, such as fractured porous systems, is still a challenge (U.S. NATIONAL RESEARCH COUNCIL, 1996[62]).

Tracer-breakthrough curves are the result of measurements containing integral information about the complete domain. Since the effects of different structures are not independent, it is not possible to use, for example, superposing techniques to obtain a decomposition of the integral information. Consequently, individual effects occurring within complex systems of different structures are often not exactly distinguishable.

As already mentioned, process information is valid for the initial and boundary con-

ditions under which it is obtained. If a domain is not infinite, but limited by impervious boundaries, the measurement results are biased by the boundaries. Depending on the distance to the boundaries, the boundary conditions and the properties of the domain, the significance of the boundary influence varies.

With this background, the aim of this dissertation is to analyse (1) the possibilities and limitations of identification of structures and structure systems based on the interpretation of tracer-breakthrough curves, and (2) the influence of boundaries on results of tracer measurements.

## 1.2 Framework

The work presented in this thesis was performed within the framework of the research project "Hard Rock Aquifer Analogue: Experiments and Modelling", financed by the German Research Foundation (DFG). Four groups from the universities of Tübingen, Karlsruhe, Aachen and Stuttgart participated in the project. The first two groups were concerned mainly with experimental work and the latter two with numerical modelling. The concept of the classical aquifer analogue approach, originally established in the petroleum industry, is to study a representative outcrop of a reservoir in detail and to directly transfer the gained knowledge to the actual reservoir. Within the "Aquifer Analogue" research project, the concept was applied on samples of fractured porous sandstone on three different scales: (1) core scale ($\sim 30\,\mathrm{cm}$), (2) bench scale ($\sim 1\,\mathrm{m}$), and (3) field block scale (several meters). On each of the scales, experimental and model investigations were combined in order to learn more about the flow and transport behaviour in such heterogeneous systems. First, experiments were designed and conducted with the aim to gain high resolution data sets of the systems. This information was then used to set up reliable models for the further analysis of the flow and transport behaviour on the different scales. A detailed presentation and discussion of this research work is given in DIETRICH ET AL. (2005[18]).

The research work presented in this thesis is focused on one of the bench scale samples for which a large amount of structure as well as process information is available. The cubic block sample was recovered from a quarry and carefully prepared for measurements under controlled conditions in the laboratory. The fractured porous sandstone block with the dimensions $60 \times 60 \times 60\,\mathrm{cm}$ was dry, i.e. saturated with air. As shown in Figure 1.2, measurement ports were distributed over all sides of the cubic block; $4 \times 4$ ports on a regular raster and additionally one central port on each block side. The rest of the surface was made impermeable by a cover of resin.

Flow and transport experiments were conducted on the block sample for a large number of port configurations. The investigations presented in this thesis are focused on tracer measurements conducted for the so called *direct port configurations* for which, during a measurement, only two opposite ports are open, whereas all the others are closed. Constant pressures with a difference of $0.5\,\mathrm{bar}$ were imposed on the two active ports. After steady state conditions had been reached, a defined amount of tracer (helium) was injected as a pulse at the input port and the concentration at the output port was recorded. This procedure was repeated for all possible configurations of opposite ports, i.e. a set of $17 \times 3$ tracer-breakthrough curves was obtained. The sample recovery and preparation as well as

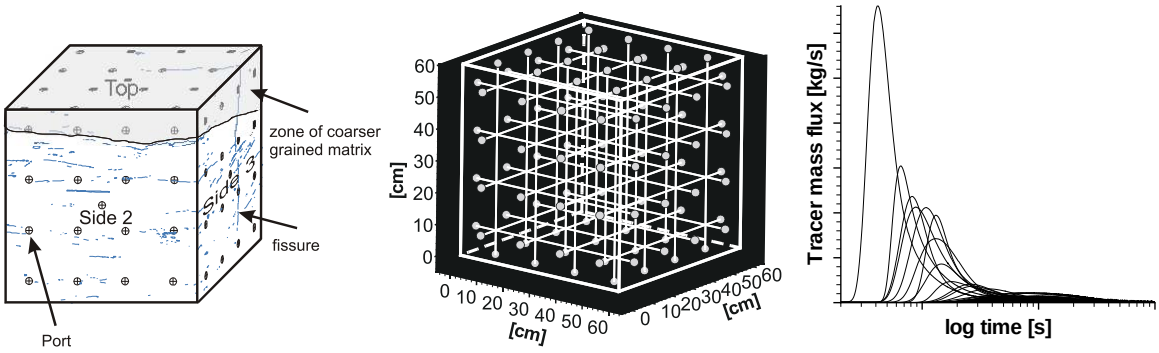


Figure 1.2: The investigated cubic ($60 \times 60 \times 60$ cm) block sample (R. BRAUCHLER, Center for Applied Geoscience, University of Tübingen, Germany). Left: Block sample with indications of ports and structures. Centre: Used direct port-port configurations. Right: Complete set of measured tracer-breakthrough curves.

the measurements were conducted by the project partners of the Center for Applied Geoscience, University of Tübingen, Germany. A detailed description of this work is given in DIETRICH ET AL. (2005[18]). Throughout this thesis, the notation *block sample* always refers to this sandstone block.

The measurements were conducted with the aim to obtain a set of data to be used for the determination of the distribution and the material properties of the inner structure of the block sample. In order to effectively use the measured tracer-breakthrough curves for this purpose, extended knowledge about the influence of structures on the characteristics of such curves was required. Additionally, due to the limited size of the sample, the influence of impervious boundaries on the measurement results was important for the interpretation of the obtained data.

The investigations and analyses presented in this thesis, are based on numerical simulations of flow and solute transport on the block sample scale (60 cm). The relevance of the two perspectives of this thesis as stated in Section 1.1 is clearly confirmed by the issues encountered within the "Aquifer Analogue" research project.

## 1.3 Structure of the thesis

In Chapter 2 the theories, concepts and models that are used for characterisation of fractured porous systems and for the mathematical and numerical solution of problems in such systems are presented. The extent of the chapter is limited to the scope of this thesis.

The first of the two main chapters (3) deals with the influence of impervious boundaries on flow and transport processes. First, the general effect on discharge and characteristics of tracer-breakthrough curves for a homogeneous system is analysed. Second, the influence of, on the one hand, boundaries and, on the other hand, of fractures is compared. Finally, it is investigated if the sensitivity to fracture system geometry variations is affected by the existence of limiting boundaries.

In the second main chapter (4) the possibilities and limitations of identification of structures by means of interpreting tracer-breakthrough curves are investigated. For a number

of test cases, containing structures such as layers, lenses and fractures, the general characteristics of the associated tracer-breakthrough curves are discussed. The possibilities and limitations of identification of such structures are then discussed for, first, known test cases, second, unknown artificial domains and, third, for a real domain.

Finally, in Chapter 5 the main issues and the most relevant conclusions are summarised and an outlook is given with suggestions for possible further research.

# 2 From natural system to numerical model

*Natural geological systems* are generally highly complex, both as far as the geological structure and the physical processes occurring within the system are concerned. In order to investigate such systems, it is necessary to understand the natural processes, their interaction with the geological structure and their relative importance on different scales for different types of problems. The transformation of a natural system to a model is illustrated in Figure 2.1. This transformation inevitably leads to simplifications of the real system. When model results are being interpreted, it is therefore essential to keep in mind that a model is merely an approximation of nature. One must always be aware of the assumptions that are made and the concepts that are used for a specific model in order to assess its results correctly.

Due to the geometrical complexity of natural systems and the large number of physical processes involved, it is not feasible to describe the exact system in great detail. The system structure and the processes occurring within it are therefore represented by *conceptual models*, designed to meet the requirements of certain types of problems on a given scale. This implies, for example, the introduction of parameters representing the material properties and physical descriptions of the relevant flow and transport processes.

In order to solve a problem for such system, a *mathematical description* of the model concept is required. Due to the degree of complexity of this type of problem, analytical solutions are not an option. The *numerical solution* involves the spatial and the temporal discretisation of the problem and the use of efficient and stable numerical algorithms.

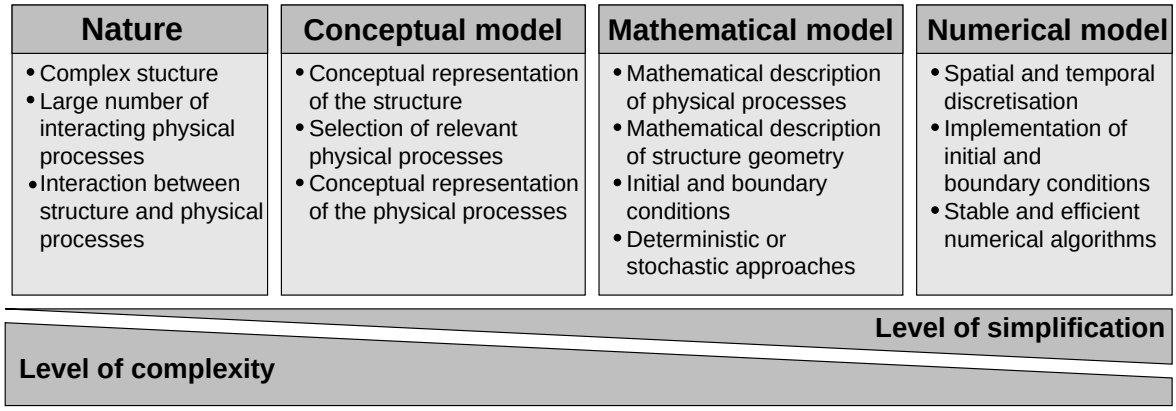


Figure 2.1: Transformation of a complex natural system to a simplified numerical model.

This chapter describes the transformation from nature to model of saturated fractured porous systems as well as flow and transport processes that are relevant for the investigations discussed in this thesis. The first part (Section 2.1) deals with the characteristics of natural fractured porous systems. This is followed by a discussion of different model concepts used on different scales and for different problem types (Section 2.2). In Section 2.3, the

governing equations of the pertinent physical processes are introduced. Finally, the model concept and the tools used for the simulations in this thesis are presented (Section 2.4).

It should be underlined that this chapter does not provide a complete overview of physical processes, theories, concepts and models. It is restricted to the scope of the research work presented in this thesis. For a more detailed discussion of the topic, references to further reading are given in the various sections.

## 2.1 Natural fractured porous systems

Solid rock can be classified according to its diagenetic characteristics (KOLDITZ, 1997[35]). Consolidated sedimentary rock evolves from the cementation of mineral grains, metamorphic rock is the result of recrystallisation under very high temperature and stress whereas igneous rock forms by the direct crystallisation of minerals from magmaic melt.

In direct response to the stress applied, which may be lithostatic, tectonic, thermal or the result of high fluid pressures, joints, faults and systems of such discontinuities occur on different scales and with different geometries. Joints are tension fractures across which no shear displacement is visible (PRICE, 1966[50]; NUR, 1982[45]) as opposed to faults, which show significant displacement. In hydrogeology, the term *fractures* is often used for all the different types of discontinuities in the rock matrix, independently of genesis or scale. This convention is followed here as well.

Tectonic fractures tend to be oriented along stress fields on a regional scale, whereas the other types of stresses give rise to local fractures that vary more greatly in orientation. Apart from stress-induced fractures, fractures may also occur at the boundaries of sedimentary layers consisting of deposits of different properties. The characteristics of existing fractures can be altered by local physical and chemical processes.

Figure 2.2 shows an exposed vertical wall of fractured sandstone containing both vertical and horizontal fractures. In this case, the horizontal fractures are separation planes between different sedimentary layers, whereas the vertical fractures are the result of mechanical stress (SILBERHORN-HEMMINGER, 2002[58]).

The hydraulic properties of hard rock are to a large extent determined by the porosity of the rock mass. Table 2.1 presents typical ranges of porosity for different types of hard rock, considering the rock as a whole, including both fractures and matrix (see below). Depending on the type of rock, the contribution of these two components to the porosity varies. For example for granite, the porosity is almost exclusively determined by the fractures, whereas for sandstone, the matrix porosity is considerable. Table 2.1 shows that there is a large difference between the total $n$ and the effective porosity $n_e$. The total porosity includes all the pores of the system whereas, for the effective porosity, only connected pores that are available to fluid flow are considered. It should be pointed out that the effective porosity is not directly correlated with the hydraulic conductivity of the system. The hydraulic conductivity varies over a wide range (several orders of magnitude) both for different rock types as well as for one single rock type.

This thesis is concerned with *fractured porous rock*, in which the rock matrix is considered to be permeable to flow. Fractured porous rock can be divided into three different components:

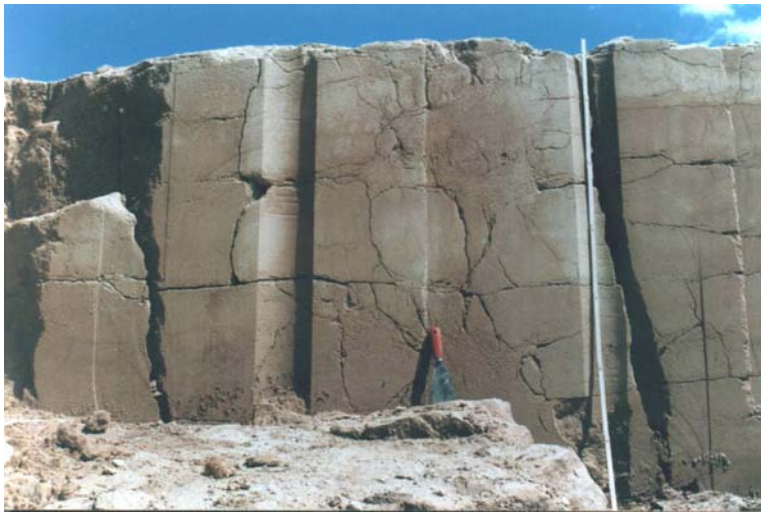

Figure 2.2: Vertical exposed wall of fractured sandstone (SILBERHORN-HEMMINGER, 2002[58]).

Table 2.1: Total porosity, effective porosity and hydraulic conductivity of selected hard rocks (DOMENICO & SCHWARTZ, 1990[19]; MATTHESS & UBELL, 1983[39]).

| Rock | Total porosity $n$ (%) | Effective porosity $n_e$ (%) | Hydraulic conductivity K ($m\,s^{-1}$) |
|---|---|---|---|
| Granite | 0.1 | 0.0005 | $5.0 \cdot 10^{-13} - 2.0 \cdot 10^{-12}$ |
| Limestone | 5 – 15 | 0.10 – 5 | $1.0 \cdot 10^{-9} - 6.0 \cdot 10^{-6}$ |
| Chalk | 5 – 44 | 0.05 – 2 | $6.0 \cdot 10^{-9} - 1.4 \cdot 10^{-7}$ |
| Sandstone | 5 – 20 | 0.5 – 10 | $3.0 \cdot 10^{-10} - 6.0 \cdot 10^{-6}$ |
| Shale | 1 – 10 | 0.5 – 5 | $1.0 \cdot 10^{-13} - 2.0 \cdot 10^{-9}$ |

- A *fracture network* is a system of partially intersecting single fractures. Its hydraulic properties are typically characterised by the distribution of fracture size, fracture permeability, fracture orientation, fracture distance, and fracture density. Due to its small volume relative to the volume of the total domain, the storage capacity of the fracture system is small.
- Within the fractures, *filling material* consisting of mineral deposits can be found. Open fractures can channel and speed up the transport of pollutants from disposal sites, e.g. leading to a locally high concentration of a pollutant at a great distance from the source, whereas filled fractures may inhibit the flow in otherwise highly permeable aquifers (ODLING, 1995[47]).
- The *matrix* blocks between the fractures have a spatially varying texture and porosity. The permeability contrast between fractures and matrix is the decisive factor for the importance of the matrix for flow and transport processes. As opposed to the fracture system, the storage capacity of the matrix is often significant as a result of its large volume.

In fractured porous systems all three components play a significant role for the characterisation of flow and transport processes.

Individual fractures can be described by size, orientation, average aperture and permeability. A fracture system is described by statistical distributions of these properties and, in addition, by fracture density and spatial correlation patterns. It is the combination of these properties as well as the permeability of the rock matrix that determine the system connectivity, hence, the interaction between individual fractures and their interaction with the rock matrix. The characteristics of the flow and transport behaviour of fractured porous systems is to a large extent determined by the system connectivity. ODLING (1995[47]) defines a measure of the connectivity as the proportion of the largest cluster that forms continuous pathways through the fracture network, where a cluster is defined as a group of connected fracture traces. Connectivity has been extensively investigated within the field of percolation theory (e.g. STAUFFER & AHARONY, 1991[60]) and many of the basic concepts are relevant to fluid flow processes through fracture systems (e.g. BALBERG ET AL., 1991[2]; BERKOWITZ, 1995[9]). Common to all of these investigations is that the matrix is considered to be impermeable to flow. The consideration of a permeable matrix leads to a less well defined problem when attempting to characterise the system connectivity.

In the following, based on SILBERHORN-HEMMINGER (2002[58]), properties that are used to characterise fractured systems are briefly presented. The discussion is focused on the influence of these properties on the system connectivity and is limited to concepts which are used in this thesis.

#### Fracture size

The fracture size, i.e. the lateral limitations of a fracture, can in most cases not be recorded and determined directly. Usually, fracture traces are detected at exposed walls (e.g. outcrops, quarries, tunnels). The fracture trace is the intersection line of a fracture with the exposed wall. In the field, the actual fracture edges are therefore often not determined, but the fracture traces are recorded and evaluated further using statistical methods. This is demonstrated in Figure 2.3: the vertical two-dimensional section, showing the fracture intersection lines with the $x$-$y$-plane at $y = 1\,\mathrm{m}$, is only a limited representation of the actual three-dimensional system (SILBERHORN-HEMMINGER, 2002[58]). An interesting aspect is whether it is possible to reconstruct the actual three-dimensional fracture system based on the determined fracture-trace distribution. Considering fractures with circular shape, BAECHER ET AL. (1977[1]) showed that a power-law and a log-normal distribution of the fracture radii both lead to a log-normal distribution of the fracture traces. Hence, a unique reconstruction of the fracture system is not possible.

The approximation of the empirical fracture trace-length distribution can be accomplished using different theoretical distribution functions. The most common distribution observed in the field, which is also often used in numerical studies of discrete fracture systems, is a power-law distribution, here expressed as

$$P(l) = 1 - e^{-\lambda l} \qquad \text{for} \qquad \lambda > 0\,, \tag{2.1}$$

where $P(l)$ is the probability that a fracture has a length less than $l$, and $\lambda$ is an exponent determining the shape of the accumulated probability-density function. The larger the expo-

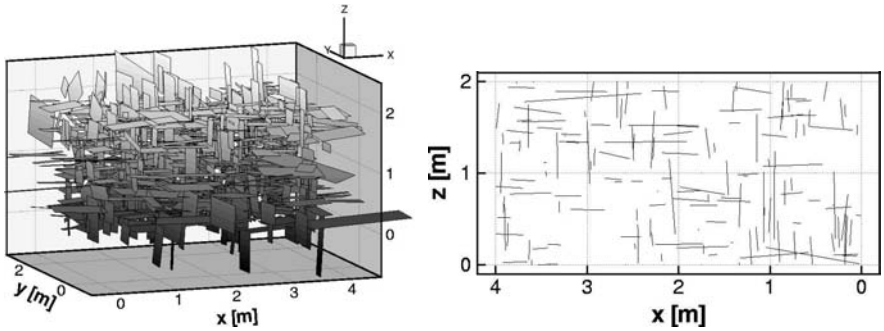


Figure 2.3: Artificial three-dimensional fracture system (left) and a vertical two-dimensional section showing the fracture traces at $y = 1$ m (right) (SILBERHORN-HEMMINGER, 2002[58]).

nent $\lambda$ is, the larger the percentage of short fracture traces within a system. Power-law length distributions can account for a broad range of lengths that are theoretically non-limited (DE DREUZY ET AL., 2002[20]; PARK ET AL., 2001[49]). ODLING ET AL., (1999[48]) observed power-law distributions for large data sets and log-normal distributions for their subsets, indicating a scale dependency of the trace-length distribution. They also state that there are cut-off lengths, limiting the validity range of power-law distributions. DERSHOWITZ & EINSTEIN (1988[17]) explain the diversity of possible distributions by the fact that, on the one hand, fracture traces and not the actual fracture sides are detected, and on the other hand, different fracture-formation processes yield different fracture shapes.

In a theoretical, numerical study BOUR & DAVY (1997[12]) investigated the connectivity of random fracture networks following power-law trace-length distributions. They conclude that for large values of $\lambda$, fracture traces smaller than the system size rule the network connectivity. On the opposite, for small values of $\lambda$, the connectivity is ruled by the largest fracture trace in the system. For intermediate values of $\lambda$, both small and large fracture traces control the connectivity in a ratio which depends on $\lambda$.

#### Fracture distance

The fracture distance $d_F$ is defined as the distance measured between two directly neighbouring fractures along a straight line. Such straight line is denoted *scanline*. It is an observation line which is positioned on an exposed wall. The determination of the fracture distance is schematically represented in Figure 2.4. The mean fracture distance can be determined from the length $l$ of the scanline, the number of fractures $n$ that intersect with the scanline and the angle of incidence $\theta$ between the scanline and the normal direction of the fractures:

$$\overline{d_F} = \frac{l}{n} \cdot \cos\theta \,. \tag{2.2}$$

This concept is only accurate if the variation of the fractures around the main direction of the cluster is small.

A decrease in fracture distance does not automatically lead to a higher system connectivity. If the fractures have the same orientation and the permeability of the matrix is low, even a small distance can prevent interaction between two neighbouring fractures. If, how-

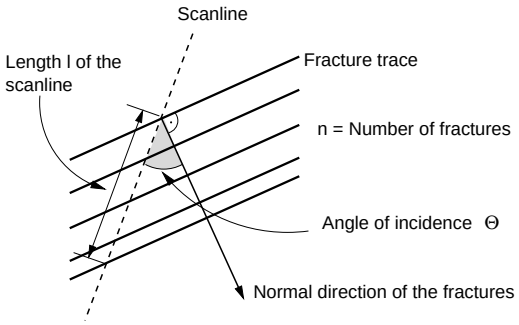


Figure 2.4: Determination of fracture distances (SILBERHORN-HEMMINGER, 2002[58].)

ever, the orientations within one set of fractures vary or if sets of different main orientations exist, a decrease in fracture distance improves the system connectivity, assuming a certain trace-length distribution.

#### Fracture density

The fracture density is determined on the basis of core samples and scanline measurements. Along the scanline, the number of intersections with fractures, the angle of incidence, etc. can be determined. The two-dimensional fracture density $d_2$ is defined as the average total fracture-trace length per unit area, whereas the three-dimensional fracture density $d_3$ is the average total fracture area per unit volume.

Similar to the fracture distance, a high fracture density alone, does not necessarily lead to a high connectivity. It is the combination of density, orientation, size and matrix permeability that determines the connectivity of the system.

#### Fracture permeability

The average permeability of a single fracture is determined by its fracture aperture distribution as well as by the properties of possible filling material within the fracture.

The fracture aperture is defined as the perpendicular distance between two directly opposing fracture walls. The aperture can be increased by, for example, dissolution and erosion processes. This is mainly observed in the weathered zones close to the ground surface. Another reason for an increase in aperture is displacement due to external forces or subsidence. The aperture generally decreases with increasing depth due to the increasing thickness of the overlying rock.

Figure 2.5 shows two opposite sides of a fracture. The roughness of the two surfaces can be clearly seen. If the two pieces are put together, the actual fracture is obtained as the space between the two surfaces. The aperture varies significantly throughout a fracture. It is therefore not possible to characterise the fracture aperture by a single measurement. Considering the simulation of flow and transport processes in single fractures, one possibility of describing the roughness of a fracture is to assume a fracture-aperture distribution within the fracture (often log-normal or with self-affine fractal properties). This approach is mainly used for fundamental experimental and numerical studies (e.g. MORENO & TSANG,

1991[41]; BROWN, 1987[14]). However, for the simulation of such processes in systems containing many fractures, this approach is not feasible due to the large computational effort which is required in order to resolve such great degree of detail. In general, for the discrete

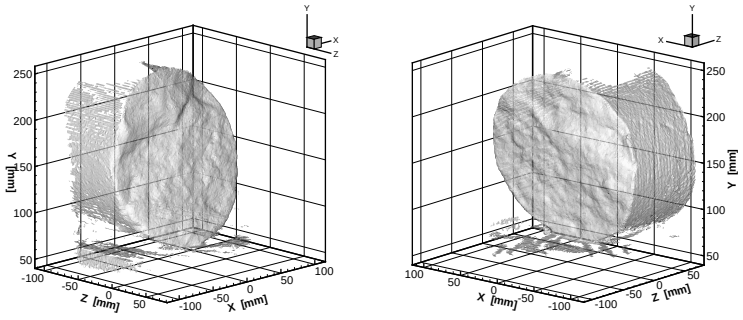


Figure 2.5: Image of the two opposite walls of a single fracture from a sandstone core sample with a diameter of approximately 20 cm (created in cooperation with the Institute for Robotics and Process Control, Technical University of Braunschweig, Germany (SILBERHORN-HEMMINGER, 2002[58])).

representation of fractures in models, the fracture aperture is described using the parallel-plate concept, yielding a mathematical expression for the relationship between fracture aperture and permeability (Section 2.4.1). It should be underlined, that the parallel-plate concept is a very strong simplification of the natural geometry as well as of the flow and transport behaviour within a real fracture. A constant aperture throughout the fracture is assumed and channelling effects are ignored.

The existence of filling material between the fracture walls, has a decreasing effect on the fracture permeability. Fractures can be completely but also partly filled, in the latter case leading to formation of preferred flow paths within the fracture. Depending on the properties of the mineral deposits, a fracture may even work as a flow barrier with a very low permeability.

According to DE DREUZY ET AL. (2002[20]) there is still a debate whether a log-normal or a power-law fracture-permeability distribution should be assign in discrete models. Using a power-law model, the probability that high permeability values occur is larger.

High fracture permeabilities have a positive influence on the system connectivity only if the fractures in the system can interact. So-called *dead-end* fractures in a matrix with low permeability do not increase the connectivity because they are not participating in the flow process of the system.

#### Fracture orientation

The orientation of geological formations in space is uniquely determined by the strike angle S or the azimuth A, and the dip D. According to MURAWSKI (1998[43]), the strike is the section boundary of a natural surface (e.g. layer or fracture) at an imaginary horizontal plane. The strike angle S is defined as the angle between the northerly direction and the section boundary. The projection of the line of greatest slope onto the horizontal plane is the dip direction which is always perpendicular to the strike. The inclination angle between the line of

greatest slope and the dip direction is the dip D. The angle between the northerly direction and the dip direction is defined as the azimuth A. It is connected to the strike angle through the equation $A = S + 90°$. Figure 2.6 summarises the relationship between strike, dip and azimuth.

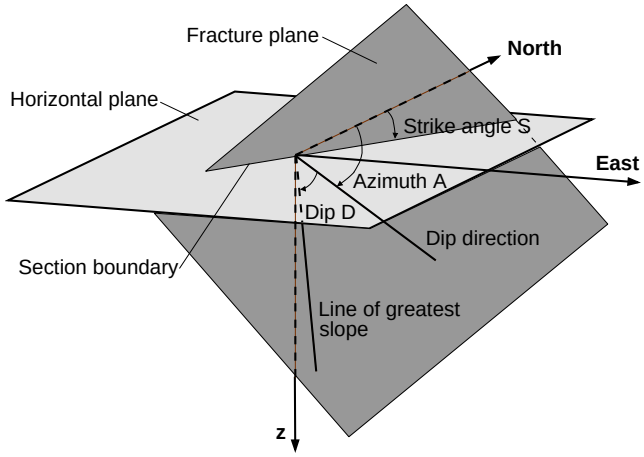


Figure 2.6: Determination of the location of a geological surface: strike, dip, azimuth. The dip direction is the projection of the line of greatest slope onto the horizontal plane (modified from SILBERHORN-HEMMINGER (2002[58])).

If fractures or layers occur in a preferred direction, the statistical distribution of the orientation is often described by the FISHER distribution, also called the spherical normal distribution. The FISHER distribution is characterised by the fact that orientations are distributed around a certain main orientation with rotational symmetry. In WALLBRECHER (1986[63]) and FISHER (1993[22]) the distribution is discussed in detail. The probability density function of the FISHER distribution has the following form:

$$f(\Theta,\phi) = \frac{\kappa}{4\pi \cdot \sinh\kappa} \cdot exp[\kappa\,(\sin\Theta\,\sin\alpha\,\cos(\phi-\beta) + \cos\Theta\,\cos\alpha)] \cdot \sin\Theta\,. \qquad (2.3)$$

Here, $\alpha$ is the $\Theta$-pole coordinate (latitude) of the main direction, $\beta$ is the $\phi$-pole coordinate (longitude) of the main direction and $\kappa$ is the concentration parameter. The concentration parameter $\kappa$ is a measure of the distribution of the orientations around the main orientation. For $\kappa = 0$, the orientations are uniformly distributed. The larger $\kappa$ is, the stronger the concentration around the main orientation.

As discussed for most of the geometrical properties above, the fracture orientation and the number of fracture clusters are essential for the connectivity of a system. More than one cluster and a small value of the concentration parameter $\kappa$, i.e. large variation around the main orientation, positively affect the connectivity.

## 2.2 Model concepts in fractured porous systems

As discussed in the introduction to this chapter, it is not possible to set up a model that is an exact representation of reality, but conceptual models are developed that are able to

describe the relevant structures and physical processes of a problem. The choice of model concept for the description of fractured media strongly depends on the scale of the problem, the geological characteristics of the area of investigation, and the purpose of the simulation. BEAR (1993[7]) classifies various problems of flow and transport in fractured porous media according to their scale. On these scales, different types and extensions of heterogeneities occur (RATS & CHERNYASHOV, 1967[52]).

- **Zone 1: The very near field.** Interest is focused on flow and transport processes within small-scale fractures (fissures) and the pore space. Single, well-defined fractures and the surrounding porous rock, which is possibly accessible to transport, are considered.
- **Zone 2: The near field.** The flow and transport processes are considered in a relatively small domain, which contains a small number of well-defined small and intermediate fractures. The location and shape of the individual fractures are either deterministically defined or can be generated stochastically, based on statistical information from the real system.
- **Zone 3: The far field.** On this scale, the flow and transport processes are regarded as taking place, simultaneously, in at least two continua. One continuum is composed by the network of large scale fractures and the other one by the porous rock. Mass of the fluid phase and its components may be exchanged between the two continua.
- **Zone 4: The very far field.** The entire fractured medium is considered as one single continuum, possibly heterogeneous and anisotropic in order to account for large-scale geological layers and fault zones.

In order to set up models of systems with such varying characteristics, different model concepts are necessary. These concepts are discussed on the basis of Figure 2.7. There are two fundamental approaches (HELMIG, 1993[26]):

1. Assuming that the concept of the representative elementary volume REV (Section 2.3.1) is valid and that the scale of the investigation area is sufficiently large, it is possible to describe the model area as a heterogeneous, anisotropic *continuum*. According to BEAR (1993[7]), this is possible on the very far scale. KRÖHN (1991[36]) also considers this to be a feasible approach for describing poorly fractured rock (type I) and rock with a very high fracture density (type II) on a smaller scale.
2. If the flow and transport processes in the fractured media are dominated by shear zones (spatially concentrated small-scale fractures) or fracture systems (type III), it is feasible to describe these features specifically, neglecting the rock matrix, using a *discrete* fracture-network model (consideration of each single fracture).

However, the rock matrix, filling the space between the fractures, is often not negligible, but plays an essential role in flow and transport processes (type IV). If the porous rock matrix can be idealised as a continuum with averaged material properties, a model can be set up where a continuum model, accounting for the matrix, is coupled with a discrete model considering the fractures. This type of model is further discussed in Section 2.4.

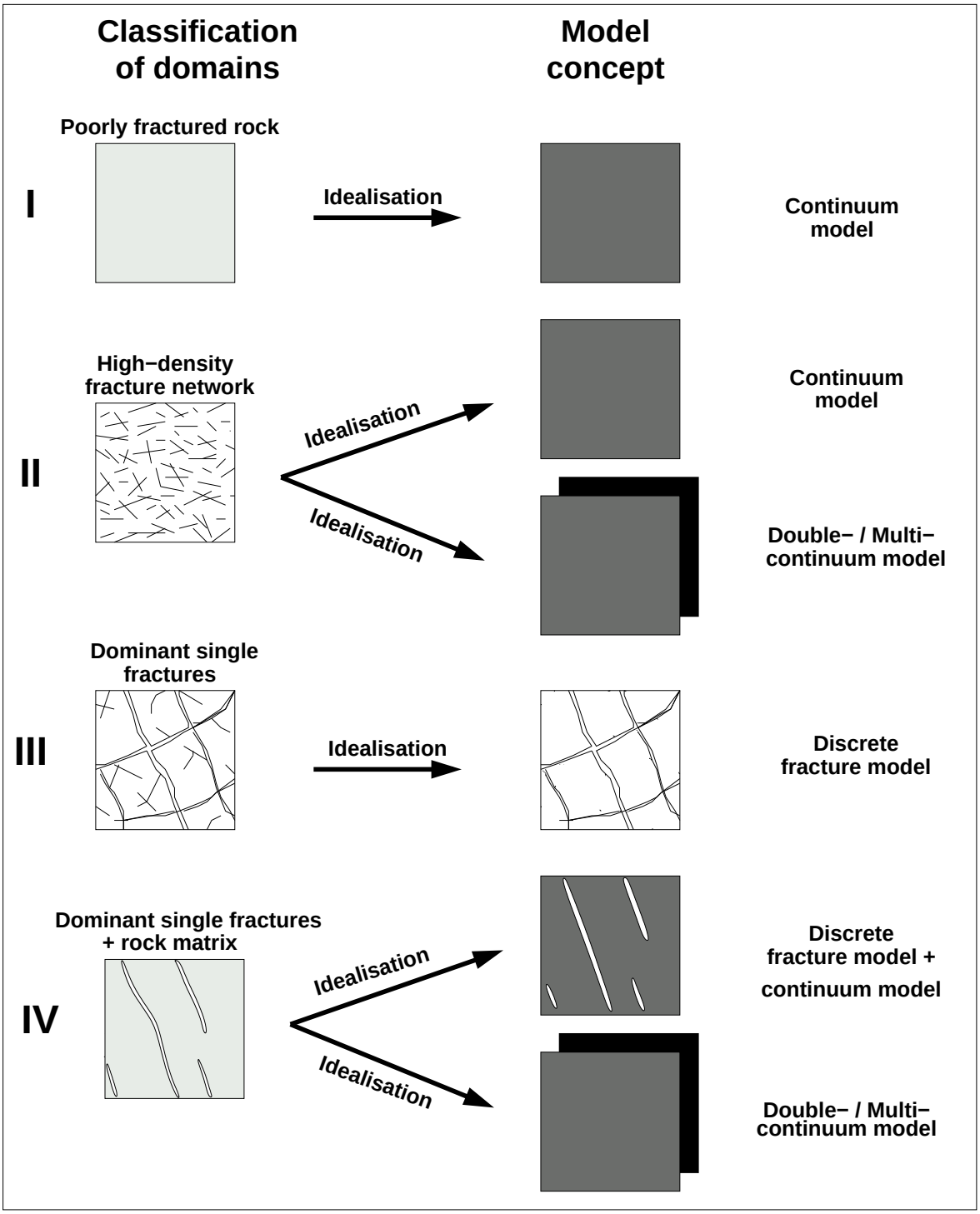


Figure 2.7: Model concepts for the description of fractured porous media (based on KRÖHN (1991[36]) and HELMIG (1993[26])).

Another widely used possibility for describing areas of type II (system with high fracture density) and IV (dominant single fractures + rock matrix) is to transform the matrix

and the fracture systems on different scales into separate homogeneous equivalent continua. This approach is mainly applied on large scales. With the concept originally presented by BARENBLATT ET AL. (1960[3]), the flow and the transport processes between the continua can be represented by coupling them via exchange terms and in this way setting up a so-called double-continuum model. It is essential to the principle of homogenisation for heterogeneous media to define equivalent model parameters and to find appropriate expressions for the interaction of the hydraulic components which are capable of describing the correct physical system behaviour. Extending this model allows the consideration of more than two continua, a multi-continuum model, if required by the geological characteristics of the investigation area and by the nature of the problem. Since this type of model concept is not used for the investigations discussed in this thesis it is not further discussed. A detailed description is found in, for example, DIETRICH ET AL. (2005[18]).

## 2.3 Governing equations of flow and transport in porous media

In this section, the mathematical description and the governing equations of flow and transport processes in *porous media in general*, i.e. without the consideration of fractures, are presented. The discussion focuses on the processes which are relevant to the research work presented in this thesis. The implementation of the discrete model concept for considering fractures is discussed in Section 2.4.

### 2.3.1 Representative elementary volume (REV)

The concept of the representative elementary volume (REV), as defined by BEAR (1972[6]), is fundamental to the mathematical description of fluid flow and transport in porous media. By means of volume averaging, the micro-scale properties of the porous medium (grain-size and pore-space geometry) are represented by an equivalent continuum on a larger scale described by new properties. On the one hand, the REV must be large enough to avoid undesirable fluctuations of the averaged properties and, on the other hand, it must be small enough to render the spatial distribution of these properties. In Figure 2.8, the definition of a suitable extent of the REV is visualised. The application of the REV approach in different model concepts for *fractured* porous media is discussed in Section 2.2.

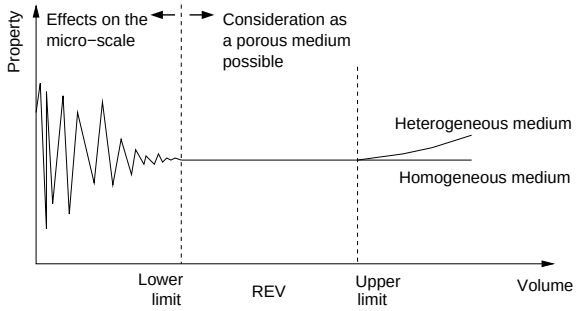


Figure 2.8: Representative elementary volume (REV) (modified from BEAR (1972[6])).

### 2.3.2 Flow processes

#### DARCY equation

The DARCY equation for laminar flow in porous media was defined by HENRY DARCY in 1856. In one-dimensional column experiments, DARCY found that the volume discharge Q is proportional to the hydraulic gradient $\Delta h/\Delta l$ as described by the following equation:

$$Q = -A\,K\,\frac{\Delta h}{\Delta l}\,. \tag{2.4}$$

Here, A is the cross-sectional area of the column, K is the hydraulic conductivity, $\Delta h$ is the difference in hydraulic head and $\Delta l$ is the distance between the measurement points. From (2.4) and the relationship

$$Q = q_i A\,, \tag{2.5}$$

the three-dimensional DARCY velocity $q_i$ is determined:

$$q_i = -K_{ij}\,\frac{\partial h}{\partial x_j}\,. \tag{2.6}$$

The hydraulic conductivity tensor $K_{ij}$ depends on the properties of the porous medium as well as of the fluid:

$$K_{ij} = \frac{\rho\, g_i\, k_{ij}}{\mu}\,, \tag{2.7}$$

where $\rho$ is the fluid density, g is the gravitational acceleration, $k_{ij}$ is the permeability tensor and $\mu$ is the dynamic viscosity. The permeability tensor $k_{ij}$ represents the directional permeability of a porous medium and is independent of the fluid. Expressing the piezometric head h in terms of pressure pressure p and geodetic head z and using the permeability $k_{ij}$ instead of the hydraulic conductivity $K_{ij}$, yields the following expression for the DARCY velocity $q_i$:

$$q_i = -\frac{k_{ij}}{\mu}\left(\frac{\partial p}{\partial x_j} + \rho g \frac{\partial z}{\partial x_{ij}}\right)\,. \tag{2.8}$$

In the case of gas flow, the gravity effect is often neglected. This is legitimate if the gravity effect, due to low density, is small compared to the effect of the pressure gradient. Neglecting the gravity effect, the equation can be simplified to

$$q_i = -\frac{k_{ij}}{\mu}\,\frac{\partial p}{\partial x_{ij}}\,. \tag{2.9}$$

This form of the equation may be applied for two-dimensional horizontal calculations as well.

The range of validity of the DARCY equation is expressed in terms of the REYNOLDS number Re which is defined as:

$$Re = \frac{q\,d\,\rho}{\mu}. \tag{2.10}$$

Here, d is a characteristic length, such as, for example, mean grain or pore size. According to BEAR (1972[6]), the upper limit of the validity of the DARCY equation is at a value of Re between 1 and 10 with $d = d50$ (mean grain size).

#### Continuity equation

The continuity equation is based on the principle of conservation of mass, and states that the temporal change of mass in a control volume is the sum of the mass flux across the volume boundaries and the mass flux due to sources and sinks. The temporal change of the mass in the control volume is described as follows:

$$\frac{\partial(n\rho)}{\partial t} = -\frac{\partial(\rho q_i)}{\partial x_i} + q_s \,. \tag{2.11}$$

Here, $q_s$ is the source and sink term, e.g. describing well withdrawal or injection, and $n$ represents the total porosity, also including the pores through which there is no flow. The porosity is slightly pressure-dependent (KINZELBACH, 1992[34]). However, this aspect is neglected here, i.e. the matrix is considered as inelastic. From this, the continuity equation is obtained in the following form:

$$n\,\frac{\partial\rho}{\partial t} = -\frac{\partial(\rho q_i)}{\partial x_i} + q_s \,. \tag{2.12}$$

If we introduce the piezometric head $h$ as the independent variable instead of the DARCY velocity $q_i$, we may express the continuity equation as

$$n\,\frac{\partial\rho}{\partial t} = \frac{\partial}{\partial x_i}\left(\rho^2 g_i\,\frac{k_{ij}}{\mu}\,\frac{\partial h}{\partial x_i}\right) . \tag{2.13}$$

The source and sink term $q_s$ is omitted for simplicity's sake. This general expression is valid for heterogeneous, anisotropic media and for compressible fluids. BEAR (1972[6]) rewrites (2.13) for the independent variable pressure $p$ using the relationship

$$g_i\,\frac{\partial h}{\partial x_i} = g_i e_{x_3} + \frac{1}{\rho}\,\frac{\partial p}{\partial x_i} \tag{2.14}$$

where $e_{x_3}$ is the unit vector in z-direction. Assuming that $k_{ij} = 0$ for $i \neq j$, this results in the expression

$$n\frac{\partial\rho}{\partial t} = \frac{\partial}{\partial x_1}\left(\rho\frac{k_{11}}{\mu}\,\frac{\partial p}{\partial x_1}\right) + \frac{\partial}{\partial x_2}\left(\rho\frac{k_{22}}{\mu}\,\frac{\partial p}{\partial x_2}\right) + \frac{\partial}{\partial x_3}\left(\rho\frac{k_{33}}{\mu}\left[\frac{\partial p}{\partial x_3} + \rho g_i\right]\right) . \tag{2.15}$$

In (2.15), the term $\rho g_i$, expresses the gravity effect. In many cases, this effect is much smaller than the pressure gradient $\partial p/\partial x_3$, and is therefore neglected (BEAR, 1972[6]).

Depending on the fluid, the pressure dependency of the fluid density $\rho$ is more or less significant, e.g. water is generally assumed to be incompressible whereas gas is highly compressible. The experiments and the numerical simulations discussed in this thesis are concerned with gas-saturated media. Assuming an ideal gas, the relationship between the density and the pressure is described by the ideal gas law:

$$\rho = \frac{p}{R_i T} \,. \tag{2.16}$$

Here, $R_i$ is the individual gas constant and $T$ is the temperature.

Introducing (2.16) into (2.15) and neglecting the gravity term, the following diction of the continuity equation is obtained:

$$n\,\frac{\partial p}{\partial t} = \frac{\partial}{\partial x_i}\left(\frac{k_{ij}}{2\mu}\,\frac{\partial p^2}{\partial x_i}\right) . \tag{2.17}$$

### 2.3.3 Transport processes

Assuming a conservative tracer, hence, no adsorption and no reactions, in an isothermal system, three mechanisms determine the transport process, namely advection, dispersion and diffusion.

#### Advection

Advective transport comprises the movement of the tracer in the direction and with the average velocity of the fluid in a control volume (KINZELBACH, 1992[34]). Here, the determining velocity is the seepage velocity $v_i$ defined as:

$$v_i = \frac{q_i}{n_e} . \tag{2.18}$$

Dividing by the effective porosity $n_e$, and not by the total porosity $n$, takes into account that the fluid can only flow through the connected pore space of the control volume, i.e. not through the dead-end pores. The seepage velocity $v_i$ is a bulk property and is therefore only indirectly measurable. The advective mass flux is expressed as

$$J_{a,i} = c v_i , \tag{2.19}$$

where c is the solute concentration of the transported substance.

#### Hydrodynamic dispersion

*Dispersion* describes the mixing due to fluctuations around the average velocity, caused by the morphology of the medium, the fluid-flow condition and chemical or physical interaction with the solid surface of the medium (SAHIMI, 1995[56]). Dispersion effects are observed both for solute transport and for transport of different miscible fluids.

The concept generally used to describe this mixing process is based on FICK's law, assuming that there is a compensation of the concentration in the direction of the negative concentration gradient. The dispersive mass flux is expressed as

$$J_{d,i} = - D_{d,ij} \frac{\partial c}{\partial x_j} , \tag{2.20}$$

where $D_{d,ij}$ is the dispersion tensor. Dispersive mixing is assumed to take place in two principal directions, longitudinal and transversal to the direction of the seepage-velocity vector $v_i$. The dispersion tensor $D_{d,ij}$ is not constant, but depends on the seepage velocity $v_i$. Provided that the system of co-ordinates is aligned with the direction of flow, the dispersion tensor $D_{d,ij}$ is diagonal:

$$D_{d,ij} = \begin{bmatrix} D_l & 0 & 0 \\ 0 & D_t & 0 \\ 0 & 0 & D_t \end{bmatrix} = \begin{bmatrix} \alpha_l v_1 & 0 & 0 \\ 0 & \alpha_t v_2 & 0 \\ 0 & 0 & \alpha_t v_3 \end{bmatrix} . \tag{2.21}$$

Here, $D_l$ and $D_t$ are the longitudinal and the transversal dispersion coefficients respectively, assuming that the vertical and the horizontal transversal dispersivity is equal. $\alpha_l$ and $\alpha_t$ are

the longitudinal and the transversal dispersion lengths. The ratio $\alpha_l/\alpha_t$ is generally larger than 1.

*Diffusion* induces a mass flux between regions of different concentration. Mass flux occurs in the direction of the negative concentration gradient and is described by FICK's law:

$$J_{m,e,i} = -D_{m,e}\frac{\partial c}{\partial x_i}\,. \tag{2.22}$$

Here, $D_{m,e}$ is the effective diffusion coefficient which takes into account that the diffusion process is dependent not only on the combination of fluids, the temperature and the pressure (REID ET AL., 1987[53]) but also on the porous medium (GRATHWOHL, 1998[25]). The diffusion coefficient for gases is higher than for liquids. Since the diffusion process is slow, the significance of this mass flux depends on its relative importance compared to the advective and the dispersive fluxes. In regions of high velocities, it may often be neglected, whereas for low velocities, it is one of the essential processes that determine the shape of the tracer-breakthrough curve.

From the above discussion, it is obvious that dispersive as well as diffusive processes are implemented according to the same concept, i.e. FICK's law. Consequently, these transport flux terms may be combined in one term, generally defined as the *hydrodynamic-dispersion* term, where $D_{d,ij}$ and $D_{m,e}$ are summarised in the hydrodynamic-dispersion tensor $D_{ij}$ (SCHEIDEGGER, 1961[57]):

$$D_{ij} = \begin{bmatrix} D_{m,e}+\alpha_l v_1 & 0 & 0 \\ 0 & D_{m,e}+\alpha_t v_2 & 0 \\ 0 & 0 & D_{m,e}+\alpha_t v_3 \end{bmatrix}. \tag{2.23}$$

The mass flux due to hydrodynamic dispersion is expressed as:

$$J_{hd,i} = -D_{ij}\frac{\partial c}{\partial x_j}\,. \tag{2.24}$$

The concept of hydrodynamic dispersion accounts for the spreading of the tracer due to the irregular pore space and due to diffusion. On a larger scale, the concept of *macro-dispersion* accounts for dispersion due to heterogeneity of the porous medium. In continuum models, a FICKIAN approach is often chosen for the macro-dispersion. In, for example, CIRPKA (1997[15]) the concept of macro-dispersion as well as different model approaches are discussed in detail.

#### Transport equation

Following the same principle as for the continuity equation (2.11), the transport equation is derived by balancing all mass fluxes across the boundaries of a control volume:

$$J_i + \frac{\partial}{\partial x_i}\left(J_{a,i} + J_{hd,i}\right) = 0\,. \tag{2.25}$$

If $J_i$ is expressed as

$$J_i = \frac{\partial c}{\partial t} + q_m\,, \tag{2.26}$$

where $q_m$ is the tracer-mass source/sink term, (2.25) can be written as

$$\frac{\partial c}{\partial t} + \frac{\partial}{\partial x_i}(v_i c) - \frac{\partial}{\partial x_i}\left(D_{ij}\frac{\partial c}{\partial x_j}\right) + q_m = 0\,. \tag{2.27}$$

A measure of the relative importance of advective and dispersive/diffusive transport is the PECLET number Pe. It is defined as

$$Pe = \frac{|v|\,l}{|D_l|}\,, \tag{2.28}$$

where $v$ is the average seepage-velocity in flow direction, $l$ is a typical length scale of the problem and $D_l$ is the hydrodynamic dispersion coefficient in the flow direction. Large PECLET numbers indicate that advection dominates the transport process.

## 2.4 Applied discrete model concept and used tools

As discussed above, in situations where the fractures as well as the matrix play a significant role for the flow and transport processes, the model domain cannot be homogenised but a model concept that includes fractures as well as matrix is required. One approach is to use the discrete model concept, where the matrix and the fractures are locally idealised as continua and the fractures are implemented discretely at their actual location within the domain. It is obvious that the amount of data required to set up a discrete model of the actual domain is very large and to some extent not measurable. Consequently, the discrete model concept is preferably used for relatively small domains and is a suitable tool for fundamental studies of flow and transport processes.

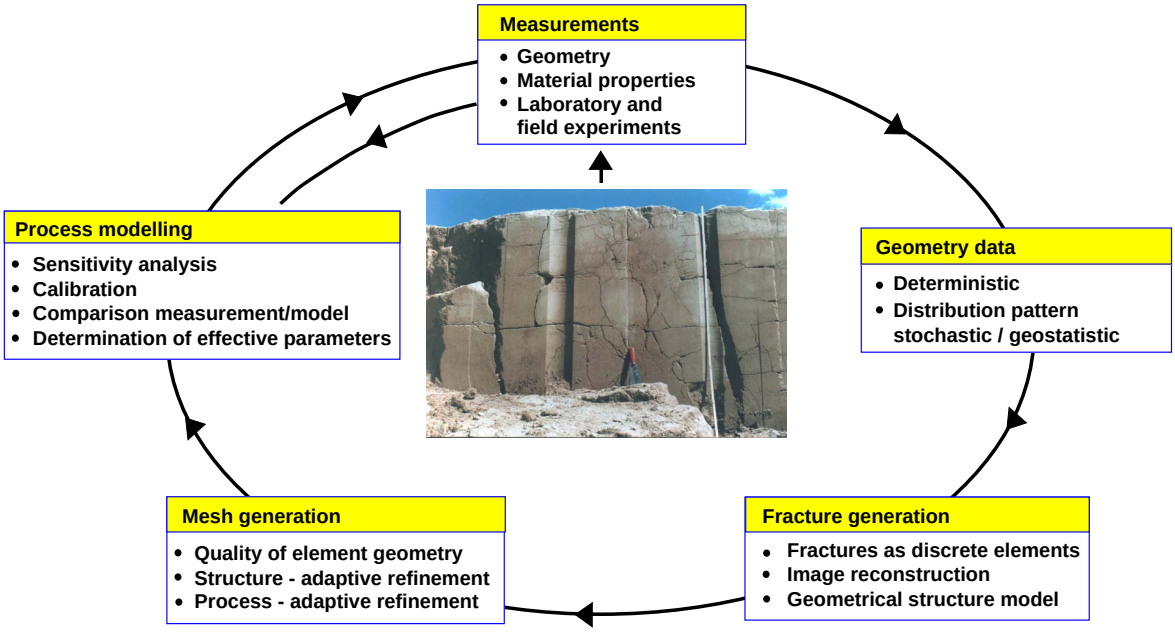


Figure 2.9: Discrete modelling of flow and transport processes in fractured porous media – necessary steps (SILBERHORN-HEMMINGER, 2002[58]).

In the previous section, the physical-mathematical description of the flow and transport processes in porous media, i.e. in the porous matrix, is presented. This section deals with the model concept specific to the fractures. The mathematical description of both the flow within a fracture and its location and geometry is discussed. An overview of the stochastic fracture generator FRAC3D is given and the implementation of the discrete model concept in the numerical model is briefly discussed. Figure 2.9 shows the steps from a natural system to a discrete process model.

### 2.4.1 Parallel-plate concept

A natural fracture is bounded on both sides by the rock surface (Figure 2.5). The rough fracture walls do not have an identical profile and the normal tension is carried by contact zones between the walls. A model concept frequently used for a fracture consists of two plane parallel plates, representing the fracture walls. As illustrated in Figure 2.10, it can be applied locally, maintaining a variation in fracture aperture throughout the fracture, or globally, assuming one constant aperture for the total fracture. It is a well-known fact that especially the latter approach is a strong simplification of nature. However, other methods proposed in the literature have not yet found general acceptance (BERKOWITZ, 2002[10]).

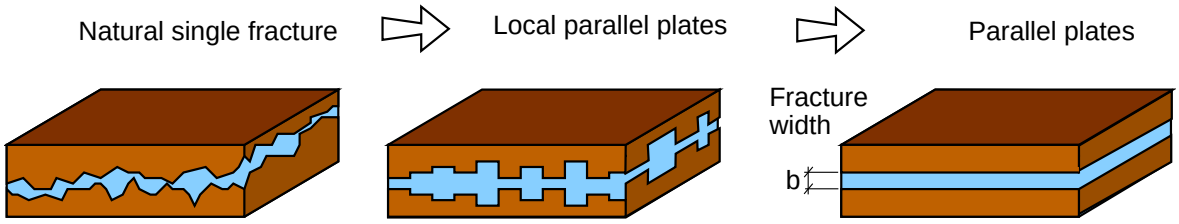


Figure 2.10: From nature to parallel-plate concept.

TSANG & TSANG (1987[61]) showed that preferential flow paths exist, hence *channelling* effects may have significant influence on the flow and therefore also on the transport processes. For multi-phase flow, the variation in entry pressure is strongly related to the distribution of the aperture; therefore, channelling effects are particularly important for simulations including more than one fluid phase.

For the numerical studies presented in this thesis, the parallel-plate concept is applied. The decision to use this simplified concept is justified by the fact that the simulations are concerned with single-phase flow only and that, for the fundamental character of the investigations, this approximation of nature is sufficient.

When the parallel plate-concept is applied, it is assumed that the length scale $l$ of the plates is much larger than the distance between them $b$ ($l \gg b$). Furthermore, hydraulically smooth walls and laminar flow are assumed, corresponding to the POISEUILLE fluid model (e.g. WOLLRATH, 1990[66]). Figure 2.11 shows the two parallel plates and the parabola-shaped velocity profile, indicating laminar flow. The NAVIER-STOKES equation for the laminar single-phase flow of an incompressible NEWTONIAN fluid yields the following equation for the velocity profile between two parallel plates (SNOW, 1969[59]; WHITE, 1999[64]):

$$v(z) = \frac{\rho g}{2\mu}\left[-\frac{d}{dx}\left(\frac{p}{\rho g} + z\right)\right](H^2 - z^2)\,. \tag{2.29}$$

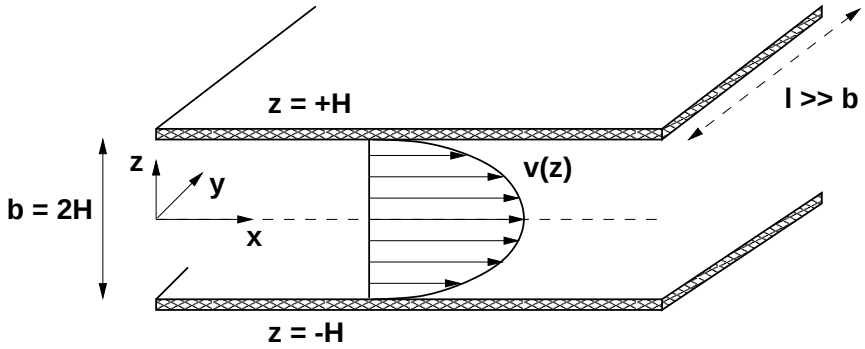


Figure 2.11: Laminar flow between two parallel plates: parabola-shaped velocity profile (SILBERHORN-HEMMINGER, 2002[58]).

The maximum velocity $v_{max}$ is reached at $z = 0$:

$$v_{max} = v(z = 0) = \frac{\rho g}{2\mu} H^2 \cdot - \frac{d}{dx}\left(\frac{p}{\rho g}\right) . \tag{2.30}$$

For a parabola-shaped profile, the mean velocity $\overline{v}$ is derived from the maximum velocity $v_{max}$:

$$\overline{v} = \frac{2}{3} v_{max} = \frac{\rho g}{\mu} \frac{H^2}{3} \cdot - \frac{d}{dx}\left(\frac{p}{\rho g}\right) . \tag{2.31}$$

From (2.31) and under consideration of the distance between the plates $b$ ($b = 2H$), the mean three-dimensional velocity $\overline{v}_i$ can be written as:

$$\overline{v}_i = - \frac{b^2}{12} \frac{\rho g}{\mu} \frac{\partial h}{\partial x_i} = - K \frac{\partial h}{\partial x_i} . \tag{2.32}$$

Here, the hydraulic conductivity $K$ and the permeability $k$ have the following relationship (see (2.7)):

$$K = k \frac{\rho g}{\mu} \qquad \text{with} \qquad k = \frac{b^2}{12} . \tag{2.33}$$

From this, it can be concluded that the permeability of a fracture, approximated by the parallel-plate concept, is proportional to the square of the fracture aperture $b$. The volume discharge $Q$ is derived by integrating the velocity over the distance between the plates (assuming a constant depth $l$ parallel to the $y$-axis):

$$Q = \int_{-H}^{+H} v(z)\, l \, dz . \tag{2.34}$$

Including (2.29) yields:

$$Q = - \frac{\rho g}{\mu} \frac{b^3}{12} l \frac{\partial h}{\partial x_1} \tag{2.35}$$

Due to the proportionality of $Q$ to the third power of the aperture $b$, (2.35) is referred to as the *cubic law* (ROMM, 1980 [54]).

### 2.4.2 Applied stochastic fracture generator – FRAC3D

The use of the discrete modelling approach for simulating flow and transport processes in fractured porous media requires a discrete spatial description of fractures. A fracture generator provides the geometrical description and the structural properties of the fracture system and therefore represents a link between the natural system and the numerical model. A fracture generator is not only used to reproduce actual fractured systems, but it is also a very useful tool for generating artificial data sets that are employed for fundamental studies.

The three-dimensional fracture generator FRAC3D was developed by SILBERHORN-HEMMINGER (2002[58]) on the basis of the work of LONG (1983[37]), LONG & BILLAUX (1987[38]), and WOLLRATH (1990[66]). A flow chart of the program algorithm can be seen in Figure 2.12. In addition to the fracture-generating routine itself, the program FRAC3D offers various methods for analysing the quality of the generated fields, and for optimising the generated fields. Interfaces for the mesh-generating program ART (Almost Regular Triangulation) (FUCHS, 1999[23]) and the flow and transport simulation program MUFTE-UG (Section 2.4.4) are included. The overview given here is based on the detailed description presented in SILBERHORN-HEMMINGER (2002[58]).

As can be seen in Figure 2.12, the algorithm for structure models for generating fractures is based on two different approaches: (1) deterministic and (2) stochastic. The choice of approach depends on the quantity and the quality of the input data available and the purpose of the subsequent simulation.

The *deterministic approach* requires exact information about a fracture network or a single fault zone. One of its main problems is that a three-dimensional system must be generated from one- and two- dimensional information. Often, this is not feasible due to lack of information.

The second basic approach is the *stochastic* one. A large sample of fracture data (e.g. length, orientation) is required and a description of these field data by parameterised theoretical distributions, such as the FISHER distribution for the spherical orientation or the power-law distribution for the fracture lengths, must be available (Section 2.1). It is important to be aware of the fact that these theoretical distributions are based on univariate statistics. They do not include any information about the spatial variability of the data.

Based on the univariate statistical input data the generating algorithm starts. With a *random number* as a starting point, the *generating routine* successively derives location of midpoint, orientation, and size for an increasing number of fractures. The newly generated fracture is included into the global list of fractures if it meets certain criteria, such as for example a minimum distance to a neighbouring fracture. New fractures are generated until the desired fracture density is reached.

The statistical characteristics of the newly generated fracture field are then analysed. For this purpose, the distribution functions of several fracture parameters are calculated. The difference between the input distribution functions and the distribution functions of the new field indicates its quality. If the differences are too large, the newly generated field is either rejected and the generating routine run again, or the *optimisation routine* starts. Because of the relatively smooth distributions of the parameters orientation and fracture length, a good agreement between the input distributions and the distributions of the generated fields is generally achieved. However, for the parameter fracture distance, optimisation is necessary

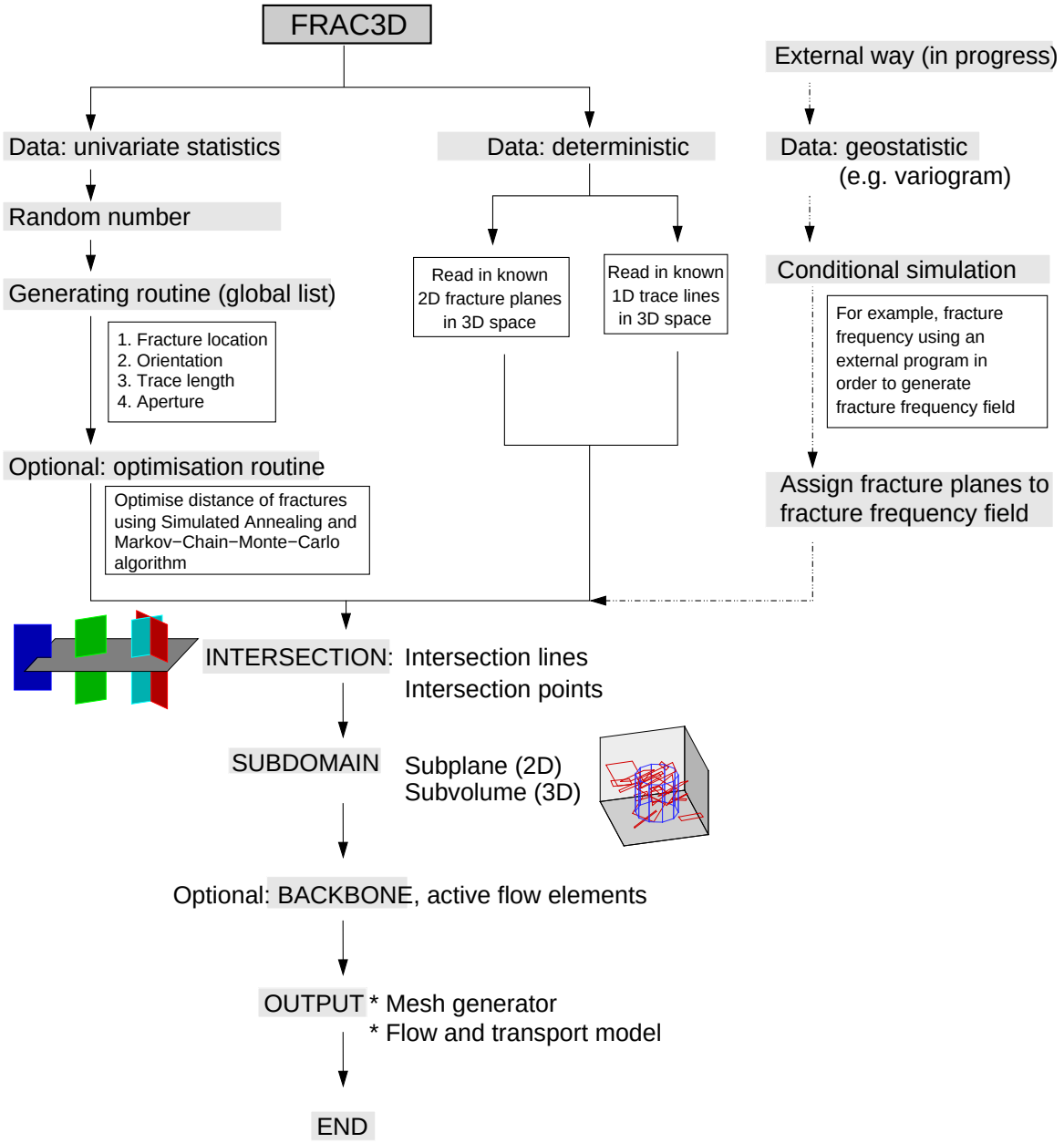


Figure 2.12: Flow chart of the program algorithm of the fracture generator FRAC3D (SILBERHORN-HEMMINGER, 2002[58]).

since information of the fracture distances cannot be taken into account in the generating routine described. In order to include this important information in the generated fracture fields, a modified scanline technique is applied. The scanline technique allows the calculation of the fracture-distance distribution and the optimisation of the distribution.

In the next step, the *intersection lines* of fracture planes and the intersection points of these lines are determined. Subsequently, a *subdomain*, which is the actual investigation domain, is extracted from the generated domain. The program additionally allows two-dimensional planes to be sampled at arbitrary locations. Figure 2.3 shows an example of a generated

three-dimensional fracture system (left) and a two-dimensional section with the resulting fracture traces (right). Optionally, the inactive, disconnected fracture elements can be removed from the fracture network, thus obtaining the *backbone* of the network.

Finally, the *output* (co-ordinates of the investigation domain, the fracture planes, the intersection lines, and the intersection points) is converted into the data format required for the following mesh generation.

There is never a perfect match between a stochastic geometrical model and the real system on which it is based. It is possible to generate different realisations which are similar in their statistical description. However, one single realisation can never exactly predict the behaviour at a certain point of the real system. Therefore, a large number of realisations must be considered for the numerical simulation, yielding simulation results of probabilistic character. Additionally, one has to be aware of the fact that single fractures sometimes control the flow and transport processes in a fracture network completely by connecting different independent fracture clusters. If such dominating fractures are known and can be described by their orientation and size, a combination of the deterministic and the stochastic approaches improves the reliability of the generated fracture network.

The generating approach discussed above incorporates deterministic and univariate stochastic information. A further improvement of the generating process is the implementation of routines for considering geostatistical information as well. Such algorithms are being developed as this thesis is being written.

### 2.4.3 Spatial and temporal discretisation

Due to the large discrepancy between the properties of the matrix and the fractures, large gradients occur in the vicinity of the fracture-matrix interface. To achieve an acceptable numerical accuracy, the mesh of the numerical model must have a high degree of refinement in these areas. Fractures may either be discretised with one dimension less than the matrix, i.e. as lines in a two-dimensional matrix or as a surface in a three-dimensional matrix, or with the same dimension as the surrounding matrix elements, i.e. equi-dimensionally (Figure 2.13).

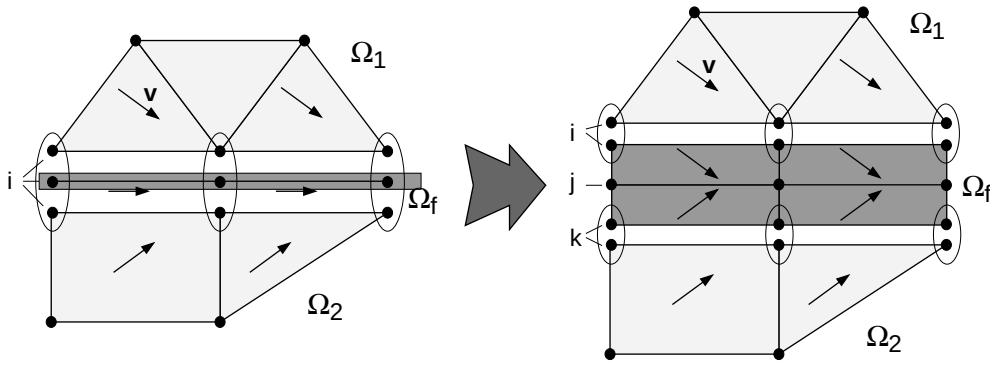


Figure 2.13: Spatial discretisation of a fracture embedded in a porous matrix in a two-dimensional domain. Left: Lower-dimensional discretisation. Right: Equi-dimensional discretisation. From OCHS ET AL. (2002[46]).

For transport simulations, NEUNHÄUSERER (2003[44]) showed that the equi-dimensional

approach yields a more accurate solution than the lower-dimensional one. However, the differences in the global solution are only significant if certain local effects accumulate in the system or if the processes are slow so that a relevant amount of tracer-mass exchange occurs between the fracture and the matrix. For time-dependent problems, steep moving pressure and concentration fronts are obtained in the fractures, suggesting the adeption of an adaptive refinement method in order to save computing time, especially for highly complex systems. For the simulations presented in this thesis a lower-dimensional non-adaptive spatial discretisation is applied.

The temporal discretisation required is in general finer in the vicinity of the fractures, where very high flow velocities occur compared to the velocities in the surrounding matrix. An implicit temporal discretisation is often chosen in order to achieve a stable solution, despite the wide range of velocities. The disadvantage of this approach is a significant influence of numerical dispersion. Due to the advantage of stability, a fully implicit temporal discretiation was used for the simulations presented in this thesis.

Detailed discussions on spatial and temporal discretisation methods, can be found in, for example, NEUNHÄUSERER (2003[44]), HELMIG (1997[27]), BASTIAN ET AL. (1999[5]), KINZELBACH (1992[34]), and HIRSCH (1984[29]).

### 2.4.4 Applied numerical model – MUFTE-UG

For the modelling investigations in this thesis the numerical model MUFTE-UG is applied. It consists of the two parts: MUFTE (Multiphase Flow, Transport and Energy Model) and UG (Unstructured Grids). Figure 2.14 gives an overview of the features of the models.

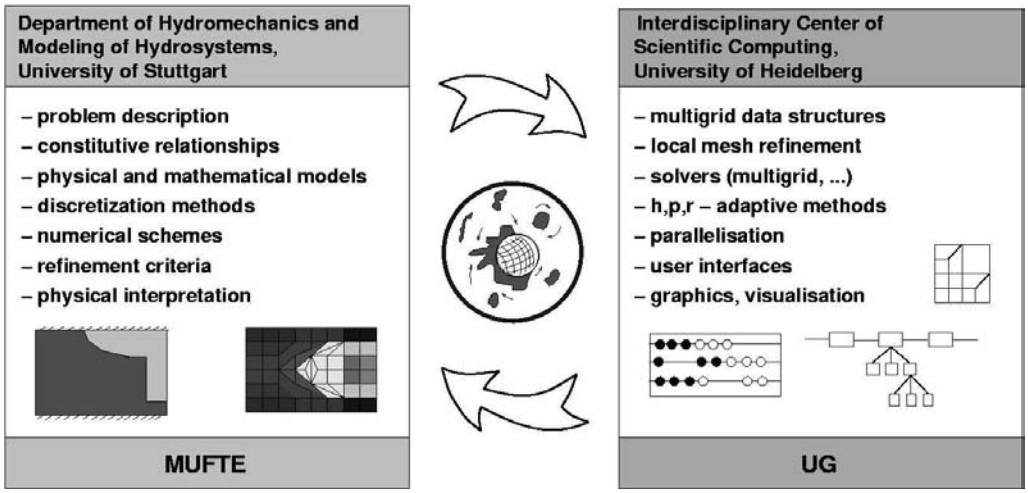


Figure 2.14: Overview of the model system MUFTE-UG.

UG is a software toolbox providing techniques for the numerical solution of partial differential equations (PDEs) on unstructured grids (BASTIAN, 1997[4]). For solving linear and nonlinear PDEs, several multi-grid solvers are available as well as adaptive and parallel techniques. MUFTE contains numerous discretisation methods and applications for modelling non-isothermal multi-phase processes in porous and fractured media (HELMIG, 1997[27]; HELMIG ET AL., 1998[28]). Geometrically complex structures, such as fractured

systems, can be simulated with MUFTE-UG due to the flexibility of the system and its compatibility with the powerful mesh generator ART (Section 2.4.2).

# 3 Analysis of the influence of boundaries on flow and transport processes

The aim of conducting flow and transport experiments is to attain a database that can be used for the determination of process behaviour and relevant parameters. For practical reasons, domain samples are often taken and measurements are conducted under controlled conditions in the laboratory. The result of measurement evaluation of one or more samples is then transfered to the domain from which the samples were taken. It is a well-known fact that the behaviour and the parameters of the samples might differ from what one would obtain for the original, larger domain due to scale effects. Other aspects to be considered when interpreting sample measurement results are, for example, the disturbance of the sample during extraction and transport or the influence of the measurement itself on the flow and transport behaviour.

This chapter deals with the fact that samples are always limited in space. The results of flow and transport measurements are therefore always, to a certain extent, influenced by impervious sample boundaries. Depending on the experimental set-up, this effect is more or less significant and may lead to incorrect measurement interpretation. The significance of the boundary influence is obviously dependent on the distance to a boundary, as illustrated in Figure 3.1. Other circumstances determining the influence of the boundaries are the choice of boundary conditions and the physical properties of the sample.

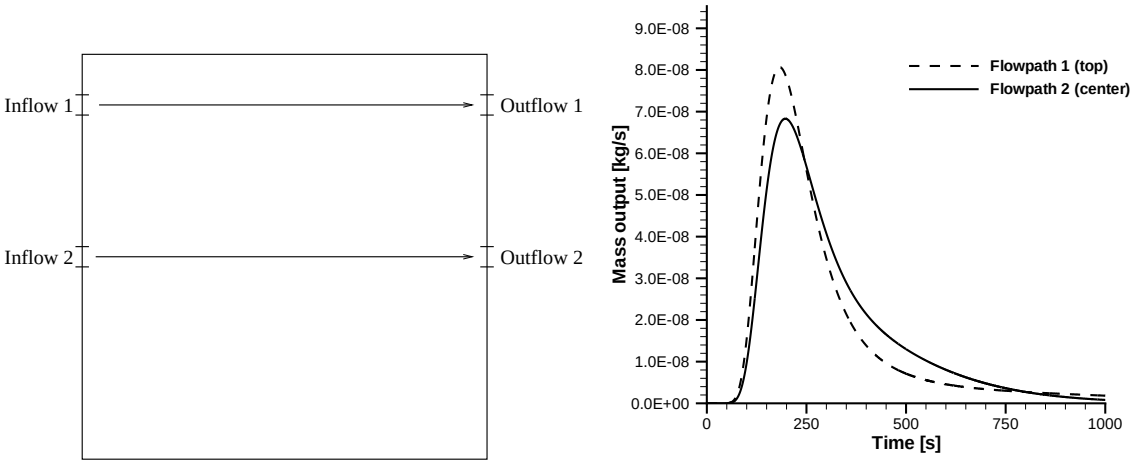


Figure 3.1: Tracer-breakthrough curves for two different port-port configurations (EICHEL, 2002[21]).

Within the framework of the "Aquifer Analogue" research project, a large number of tracer measurements were performed for different port configurations in the laboratory on

a cubical sandstone block with an edge length of 60 cm as mentioned in Section 1.2 and illustrated in Figure 1.2. The tracer-breakthrough curves obtained were statistically evaluated and used to determine the structure distribution within the block and their permeabilities (Section 4.6.1). For the quality of a statistical evaluation, it is essential to have a sufficient number of comparable measurements. However, due to the difference in boundary influence, the measurements first had to be divided into groups with equal distance to the boundaries, in order to ensure comparability. A detailed presentation of this work is given in DIETRICH ET AL. (2005[18]).

This example calls the attention to a number of questions concerning the influence of boundaries on flow and transport processes:

- What is the fundamental influence of impervious boundaries on relevant flow and transport variables?
- How significant is the influence of the boundaries compared to that of structures? Must the boundary influence really be considered or is the system dominated by the influence of structures?
- Does the sensitivity of tracer-breakthrough curves to structure and parameter changes vary with the distance to a boundary? Is the effect of structures and parameter variations on the tracer-breakthrough curve the same if the measurement is conducted or simulated at different distances from a boundary?

These questions are essential to both experimental and model design. They are also of great importance for the correct interpretation of measured and simulated data.

For the investigations that are discussed in this chapter, a flexible model set-up which is presented in Section 3.1 is used. The first investigation is a qualitative analysis of the fundamental influence of boundaries for a homogeneous system (Section 3.2). The difference between the influence of, on the one hand, boundaries and, on the other hand, of structures on tracer-breakthrough curves is evaluated and discussed in Section 3.3. Section 3.4 is concerned with the variation of the sensitivity to structure and parameter changes depending on the distance to a boundary. The chapter is finally summarised in Section 3.5.

## 3.1 Model set-up

The investigation of the boundary influence requires a flexible model set-up that allows to simulate

- flow and transport using different port configurations with an adjustable distance to the boundaries,
- "normal" as well as periodic systems,
- homogeneous as well as heterogeneous domains.

The model set-up is based on the experimental set-up used for bench scale measurements within the "Aquifer Analogue" research project as introduced in Section 1.2. A two-dimensional domain is chosen due to the fundamental character of the investigation. As showed in Figure 3.2, the domain has the dimensions $60 \times 60$ cm. Along each of the four sides 13 measurement ports are distributed, where port number 07 is located exactly in the centre of one side. Each port is 3 cm wide and the distance between two ports is 1.5 cm. During a simulation run, only two ports (e.g. W10 and E04) are open to flow and transport.

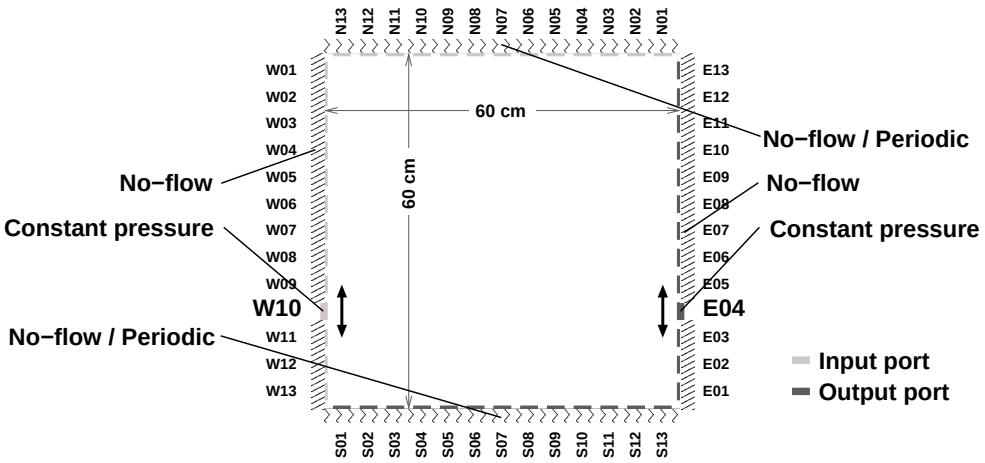


Figure 3.2: Sketch of the model set-up indicating the flow boundary conditions with one of the possible port configurations (W10-E04) as an example.

In most cases only configurations including two opposite ports are used. A driving force for the flow is induced by applying different constant pressures at the in- and the output port. Depending on the purpose of the simulation, all other boundaries are impervious *or* the boundaries without an open port (e.g. north and south) are assigned periodic boundary conditions. The use of periodic boundary conditions yields a system where, for example, tracer leaving the domain at a certain position over the south boundary, simultaneously enters it at the corresponding position over the north boundary. In this way a periodic system repeating itself is achieved.

Concerning the transport problem, only the boundary conditions of the in- and the output ports are different from the flow simulation. At the input port a tracer-mass flux is kept constant during the first time step in order to simulate the injection of a tracer pulse. After the first time step the flux is set to zero. In this way a defined mass enters the system,

independently of the flow conditions at the port. At the output port, a freeflow boundary is assigned, setting the concentration gradient to zero, which makes it possible to obtain a tracer-breakthrough curve at this boundary.

Any types of heterogeneities such as fractures or block-shaped structures may be included into the domain. Depending on the implemented structures, different finite volume meshes are generated that are adapted to the varying geometries.

In Table 3.1 the flow and transport parameters, used for the description of the matrix are listed. The permeability and the porosity values are based on approximated parameter values of the real block sample. The dispersion and diffusion parameters are minimised in order to compensate for numerical dispersion (see below).

Table 3.1: Matrix flow and transport parameters.

| | | |
|---|---|---|
| Permeability $k_M$ | $1.0 \cdot 10^{-13}$ | ($m^2$) |
| Effective porosity $n_{e,M}$ | 0.13 | (-) |
| Longitudinal dispersivity $\alpha_{l,M}$ | $1.0 \cdot 10^{-9}$ | (m) |
| Transversal dispersivity $\alpha_{t,M}$ | $1.0 \cdot 10^{-9}$ | (m) |
| Effective diffusion coefficient $D_{m,e,M}$ | $1.0 \cdot 10^{-9}$ | ($m^2\,s^{-1}$) |

Before the model is actually used for simulations, the accuracy is tested. It is assured that both the flow and the transport simulations are mass conservative and that there are no oscillations. Due to the fully implicit temporal discretisation, artificial numerical dispersion must be taken into account. By choosing a relatively small time step this effect is decreased and by minimising the assigned dispersivities and the diffusion coefficient it is counterbalanced.

## 3.2 Qualitative analysis of the boundary influence

In this section, the general influence of impervious boundaries on certain flow and transport variables in homogeneous domains is discussed. The result of this investigation is an important pre-requisite for the further discussion of the boundary influence in the remaining sections of this chapter as well as for the understanding of boundary influence in general.

### 3.2.1 Database

The simulations are based on the model set-up presented in Section 3.1. Port configurations connecting the east and the west boundaries are used. The north and the south boundaries are impervious to flow and transport. The various model runs are all based on the same mesh; solely the boundary conditions applied to the ports are changed. Using an identical mesh for all simulations prevents deviations due to differences in the element geometry.

In total, 13 model runs are conducted. Seven simulations are conducted for port configurations with the in- and output ports directly opposite to each other, while varying only the distance to the nearest boundary $L_b$ (W01-E13 – W07-E07). The remaining six simulations

connect ports with an off-set of 0.045 m (one port). All configurations are listed in Table 3.2 together with the characteristic variables that serve as a basis for the evaluation.

Table 3.2: Discharge Q, initial arrival time $t_{1\%}$, peak arrival time $t_{peak}$, peak tracer-mass flux $q_{M,peak}$, temporal variance $\sigma_t^2$, shortest average boundary distance $L_b$, and distance between in- and output ports $L_p$ for the thirteen different port-port configurations.

| | Q ($m^3\,s^{-1}$) | $t_{1\%}$ (s) | $t_{peak}$ (s) | $q_{M,peak}$ ($kg\,s^{-1}$) | $\sigma_t^2$ ($s^2$) | $L_b$ (m) | $L_p$ (m) |
|---|---|---|---|---|---|---|---|
| *Directly opposite configurations* | | | | | | | |
| W01-E13 | $0.764 \cdot 10^{-4}$ | 163 | 230 | $1.005 \cdot 10^{-7}$ | 84118 | 0.030 | |
| W02-E12 | 0.904 | 165 | 232 | 1.137 | 75460 | 0.075 | |
| W03-E11 | 0.985 | 172 | 244 | 1.137 | 65911 | 0.120 | |
| W04-E10 | 1.037 | 179 | 252 | 1.103 | 58210 | 0.165 | 0.600 |
| W05-E09 | 1.070 | 184 | 260 | 1.065 | 49734 | 0.210 | |
| W06-E08 | 1.088 | 188 | 264 | 1.034 | 41968 | 0.255 | |
| W07-E07 | 1.093 | 189 | 266 | 0.975 | 44701 | 0.300 | |
| *Off set configurations* | | | | | | | |
| W01-E12 | 0.828 | 166 | 234 | 1.130 | 78060 | 0.053 | |
| W02-E13 | 0.828 | 167 | 236 | 1.017 | 81736 | | |
| W03-E10 | 1.010 | 177 | 250 | 1.121 | 62048 | 0.143 | 0.602 |
| W04-E11 | 1.010 | 177 | 250 | 1.110 | 61707 | | |
| W05-E08 | 1.078 | 187 | 264 | 1.048 | 45382 | 0.233 | |
| W06-E09 | 1.078 | 187 | 264 | 1.042 | 45669 | | |

Figures 3.3 and 3.4 present the simulated tracer-breakthrough curves as tracer-mass flux $q_M$ over time t. For a better differentiation of the curves, zooms of the peak and the tailing area are given as well.

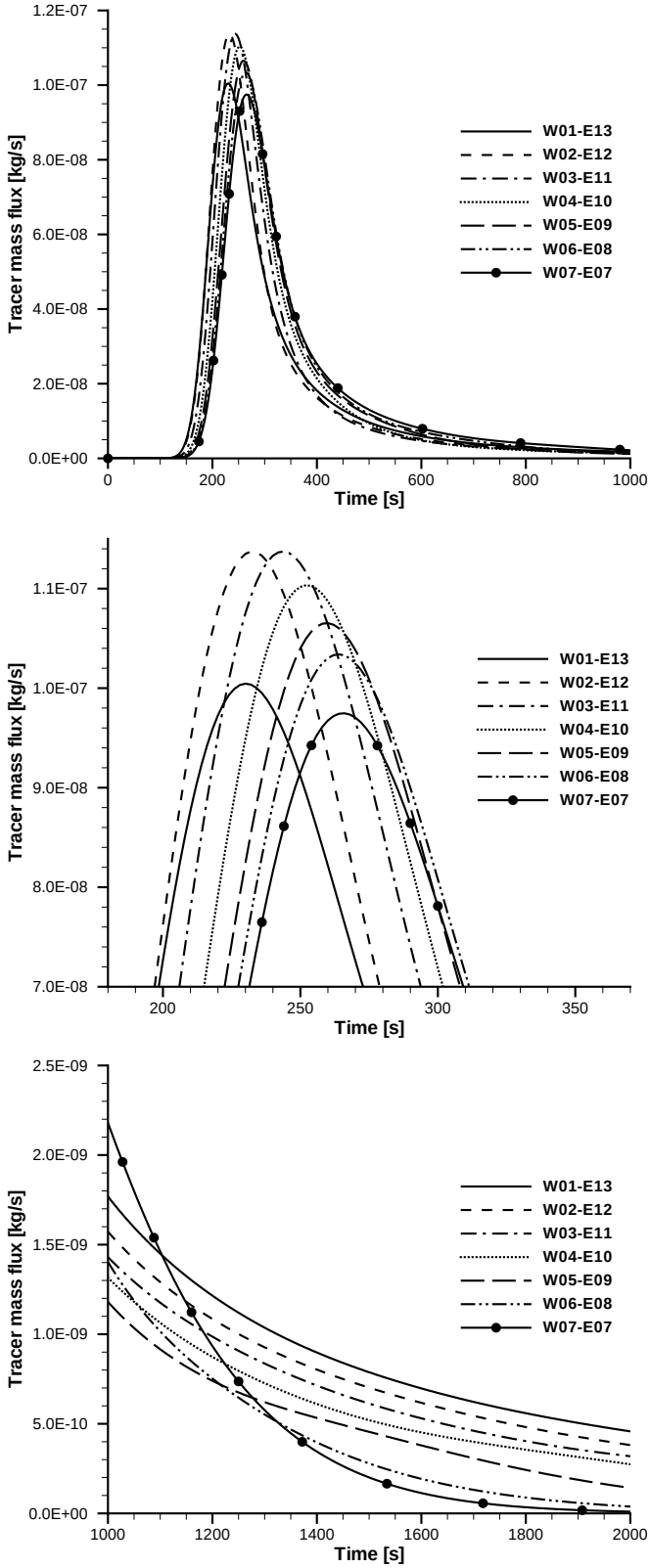


Figure 3.3: Tracer-breakthrough curves of the directly opposite port configurations (top) and zooms of the peaks (centre) as well as of the tailing (bottom).

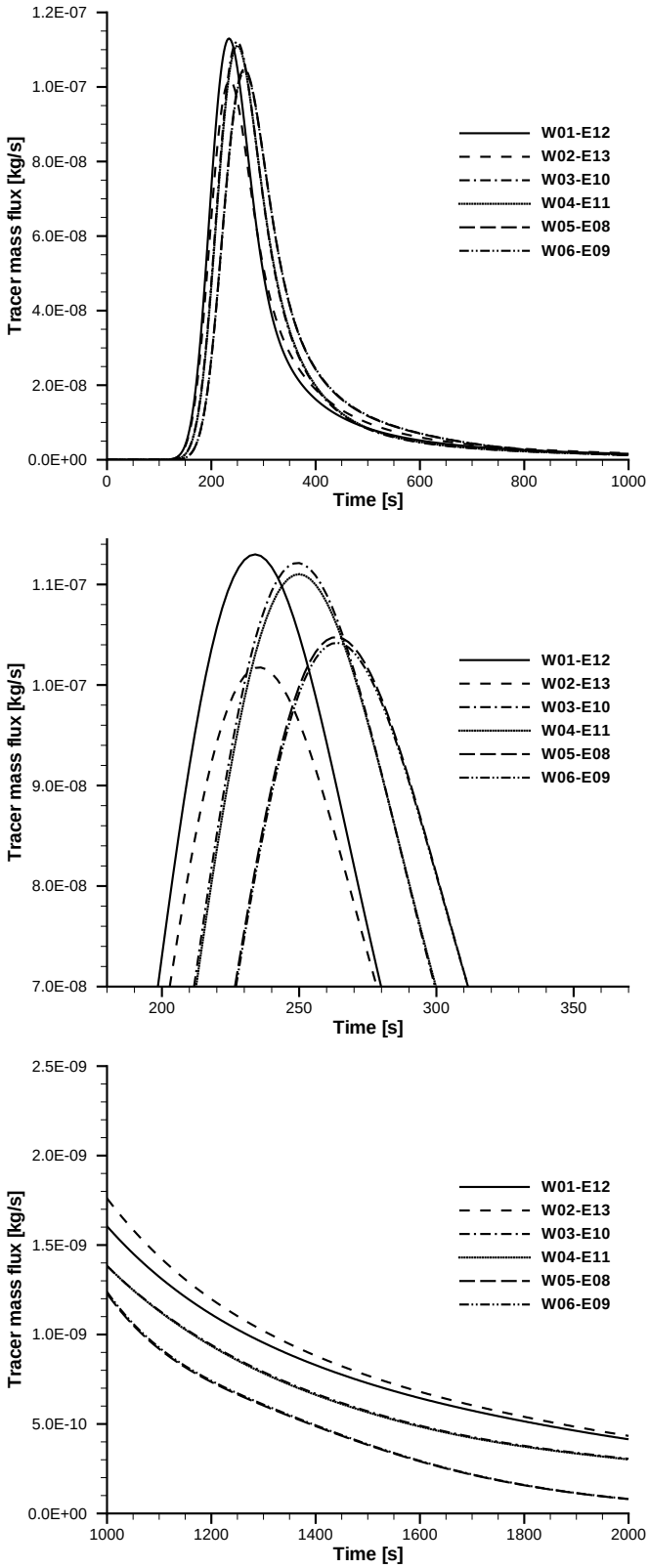


Figure 3.4: Tracer-breakthrough curves of the off set port configurations (top) and zooms of the peaks (centre) as well as of the tailing (bottom).

### 3.2.2 Evaluation

In the following, the characteristic variables, listed in Table 3.2, are discussed with respect to their dependence on the distance to the nearest boundary.

Since the driving force for the flow is a constant pressure difference between the in- and the output port, the resulting difference in average pressure gradient for configurations with different port-port distance must be considered. Consequently, only curves of equal port-port distance are compared.

#### Discharge

First, the configurations with directly opposite ports are considered (W01-E13 to W07-E07). Plotting the discharge Q over the distance to the nearest boundary $L_b$ (Figure 3.5) shows that there is a clear increase in discharge as the ports are shifted away from the boundary. The dependency is not linear, but the gradient of the curve decreases with increasing boundary distance. This behaviour is controlled by the following equation:

$$Q = \overline{q}\,\overline{A} = -K\frac{(h_{out} - h_{in})}{\overline{L}}\,\overline{A}. \tag{3.1}$$

The conductivity K as well as the difference in hydraulic head are constant. Dividing the domain in two parts, i.e. above and below the line between the two ports, and calculating the ratio $\overline{A}/\overline{L}$ for each of the two parts, shows that the ratio decreases for the area that is diminishing. At the same time the ratio for the increasing area grows larger. On average, however, the ratio decreases as the port configuration is shifted closer to a boundary. This explains the decrease in discharge closer to the boundary.

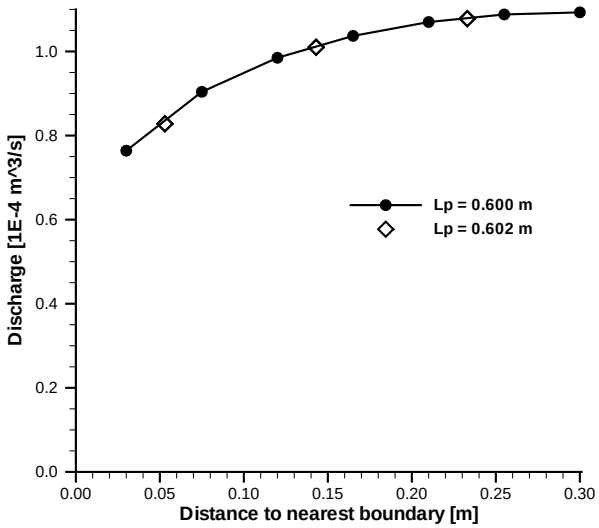


Figure 3.5: Discharge vs. distance to the nearest boundary.

Second, the port configurations with a vertical off-set are compared. From Table 3.2 it can be seen that port configurations with equal average distance to the nearest boundary $L_b$

(and equal port-port distance $L_p$) are equal. This proves that it does not make a difference to the discharge whether the in- or the output port is closer to a boundary. The determining condition is the average distance hereof.

The port-port distance $L_p$ for the off set configurations (W01-E02 to W06-E09) is only slightly larger ($L_p = 0.602\,m$) than for the direct ports ($L_p = 0.600\,m$). Plotting the simulated discharge of these six configurations together with the discharges of the directly opposite ones confirms the above statement (Figure 3.5).

### Arrival time and tailing

The initial arrival as well as the arrival of the peak are evaluated. The initial arrival is represented by the arrival time of 1% of the total tracer mass. This approach is used in order to define clearly the initial arrival time.

Since the total discharge increases as the ports are shifted away from the boundary, one would expect a faster arrival as well. From Figure 3.6, however, it can be seen that this is not the case. Both the initial and the peak arrival time increase with increasing distance $L_b$.

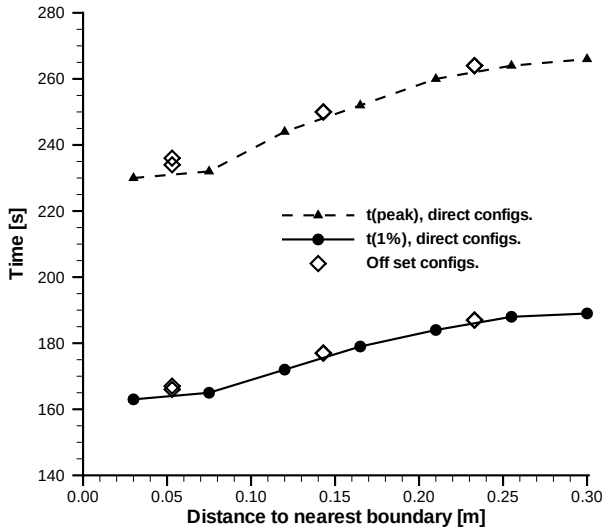


Figure 3.6: Initial and peak arrival time vs. distance to the nearest boundary.

This behaviour is explained by considering the distribution of the velocity in the domain for different port configurations. The connection between two ports can, *as a first approximation*, be looked upon as a dividing streamline. Moreover, it can be assumed that half of the flow and thus half of the tracer flows on each side of that line. The closer the port configuration is to the boundary, the smaller the cross-sectional area above the imaginary line, inferring that half the discharge flows only through a small slice at high velocities. This overrides the effect of the decreasing total discharge which explains why, for configuration W01-E13, the initial and the peak arrival is the fastest.

The same concept is used to explain the behaviour of the curve tailing. Below the imaginary line, a large cross-sectional area yields low velocities. This means that the tracer flows

along a long flow path at a low velocity, resulting in long travel times. Figure 3.3 (bottom) shows that port configuration W01-E13 exhibits the strongest tailing, whereas the concentration of the central configuration W07-E07 decreases fast.

This concept is just a first-order approximation, as the streamlines will bulge away from the nearest boundary, thus reducing the difference in cross-sectional area. Nevertheless, the concept is a valid approximation.

The plot of the arrival times of port configurations W01-E02 to W06-E09 in Figure 3.6 indicates the slight delay due to the longer port-port distance $L_p$. The data points of the smallest boundary distance are not exactly equal in time. From Table 3.2, it is seen that the configuration W02-E13 yields the slightly delayed data points. This is the configuration with the output port close to a boundary. This observation is further discussed for the peak tracer-mass flux (below).

### Peak tracer-mass flux

For the peak tracer-mass flux, the dependency of the distance to the boundary is not as clear as for the other variables as seen in Figure 3.7. In order to obtain a clearer problem involving less variables, the concentration c ($\mathrm{kg\,m^{-3}}$) is plotted in the same figure as well. This excludes the variation due to the discharge Q.

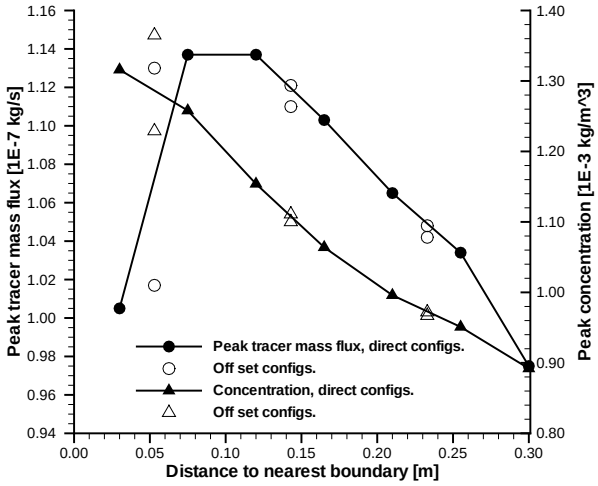


Figure 3.7: Peak tracer-mass flux and peak concentration vs. distance to the nearest boundary.

Using the same concept as for the arrival times, it can be explained why the peak concentration increases with decreasing distance to the boundary. Assuming that half of the injected tracer mass travels on each side of the dividing streamline, the part of the mass travelling through a narrow cross-section is forced together and arrives early with only little spreading in time. Consequently, the highest peak concentration is obtained for port configuration W01-E13, which is located closest to a boundary.

The non-monotonic shape of the plot of the peak tracer-mass flux is explained by considering the shape of the plot of the discharge over the boundary distance shown in Figure

3.5. The discharge decreases clearly as the distance decreases. Multiplying the concentration with the discharge therefore yields a curve with a turning point, from which the peak tracer-mass flux decreases for decreasing distance to the boundary.

In Figure 3.7, the data points of the configurations with one port off-set are plotted as well. It is observed that for larger boundary distances, the deviation from the curve of the direct configurations is not very significant. Table 3.2 shows that the peak of the configuration with the output port closest to the boundary is always the lowest one for each pair of equal average boundary distance. This effect is very strong close to the boundary. There are no arguments concerning the advective transport to explain this difference since the two pressure distributions are equal, except that they are reversed. The solution to the problem is therefore assumed to be connected to the influence of the dispersive and diffusive processes. Strong dispersive/diffusive effects are obtained for steep concentration gradients, which can be observed mainly around the input port. If the input port is close to a boundary, the spreading of the tracer is inhibited. In the region of the output port, the concentration gradients are not as steep as around the input port and therefore, the limiting effect of the boundaries are not as strong. It is emphasised that this is only one possible explanation of the observed effect and that it has not been investigated in further detail. The main conclusion, that is drawn from this observation, is that the tracer-breakthrough curve is more sensitive to boundary influence than the discharge.

### Temporal variance

The temporal variance is a measure of the spreading of the tracer arrival in time (p. 43). The general trend of the temporal variance is that it decreases with increasing distance to the nearest boundary (Figure 3.8). However, if the distance continues to grow, the temporal variance increases again.

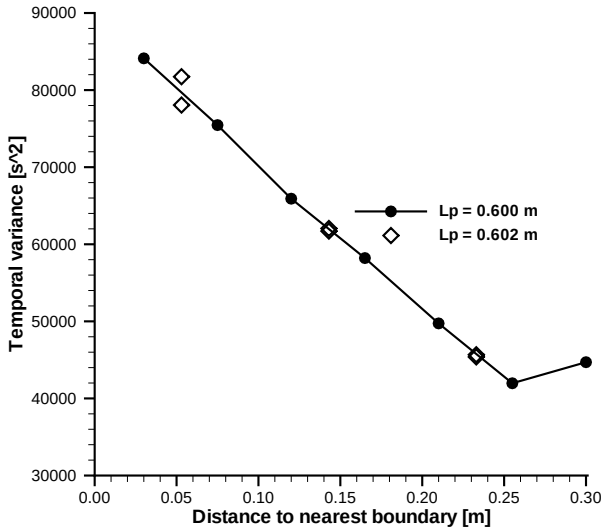


Figure 3.8: Temporal variance vs. distance to the nearest boundary.

Port configurations close to the boundary yield curves with a high peak and augmented

tailing, resulting in a large variance, that decreases as the significance of the tailing decreases. At one point however, the influence of the tracer-mass flux values of the early tailing gains influence on the variance, yielding the non-monotonic behaviour of the curve in Figure 3.8. The variance is always calculated for the same range in time, namely over the complete simulated time from 0 to 2000 s.

### 3.2.3 Conclusions

Using a model set-up that allows to simulate flow and transport for port-port configurations with varying distance to the nearest boundary, the influence of impervious boundaries on discharge and on selected characteristic variables of tracer-breakthrough curves is investigated. It is shown that, for the chosen model set-up, the boundaries have a clear influence on both flow and transport. As a port configuration is shifted closer to a boundary, the discharge decreases. Due to the velocity distribution, however, initial and peak arrival occur earlier. No linear dependencies are observed but the significance of the boundary influence clearly decreases as the distance to the boundary increases. The tracer-breakthrough curve reacts more sensitively to varying boundary distance than the discharge.

## 3.3 Comparison of the influence of boundaries and of structures on tracer-breakthrough curves

The purpose of conducting tracer measurements is to create a data basis that enables the characterisation of the investigated domain. Depending on the shape of the tracer-breakthrough curve, conclusions can be drawn about material properties and their distribution within the system. For the assessment of such data, it is essential that the domain boundaries do not dominate the system, but that the shape of the tracer-breakthrough curve is determined by the distribution of the material properties.

In the previous section (3.2) the behaviour of certain flow and transport variables depending on the distance to the nearest boundary is investigated. The conclusion is drawn, that there is a significant influence of the boundaries on the discharge and the tracer-breakthrough curve. This section serves the purpose of comparing (1) the influence of the boundaries with (2) the influence of fracture systems on the results of flow and transport simulations. Is it really necessary to consider the boundary influence, or do the heterogeneities have a much stronger effect on flow and transport? In order to answer this question, the simulations of the same homogeneous system as discussed in Section 3.2, experiencing influence only from boundaries, and simulations from systems with periodically repeating fracture patterns are evaluated. In this way the variations, on the one hand, due to the boundaries only and, on the other hand, due to the fractures only can be assessed.

First, the assessment approach designed to achieve a meaningful comparison of boundary and structure influence is described (Section 3.3.1). Second, the properties of the generated fracture systems, used to determine the influence of structures are presented (Section 3.3.2). In Section 3.3.3 the evaluation results are discussed.

### 3.3.1 Assessment approach

As briefly mentioned above, the assessment requires two different types of model systems yielding two different data sets. The flexible model set-up introduced in Section 3.1 is used.

The first set of curves is obtained from a homogeneous system which is limited by no-flow boundaries. By varying the configuration of the measurement ports, seven different curves are obtained (W01-E13 to W07-E07), due to the different distances to the model boundaries (Figure 3.2). This is the same system as discussed in Section 3.2, considering only the direct port configurations. The fundamental influence of the boundaries on the result of these configurations is known from the discussion in that section.

The second set of curves is simulated based on fractured porous systems with lateral periodic boundary conditions, allowing flow and transport to cross a boundary and enter again over the opposite boundary of the model domain. This set-up represents a system that is determined by the fracture pattern and not by the limiting lateral boundaries. Different types of porous fractured systems are investigated. Using the stochastical fracture generator FRAC3D (Section 2.4.2), five ensembles of systems with different characteristics are generated (Figures 3.9 – 3.13). The characteristics of these ensembles are discussed in detail in Section 3.3.2. Including different ensembles into the investigation allows the influence depending on the system characteristics to be assessed. For each of the five ensembles, 104 curves (4 realisations $\times$ 26 port configurations) are obtained.

The comparison of the two sets of data is based on comparing certain variables, that can be derived from each simulation. The chosen variables have a good interpretability and together they describe the flow as well as the shape of the tracer-breakthrough curve. The following variables are chosen:

- The *discharge* Q ($m\,s^{-1}$) varies according to the equivalent domain permeability, since the driving force of the flow is the pressure difference between the in- and the output port.
- The *mean effective arrival time* $t_{eff}$ (s) is defined as the first monic moment of the tracer-breakthrough curve. It can be interpreted as the co-ordinate of the "centre of gravity" of the area under the curve along the time-axis.
- The *peak concentration* $c_{peak}$ ($kg\,m^{-3}$) is taken from the first peak (in case there is more than one) of the tracer-breakthrough curve.
- The *temporal variance* $\sigma_t^2$ ($s^2$) is the second central monic moment of the tracer-breakthrough curve. It is a measure of the spreading of the tracer arrival in time.

The mean effective arrival time as well as the temporal variance is based on the complete simulated time (0 – 2000 s). The chosen variables obviously have different units. In order to enable a direct comparison of the variation of the variables, the complete data set is scaled. Each variable vector is centred around its mean value $\overline{x}$ and scaled with its standard deviation $\sigma_x$ applying the following equation:

$$x_i^* = \frac{x_i - \overline{x}}{\sigma_x} \,. \tag{3.2}$$

This makes a direct comparison of the records of the different variables possible.

The configuration that represents the least disturbed simulation is the central port configuration of the homogeneous case with no-flow boundaries. The same set-up, but with periodic boundaries yields an identical result, since the ports are repeated periodically as well. In the following, the central port configuration of the homogeneous domain is used as a reference . The comparison of the influence of boundaries and of fractures is based on the analysis of deviations from the reference value. For each of the chosen variables and for every fracture system ensemble, the average value and the standard deviation is calculated. In addition the minimum and the maximum values are recorded.

The fundamental influence of only boundaries on flow and transport is known from Section 3.2 for the homogeneous system. By analysing the *average values* of the selected variables of the the ensembles of fractured domains, the understanding of the general influence of the fractures on the chosen flow and transport variables is improved. The comparison of the *standard deviation and the extreme value range* to the value range of the homogeneous domain enables the determination of the relative importance of boundaries and of fracture systems of different types.

### 3.3.2 Generated fracture distributions

The result of flow and transport simulations of heterogeneous domains is dependent on the characteristics of the structures in the domain. Consequently, the evaluation of the influence of fracture systems is conducted for several different systems, each with different stochastic characteristics.

Five different ensemble types are defined. For each type, four realisations are generated. Since for one realisation 26 different port configurations are available, 104 ($4 \times 26$) simulations are obtained for each ensemble. The fracture systems are created by means of the fracture generator FRAC3D (Section 2.4.2).

Common to all five systems are the flow and transport properties of the fractures as well as of the matrix. The matrix has the same properties (permeability, porosity, dispersivity and diffusivity) as the homogeneous case (Table 3.1). All fractures are assigned a constant aperture, which yields a constant permeability according to the cubic law (2.35). The fracture parameters that are relevant to the transport simulation are constant as well. In Table 3.3 the values of the complete set of flow and transport parameters of the fractures are given.

Table 3.3: Fracture flow and transport parameters.

| | | |
|---|---|---|
| Aperture b | $1.0 \cdot 10^{-4}$ | (m) |
| Permeability $k_F$ | $8.3 \cdot 10^{-10}$ | ($m^2$) |
| Effective porosity $n_{e,F}$ | 0.30 | (-) |
| Longitudinal dispersivity $\alpha_{l,F}$ | 0.0 | (m) |
| Transversal dispersivity $\alpha_{t,F}$ | 0.0 | (m) |
| Effective diffusion coefficient $D_{m,e,F}$ | $1.0 \cdot 10^{-9}$ | ($m^2\,s^{-1}$) |

In Section 2.1, numbers and distributions that are used for the characterisation of fracture systems are discussed under consideration of their implication on the system connectivity. Table 3.4 summarises the parameter combinations used for this investigation. The parameter

sets are chosen with the objective of varying the system connectivity in different ways. From Table 3.4 it becomes clear, that only the two-dimensional fracture density $d_2$, the number of fracture clusters and the fracture trace length distribution are varied. All other parameters are kept constant. The orientation distribution within a cluster is determined by the FISHER distribution with a constant concentration parameter of $\kappa = 20.0$. The fracture trace lengths follow a power-law distribution with a varying value of the exponent $\lambda$. The generated realisations of each ensemble are visualised in Figures 3.9 – 3.13. The effect of the variation of the distribution parameters is clearly seen.

Table 3.4: Parameter combinations used for the generation of fracture systems.

| Ensemble | 1 | 2 | 3 | 4 | 5 | |
|---|---|---|---|---|---|---|
| Fracture density $d_2$ | 15.0 | **25.0** | 15.0 | 15.0 | 15.0 | ($m/m^2$) |
| Strike angle $S_1$ | 90.0 | 90.0 | 90.0 | 90.0 | **0.0** | (deg) |
| Strike angle $S_2$ | 0.0 | 0.0 | 0.0 | 0.0 | - | (deg) |
| Power-law exponent $\lambda$ | 5.0 | 5.0 | **1.0** | **15.0** | 5.0 | (-) |

- The *first ensemble* is used as a reference case. It has two clusters of fractures with perpendicular main orientations. The fracture density is set to $15.0\,m/m^2$ and the length distribution is determined by $\lambda = 5.0$.
- The *second ensemble* consists of realisations of an increased fracture density of $25.0\,m/m^2$. The result is a larger portion of directly connected fracture traces.
- The effect of a decreasing and increasing $\lambda$ is represented by the *third and fourth ensemble*, respectively. Since the fracture trace density is the same as for the reference case, a smaller value of $\lambda$ yields a limited number of long fracture traces. Due to the chosen density, the connectivity seems to be relatively good. On the opposite, a larger value of $\lambda$ results in a large number of short fractures that are badly connected.
- Finally, the realisations of the *fifth ensemble* consist of one fracture cluster only. The connectivity is higher in the horizontal than in the vertical direction. Due to the lack of the second perpendicular cluster, it seems that even the horizontal connectivity of this ensemble is not as good as the connectivity of the first ensemble.

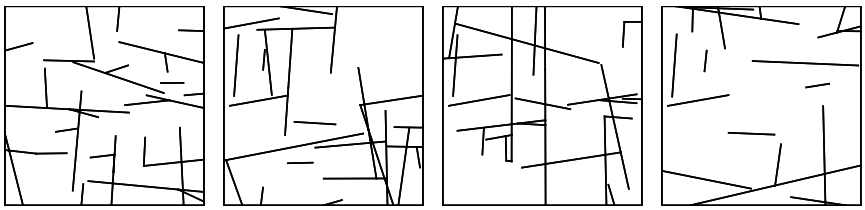

Figure 3.9: Ensemble 1, realisation a–d. Reference ensemble.

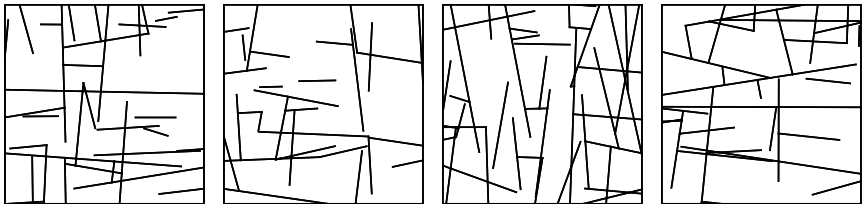

Figure 3.10: Ensemble 2, realisation a–d. Higher fracture density.

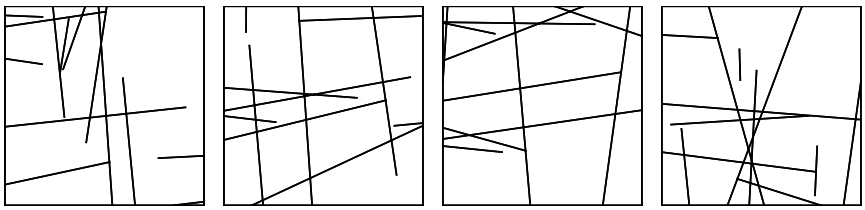

Figure 3.11: Ensemble 3, realisation a–d. Smaller value of $\lambda$, i.e. longer fracture traces.

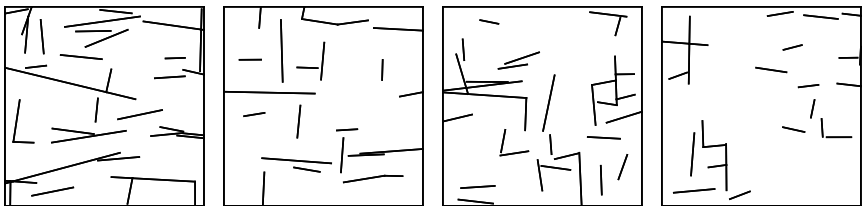

Figure 3.12: Ensemble 4, realisation a–d. Larger value of $\lambda$, i.e. shorter fracture traces.

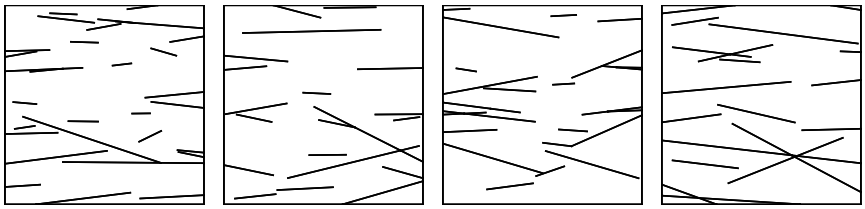

Figure 3.13: Ensemble 5, realisation a–d. One fracture cluster only.

### 3.3.3 Evaluation

The evaluation is divided into two parts. First, in order to understand how the different fracture distributions affect the flow and transport processes in principle, the average values of the selected variables are discussed and compared to the reference value. Second, the variations around the average values of the fracture ensembles are compared to the value range of the homogeneous domain. The aim is to investigate the magnitude of the variations due to boundaries on one hand, and different fracture systems on the other hand.

In Figure 3.14, the reference value (i.e. central port configuration of the homogeneous domain) and the average values are plotted. The standard deviation is plotted symmetrically

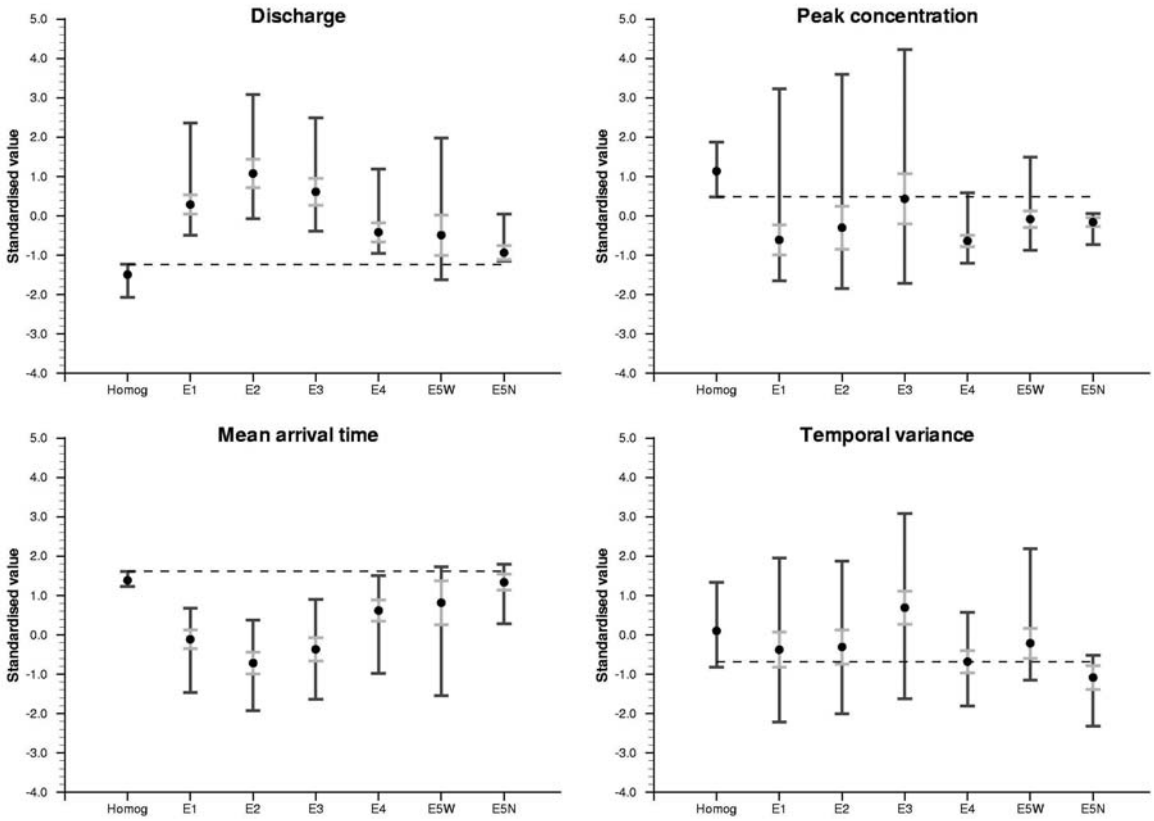


Figure 3.14: Results of the homogeneous domain with no-flow boundaries and fractured porous ensembles with periodic boundaries. Average values of the selected variables in addition to extreme values (min/max) as well as standard deviation (symmetrically plotted around the average value). The dashed line represents the reference configuration (p. 44).

around the average value. The range of extreme values is represented by a bar that connects the minimum and the maximum value. For the homogeneous domain, the range between the extreme values is a direct measure of the variations due to the boundaries and therefore a statistical measure, such as the standard deviation, is not required. For the ensembles of fractured systems, each of them consisting of 104 simulations, the standard deviation is a rel-

evant measure in addition to the extreme values. The very left record of each plot represents the homogeneous domain with no-flow boundaries. The other six records are the result of the simulations from the fractured porous domains with periodic boundaries, hence "E1" represents the simulations of the first ensemble. For ensemble five, consisting of one horizontal cluster only, a directional dependency is expected and the data data set is therefore divided according to main flow direction. "E5W" represents the horizontal port configurations and "E5N" the vertical ones.

#### 3.3.3.1 Average variable values

In the following, the average values of each of the selected variables are discussed. The discussion has two perspectives:

- investigating the deviation of the average value of *each variable* from the reference value, and
- comparin the behaviour of the average values of *different variables*.

##### Discharge

All five fracture ensembles are observed to have a higher average discharge than the reference discharge, independently of the main direction of flow. This is the response to the increase in equivalent domain permeability due to the fractures.

The highest average discharge is obtained for ensemble E2, which has an increased fracture trace density. The lowest average discharge, except for the homogeneous domain, is obtained for the north-south port configurations of the fifth ensemble (E5N). This is explained by the fact that there is only a horizontal fracture cluster and no vertical one. This shows the significance of the fracture orientation concerning the influence on the equivalent domain permeability. It is, however, underlined that the average discharge of E5N is still higher than the reference discharge.

##### Peak concentration

The average peak concentrations of the fracture ensembles are in general lower than for the reference case. For the reference case the tracer plume is not disturbed by heterogeneities and the domain boundaries still have a small increasing effect on the concentration peak (Section 3.2.2).

The highest average peak of the fractured cases has the same magnitude as the reference case and is observed for ensemble E3, containing fracture traces of increased length, often directly connecting one domain side with the opposite one. Such direct paths attract the tracer and decrease its spreading within the domain. Generally, a large portion of the tracer arrives relatively fast at the output port. Snapshots of two exemplary simulations, visualising this effect are shown in Figure 3.15. On the left is a simulation of port configuration W07-E07 for realisation E3c and on the right is the simulation of the same port configuration of one of the reference realisations (E1a). In time step 09, the degree of spreading is rather similar, whereas in time step 21, the tracer plume is more diffuse for the reference realisation.

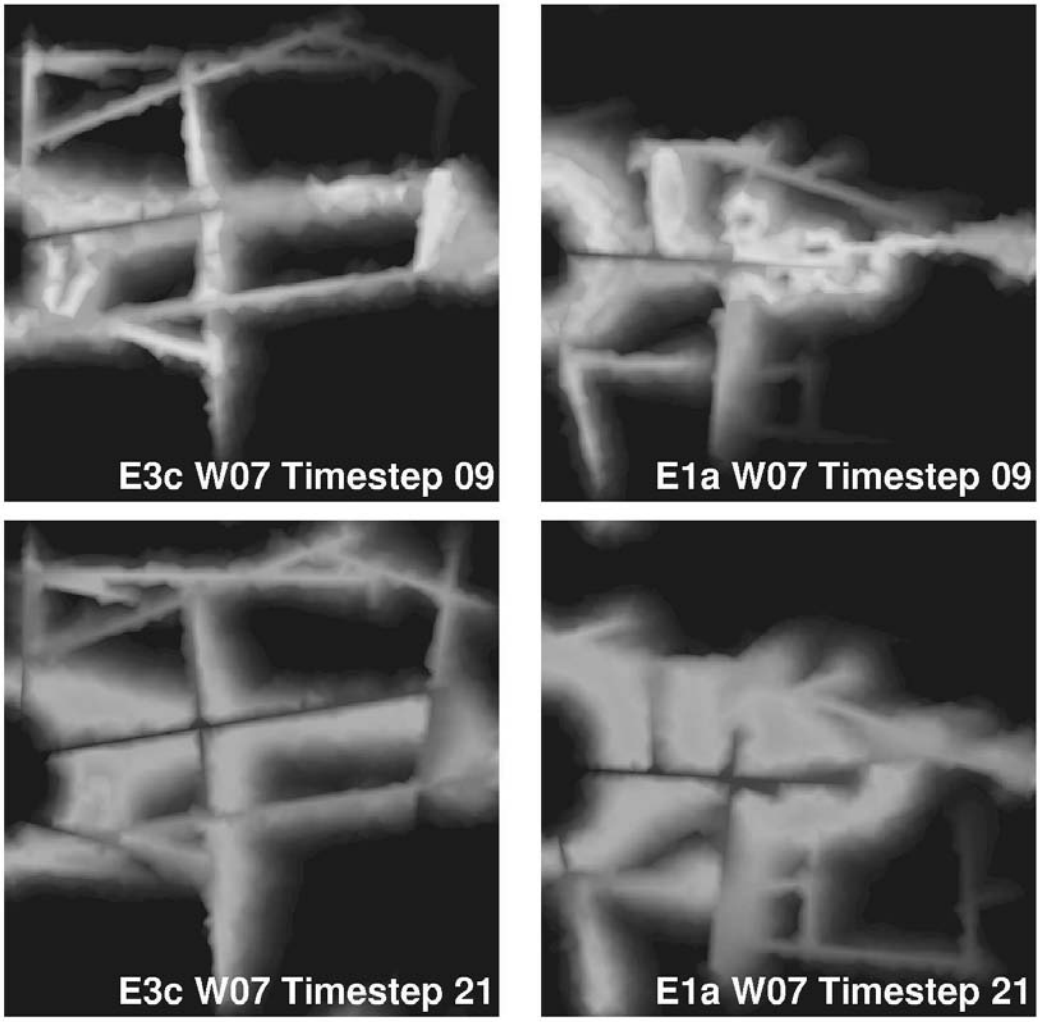


Figure 3.15: Exemplary concentration distributions for time step 09 and 21: realisation E3c (left) and realisation E1a (right).

The lowest average peak of the fracture ensembles is obtained for ensembles E1 and E4 for the following reasons:

- The connectivity of *ensemble E1* is lower than the one of the second ensemble, which has a higher fracture density. The spreading of the tracer is higher than for the third ensemble, for which the tracer is strongly focused on a few preferred flow paths. The dispersive effects are also more significant than for both directions of the fifth ensemble. The fifth ensemble contains only one horizontal fracture cluster which leads to low transversal macro-dispersion for the east-west main flow direction (E5W). In the north-south main flow direction (E5N) there is only a limited influence by the fractures, since the pressure gradient parallel to the fractures is negligible.
- The connectivity of *ensemble E4* is low due to the short fracture traces. The tracer is therefore not focused on a few preferential flow parts. Compared to the homogeneous

reference configuration the dispersive effect is enhanced by the short fractures as visualised in Figure 3.16.

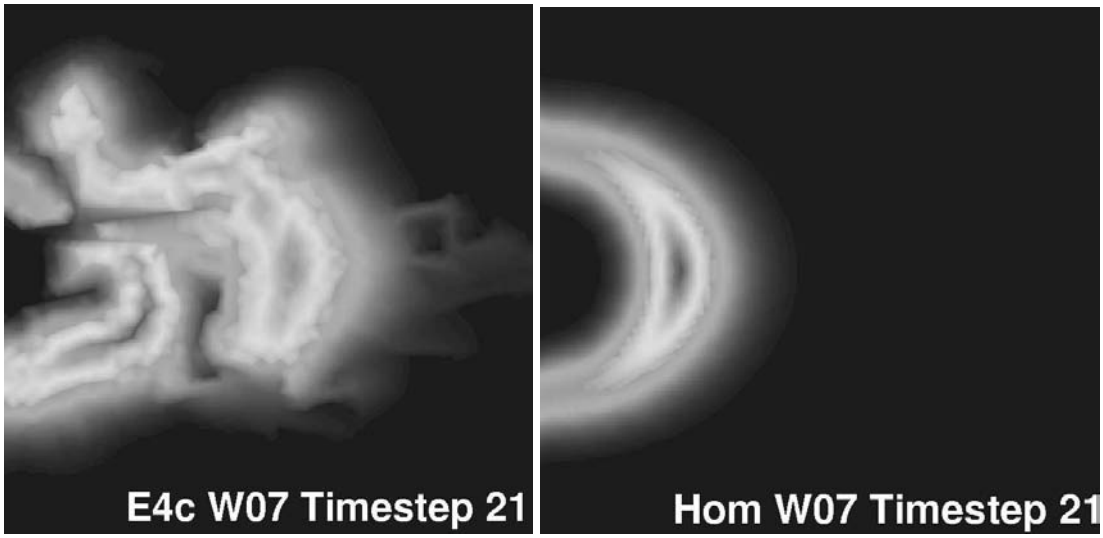


Figure 3.16: Exemplary concentration distributions for time step 21: Realisation 4c (left) and the homogeneous reference configuration (right).

There is no strict relation between the average discharge and the average peak concentration of the fractured ensembles.

#### Mean effective arrival time

The course of the average values of the mean effective arrival time is observed to be a mirror of the course of the average discharge values. This is logical considering the fact that a high discharge implicates a high average velocity and therefore short average travel times.

It is refrained from discussing this variable in detail for the individual ensembles, since the conclusions are equal to the ones for the discharge.

#### Temporal variance

The average values of the mean temporal variance of the fractured ensembles are generally higher than for the homogeneous reference configuration, except for ensembles E4 and E5N. These are both ensembles with bad connectivity. The few fractures that are there, however, promote the tracer transport and decrease the significance of the tracer-breakthrough curve tailing.

The highest variance is obtained for ensemble E3. It consists of very long fractures, often almost directly connecting one side of the domain with the opposite one. This results in tracer-breakthrough curves with a high first peak, in many cases a second clear but strongly delayed peak and a significant tailing. All these characteristics promote an increase in temporal variance.

#### 3.3.3.2 Variations of the variable values

Above, the average behaviour of domains influenced by fractures is discussed. Here, the variations of the selected flow and transport variables are analysed. The standard deviation and the extreme value range of the fracture ensembles are discussed and compared to the value range of the homogeneous domain.

##### Discharge

The range of the discharge values of the homogeneous domain is of approximately the same magnitude as for the standard deviations of the fractured domains. The ranges of the extreme values are, however, clearly wider due to the fractures than due to the boundaries.

As expected for the fracture systems, a small standard deviation corresponds to a small range of extreme values. The largest variation is observed for ensemble E5W, containing one fracture cluster only, parallel to the main flow direction. This yields a system where, depending on the location of the ports, the connectivity varies strongly, since, due to the lack of vertical fractures, the horizontal fractures are only locally well connected. The standard deviation is approximately the same as for the value range of the homogeneous domain, whereas the range of the extreme values is clearly wider. The smallest variation of the fractured domains occurs for ensemble E5N, perpendicular to the single fracture cluster. The range of the extreme values is comparable to the one of the homogeneous case and the standard deviation is very small (smaller than the value range of the homogeneous domain). This indicates the weak influence of fractures perpendicular to the main flow direction.

##### Peak concentration

Except for ensemble E3, the standard deviation of the peak concentration of the fractured systems is smaller than the value range of the homogeneous case. The range of extreme values is in general larger, apart from ensemble E5N.

Ensemble E3, consisting of two clusters of relatively long fracture traces, shows the strongest variations. Depending on whether the tracer finds its way through the relatively coarse fracture network easily or if it is widely spread over several paths, the resulting first peak is high or low, respectively, yielding a strong variation. For more homogeneously connected systems, such as ensembles E1 and E2, the variations are slightly weaker. The weakest variations, however, are obtained for poorly connected systems, such as ensemble E4 and both directions of ensemble E5. The variations of ensemble E5N, both standard deviation and the range of extreme values, are smaller than the range of values of the homogeneous case. This is unique and does not occur for other ensembles or for other variables.

##### Mean effective arrival time

In accordance with the discussion of the average values of the mean effective arrival time, the variations of this variable follow the pattern of the variations of the discharge. It is however observed that the range of the extreme values of the mean effective travel time is generally smaller than for the discharge. The magnitudes of the standard deviation are similar to the ones of the discharge.

The mean effective arrival time is the only variable for which the standard deviation of the fracture ensembles is generally larger than the range of values of the homogeneous domain.

#### Temporal variance

If for the previous variables, the standard deviation of the fracture ensembles is of similar magnitude or larger than the corresponding value range of the homogeneous case, the temporal variance is the only variable for which the standard deviation of the fracture ensembles is clearly smaller than the value range of the homogeneous domain. The ranges of the extreme values of the fracture ensembles, except for ensemble E5N, however, exceed the value range of the homogeneous domain.

The standard deviations of all records are of approximately the same magnitude. Similar to the peak concentration, the range of extreme values is large for ensembles E1 – E3 and smaller for the remaining three ensembles E4 – E5N.

### 3.3.4 Conclusions

From the discussion of the average values of the chosen variables, knowledge about the general influence of fracture systems is gained. The fractures have two essential effects on flow and transport behaviour:

- As expected, the equivalent domain permeability is increased. This effect is strongest for well connected systems and systems with a high fracture density.
- The fractures tend to spread the tracer within the domain, which yields stronger macro-dispersion. The characteristics of the macro-dispersion is different depending on if a fracture system offers many well connected flow paths, only a few but very direct paths or has a bad connectivity.

The increased equivalent permeability results in increased discharge and decreased mean effective arrival time. The increased macro-dispersion yields a decreased peak concentration. The influence on the temporal variance is not as distinct, however the majority of the systems exhibit an increase due to the fractures.

The key question asked in the introduction to this section is if the influence of the boundaries or of the fracture patterns is stronger and if it is necessary to consider the boundary influence.

In general, the magnitude of the standard deviation of the fracture ensembles is comparable to the value range due to boundary influence only. The ratio is not consequently larger or smaller than one. Concerning the extreme value range of the fracture ensembles, they are with very few exceptions, wider than the value range of the homogeneous domain.

Due to the similar magnitude of the standard deviation of the fracture ensembles and the value range due to boundary influence only, and due to the lack of a consequently higher influence of the fractures, the conclusion of the presented investigation must be that the boundary influence may not be neglected for the type and scale of model set-up discussed here.

## 3.4 Boundary influence on the sensitivity of tracer-breakthrough curves to fracture system changes

In the previous section, it is shown that the magnitude of variations due to boundary influence is comparable to variations caused by fracture systems. In this section, the aim is to compare if the sensitivity of the selected flow and transport variables is affected by limiting the fracture domains in space.

### 3.4.1 Assessment approach

For the purpose of this investigation, the existing database is extended by conducting the same simulations of the fracture ensembles as in the previous section, however now with no-flow boundaries instead of periodic ones. The results are statistically evaluated, yielding average values, standard deviations and extreme values for the selected variables.

The magnitude of the standard deviation is used as a measure for the sensitivity of the flow and transport results to disturbance of the system. It is considered to be a more reliable measure than the extreme values, where a large deviation of one value can have a very strong impact on the extreme value range of a variable.

In order to compare the sensitivity of the system limited by no-flow boundaries and the periodic system, the average values and the standard deviations are plotted as presented in Figure 3.17. The standard deviation is plotted symmetrically around the average value. In each plot, the value of the homogeneous reference configuration is marked by the dashed line. First, by comparing the average values to the reference configuration, the impact of the two systems on the average behaviour is assessed. Second, a comparison of the standard deviations of the two systems yields information about the difference in sensitivity, depending on the imposed boundary conditions.

### 3.4.2 Evaluation

The discussion and assessment of the sensitivity is based on the plot of the average values and the standard deviations shown in Figure 3.17.

#### Discharge

The increasing effect of the fractures on the discharge, observed in the previous section is weakened by the spatial limitation of the domain. For all ensembles, the average discharge of the domains with no-flow boundaries is lower. This confirms the conclusion drawn in Section 3.2, that the boundaries act as a resistance to flow, decreasing the equivalent permeability of the domain. An interesting observation is that the average value of ensemble E5N is the same as for the homogeneous reference configuration. This indicates that the effect of fractures perpendicular to the main flow direction, is even weaker if the fractures are terminated by a no-flow boundary.

For all ensembles, the standard deviation is lower for the periodic system than for the no-flow system. This indicates that the boundaries increase the sensitivity of the discharge

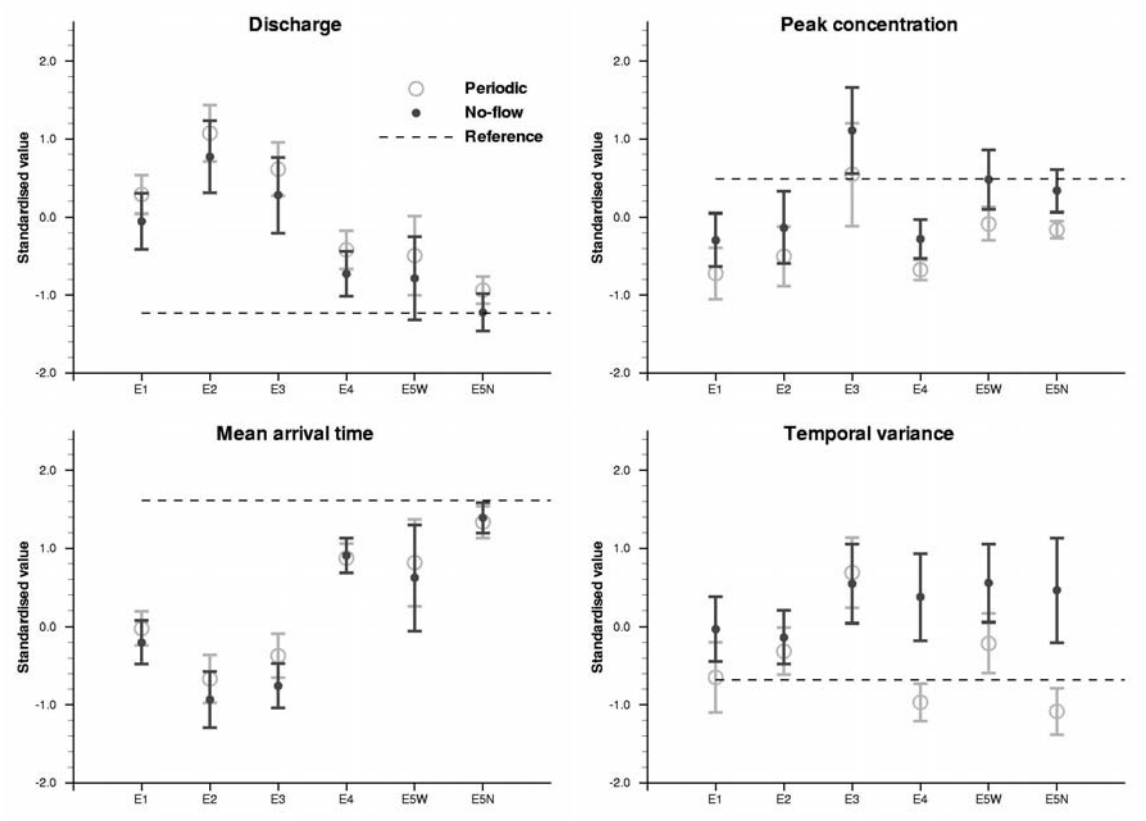


Figure 3.17: Average values and standard deviation of the fracture ensembles for different boundaries.

to the disturbance caused by the fracture pattern. The difference in standard deviation is strongest for ensembles E1 – E3, which have a good connectivity.

### Peak concentration

Comparing the average values, it is observed that the peak concentration of the no-flow systems is always higher than for the periodic systems. The limiting boundaries inhibits the spreading of the tracer plume across the boundaries and consequently the peak increases. The highest peak value is observed for the no-flow system of ensemble E3. Here, a few long fractures rapidly transport the tracer. If an impervious boundary is reached, the tracer flows along the boundary until it reaches an output port or another fracture. This effect is combined with the explanation for high peaks close to a boundary, given in Section 3.2.2.

The standard deviation of the no-flow systems is larger than for the periodic systems, except for ensemble E3. This means that, in general, the sensitivity is increased by the no-flow boundaries.

#### Mean effective arrival time

In contrast to what is expected, the mean effective arrival time of the no-flow systems is lower than for the periodic systems, despite of the lower average discharge. This is the same behaviour as found for the homogeneous system with varying distance to the nearest boundary (Section 3.2.2). There, a decrease of both discharge and arrival time is observed for decreasing boundary distance. This behaviour is explained by the increase in velocity in the narrow cross-sectional area between the direct flow line connecting the two ports and the near domain boundary. This explanation holds for the decreased mean effective arrival time for the no-flow systems compared to the periodic systems as well.

Concerning the standard deviation, the magnitudes of the periodic and the no-flow systems are relatively similar, i.e. no significant influence on the sensitivity is observed.

#### Temporal variance

Except for ensemble E3, the average temporal variance is larger for the no-flow systems than for the periodic systems. This corresponds to an increase in temporal variance for the homogeneous system as the distance to the nearest boundary in decreased. This effect is especially strong for the poorly connected systems of ensembles E4 – E5N. For ensemble E3, consisting of a few long fractures, the effect of the fractures seems to overrule the boundary effects.

For the well connected ensembles E1 – E3, the magnitude of the standard deviation of the no-flow and the periodic systems is relatively similar. For the remaining ensembles E4 – E5N, the standard deviation of the no-flow systems is clearly larger than for the periodic systems, indicating the importance of the boundaries for systems of poor connectivity.

### 3.4.3 Conclusions

The effect of limiting fractured porous domains by impervious boundaries is investigated by comparing periodic systems to systems with no-flow boundaries. The assessment is based on the comparison of selected variables, characterising the flow and transport behaviour.

Limiting the domain by impervious boundaries has different effects on the average values of the selected variables:

- The *discharge* decreases, which confirms the conclusion drawn in section 3.2.2.
- The *peak concentration* increases and the *mean effective travel time* decreases. Again, this is the same behaviour as for the homogeneous case with decreasing distance to the nearest boundary. Half of the discharge flows through a narrow cross-sectional area yielding high velocities and hence, fast transport. Half of the injected tracer travels through the narrow cross-sectional area as, yielding a higher peak due to the boundary limitation.
- The influence on the *temporal variance* is not as distinct. Only ensembles with a poor connectivity are significantly affected, exhibiting a larger temporal variance than the periodic systems. This corresponds to the increase in temporal variance for decreasing distance to a boundary as observed for the homogeneous case. For well connected

systems, the difference of the average values of the periodic and the no-flow systems is negligible.

From the observed effects on the average values of the selected variables, it is concluded that the general influence of limiting impervious boundaries for homogeneous domains holds for fractured domains as well. The lower the connectivity of the fracture pattern, the stronger the influence of the impervious boundaries.

The sensitivity of the no-flow systems compared to the periodic systems is assessed by analysing the standard deviation of the selected variables:

- The standard deviation of the *discharge* is increased, especially for ensembles of good connectivity.
- For the *peak concentration*, there is a similar increase in standard deviation for all ensembles.
- The influence of the no-flow boundaries on the standard deviation of the *mean effective travel time* is negligible.
- There is a general increase in standard deviation, especially for poorly connected ensembles.

From these observations it is concluded that the sensitivity of the flow and transport results of the fractured porous systems is in general increased as the domain is limited by impervious boundaries. In accordance with the previous sections, this shows that the awareness of the influence of boundaries on flow and transport simulations as well as experiments is essential for set-up and interpretation.

## 3.5 Synopsis

The discussions presented in this chapter have the purpose of showing the importance of considering the influence of boundaries when designing an experimental set-up, setting up a numerical model or when interpreting measured or simulated data.

First, this chapter presents a discussion of the fundamental influence of impervious boundaries to flow and transport behaviour on the laboratory scale. Results of numerical simulations of port-port set-ups with varying distance to the model boundaries, show that the boundaries have a significant influence on the discharge and the shape of the tracer-breakthrough curve. With the in- and output ports located closer to the lateral boundary, the discharge decreases, the peak concentration increases, the tracer arrival time decreases, and the temporal variance increases.

Second, in order to answer the question if the magnitude of influence due to boundaries is essential or if it can be neglected, it is compared to the influence of fracture patterns of varying characteristics on certain chosen flow and transport variables. A detailed investigation of the average values and the variations due to boundaries on one hand, and fractures on the other hand, leads to the conclusion that the influence is generally of the same order of magnitude. Consequently, the boundary influence is an essential factor that determines the system behaviour significantly.

Finally, it is investigated how sensitive the flow and transport results are to changes in the fracture pattern depending on the existence of impervious boundaries. Periodic fracture systems are compared to the same systems, however, spatially limited impervious boundaries. The general influence of impervious boundaries observed for homogeneous domains apply for the fracture ensembles with boundary influence as well. The sensitivity of the systems is measured by the standard deviation of certain chosen flow and transport variables. It is concluded that the sensitivity of these variables increases if the domain is limited by impervious boundaries. This is more evidence of how important it is to consider boundary effects.

# 4 Possibilities and limitations of structure identification

The concept of using tracer-measurement data for determining structure geometries and material properties is based on the idea, that the characteristics of the obtained tracer-breakthrough curves are determined by the distribution of flow and transport properties of the domain. Figure 4.1 visualises the *ideal* procedure. By inspection of exposed surfaces of

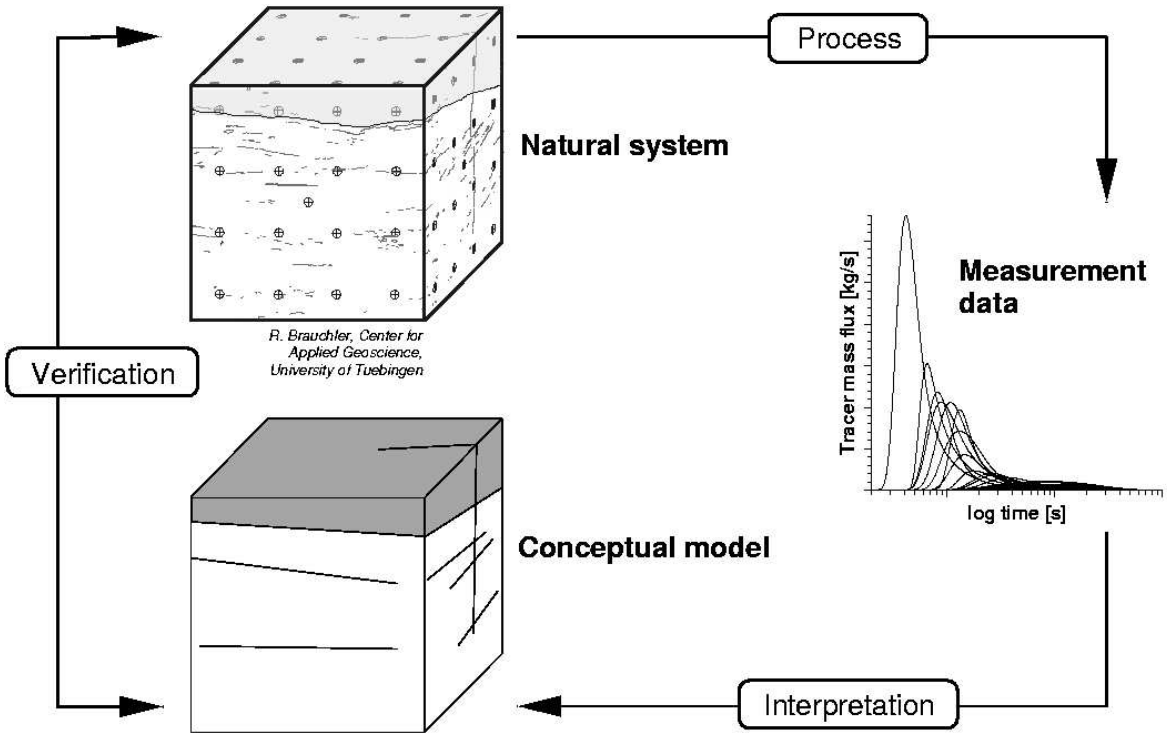


Figure 4.1: Ideal procedure of characterisation of the geometry of structures as well as their flow and transport properties in a sample domain.

the natural system, here represented by the block sample, a first qualitative impression of the characteristics is obtained. In order to localise inner structures and to quantify the material properties, tracer tests are conducted and breakthrough curves are obtained. The curves are evaluated and conclusions about the structures and the properties that caused their shape are drawn. The interpretation yields a conceptual model with a certain inner geometry and distribution of flow and transport properties. The validity of the conceptual model is verified by considering geological plausibility, the information gained from the inspection of the exposed surfaces, any other available information, and by numerical simulation based

on the assumed conceptual model. This is the description of the ideal procedure. It is clear, that the interpretation of the tracer-breakthrough curve is the key task of the described procedure. In reality, there are several difficulties that lead to uncertainty and inaccuracy of the evaluation results.

For quasi-homogeneous domains, well developed evaluation techniques exist that allow the properties of a domain to be determined. Assuming homogeneity, and well defined initial and boundary conditions the desired properties can be determined analytically from the tracer-breakthrough curve (e.g. KÄSS, 1992[32]).

In reality, porous media is always to a certain extent heterogeneous. Since the exact true spatial distribution of material properties can never be determined, stochastic approaches are often used. Stochastic approaches consider the permeability $k(x_i)$ as a random function. Through the flow and transport equations, the velocity $v_i(x_i)$ and the concentration $c(x_i)$ are also defined as random variables. The goal is to predict their statistical moments, rather than deriving one single estimate (e.g. GELHAR, 1993[24]; RUBIN, 1991[55]). Such approaches can be applied both for theoretical process analysis and for evaluation of measured data.

The stronger the contrast of the prevailing material properties is, the more difficult the interpretation of measurement data. For strongly heterogeneous domains the definition of an REV (Section 2.3.1) is no longer possible and single structures are essential to the flow and transport behaviour within the domain. Fractured porous systems are typical examples of such problems. The use of tracer-breakthrough curves for characterising such systems is challenging due to several reasons:

- The tracer-breakthrough curves yield integral information, i.e. they are the result of flow and transport processes within the total domain.
- Exact analytical decomposition of the integral signal into several components, representing certain typical features of the system, is not possible because the effect of one heteogeneity is not independent of the influence of another one.
- An indefinite number of structure and property distributions yield the same output signal, i.e. the problem is not unique.

Usually, inverse modelling methods are used for the characterisation of such systems. How well the real system is represented by the model is always dependent on the physical, mathematical and numerical concepts that are used to set up the model and on the quality and amount of available information.

Within the "Aquifer Analogue" research project (Section 1.2), a new approach was developed for characterising heterogeneous fractured porous samples. For this purpose, multiple tracer measurements were conducted on the block sample. The block sample with its measuring ports and used port configurations is shown in Figure 1.2. The concept was to minimise the problem of integral information and non-uniqueness by conducting a large number of measurements between pairs of ports that were distributed on a regular grid over the six sides of the block. The combination of measurements in different directions and at different locations, restricts the number of possible structure and property distributions that would yield the same flow and transport result. An essential part of the approach was to classify the obtained tracer-breakthrough curves according to their shape properties the

associated measured discharge. The concept was to identify zones of similar behaviour and, based on the interpretation of typical curves for the zones, to characterise the block sample. A detailed description of the experimental set-up and the evaluation approach is given in DIETRICH ET AL. (2005[18]).

The proposed evaluation approach was successfully applied to the block sample. However, the true structure geometry and property distribution of this real sample cannot be known. Therefore, the aim of the work presented in this chapter is twofold:

- Based on certain defined test cases, deliberately designed to contain simple geometries, the *possibilities* of identification of the geometry of structures and the determination of their properties are discussed using numerical simulation.

- The intention is also to show that, even for such simple geometries, there are *limitations* in both localising structures and determining their properties.

The same model set-up as introduced in Section 3.1 is used for the simulations, considering several port configurations and imposing periodic boundary conditions on the two boundaries parallel to the main flow direction (Figure 3.2). Due to the periodic boundaries, the emphasis is put on the influence of the structures and, hence, effects caused by no-flow boundaries are eliminated. This is an essential pre-requisite for a well defined analysis of structure influence as discussed in Chapter 3.

As already mentioned above, the possibilities and limitations of structure identification are investigated using transport simulations from a number of test cases of different characteristics. The test cases are designed to contain very simple structure geometries. The first group of test cases (A) contains no fractures, but block-shaped geometries. The domains of the second group (B) are composed of a porous matrix and a few distinct fractures. The third group (C) consists of domains with a porous matrix and regular systems of fractures. The geometry as well as the flow and transport properties of the test cases are presented in Section 4.1. From the various possible port configurations of the introduced test cases, a large number of tracer-breakthrough curves and associated discharges serve as a data basis for the investigations presented in this chapter.

An essential part of this chapter consists of discussions of properties of transport simulation results, i.e. the shape characteristics of tracer-breakthrough curves and the associated discharge. In Section 4.2, first, the influence of permeability in homogeneous domains on the shape of the tracer-breakthrough curve is demonstrated. Second, exemplary tracer-breakthrough curves of the test cases are discussed. The problem of non-uniqueness is discussed as it is revealed that different domains yield the same type of output.

In Sections 4.3 and 4.4, ways of localising structures and determining the domain permeabilities are investigated. Possibilities and limitations of the proposed procedures are discussed.

The applicability of the gained knowledge is tested in Section 4.5 by attempting to localise and determine the permeabilities of structures of certain artificial domains. Except for the boundary and initial conditions as well as the ”measured” tracer-breakthrough curves, nothing is known about the domains, corresponding to the conditions under which real measurements are evaluated. Since for the artificial cases, the true structure geometry and

properties are revealed after the evaluation, a verification of the proposed identification result is possible.

Finally, the results of an application to a real case are presented in Section 4.6.

## 4.1 Definition of test cases

In order to create a database that can be used to investigate the possibilities and limitations of the identification of structures and their properties, certain test cases are defined. There are three different groups of test cases, representing systems of different type: The first group (A) contains domains with one block-shaped structure, the second (B) is concerned with a few possibly intersecting single fractures in a porous matrix, and the third (C) with systematically distributed fractures in a porous matrix. If not specified below, the matrix and fracture properties correspond to the data given in Tables 3.1 and 3.3.

The properties and geometries of the three groups of test cases, are selected to represent potential features of natural fractured porous domains. It should be emphasised, that the chosen geometries are strongly simplified compared to structures which are to be expected in real domains. However, in order to see clearly the effects of certain geometries or properties, a reduction of the number of influencing factors is required. This is achieved by selecting artificial structures with clear geometries instead of more natural irregular structure shapes.

### 4.1.1 Group A: Block-shaped structures

The first group of test cases is concerned with block-shaped structures as shown in Figure 4.2. These structures represent, for example, lenses or layers of a different permeability than the background material.

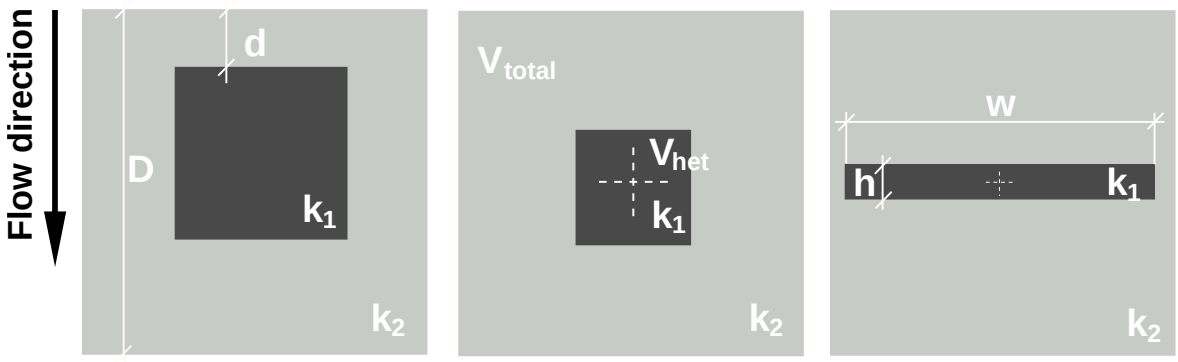


Figure 4.2: Sketches of the three cases of group A. Left: Case A1 (fracture length). Centre: Case A2 (relative volume). Right: Case A3 (shape of the structure).

For all three cases the simulations are performed for $k_r = k_1/k_2 < 1.0$ as well as for $k_r = k_1/k_2 > 1.0$. The absolute values of the used permeabilities are listed in Table 4.1. These values are chosen according to the permeabilities relevant for the type of domains, which are investigated within the "Aquifer Analogue" research project, i.e. fractured porous sand-

stone. They represent a small and a large permeability ratio. The general flow direction is always from the north to the south.

Table 4.1: Combinations of permeabilities used for the test cases of group A.

| | Ratio $k_1/k_2$ (-) | Structure $k_1$ ($m^2$) | Background $k_2$ ($m^2$) |
|---|---|---|---|
| (a) | 1/2 | $1.0 \cdot 10^{-13}$ | $2.0 \cdot 10^{-13}$ |
| (b) | 2 | $2.0 \cdot 10^{-13}$ | $1.0 \cdot 10^{-13}$ |
| (c) | 1/10 | $1.0 \cdot 10^{-13}$ | $10.0 \cdot 10^{-13}$ |
| (d) | 10 | $10.0 \cdot 10^{-13}$ | $1.0 \cdot 10^{-13}$ |

The *first test case (A1)* is designed to investigate the influence of the distance of the structure to the in- or to the output boundary. The structure is gradually shifted away from the northern boundary closer to the southern one, i.e. $d$ is increased in steps of 0.05 m from $d = 0.0$ m to $d = 0.15$ m. This yields a total of 112 curves for test case A1, neglecting symmetric port configurations and considering the different permeability ratios, as listed in Table 4.1. The edge length of the square structure is half the edge length of the domain.

In the *second test case (A2)*, the relative volume $V_r$ (assuming a domain thickness of 1 m) is varied, while the centred position of the structure is maintained. The relative volume $V_r$ is determined according to the following expression:

$$V_r = \frac{V_{\text{structure}}}{V_{\text{domain}}} \,. \tag{4.1}$$

The edge length of the square structure is increased from 0.06 m to 0.60 m in steps of 0.06 m, yielding relative volumes ranging from $0.01 \leq V_r \leq 1.0$. In total, 280 different transport simulations are obtained for test case A2.

Finally, the *third test case (A3)* deals with the shape of the block structure. The shape is described by the shape ratio P, defined as

$$P = \frac{w \quad \text{(width of the structure)}}{h \quad \text{(height of the structure)}} \,. \tag{4.2}$$

The volume of the centred structure is kept constant. In order to allow long thin shapes, the relative volume is set to $V_r = 0.09$. There are 9 different shape ratios in the range of $0.01 \leq P \leq 9$ ($w = 0.06$, 0.09, 0.12, 0.15, 0.18, 0.216, 0.27, 0.36, 0.54 m). This yields a total of 252 transport simulations for test case A3.

### 4.1.2 Group B: Single fractures

The second group of test cases contains domains with single fractures or a few, intersecting fractures. It contains three test cases as presented in Figure 4.3.

Common to all cases is the constant fracture permeability of $k_F = 8.33 \cdot 10^{-10}\,m^2$, which, according to the cubic law (Section 2.4.1), corresponds to a fracture aperture of $b = 0.1$ mm. Similar to the test cases in group A, the matrix permeability is either $k_M = 1.0 \cdot 10^{-13}\,m^2$ or $k_M = 1.0 \cdot 10^{-12}\,m^2$, allowing for the assessment of the influence of different permeability contrasts.

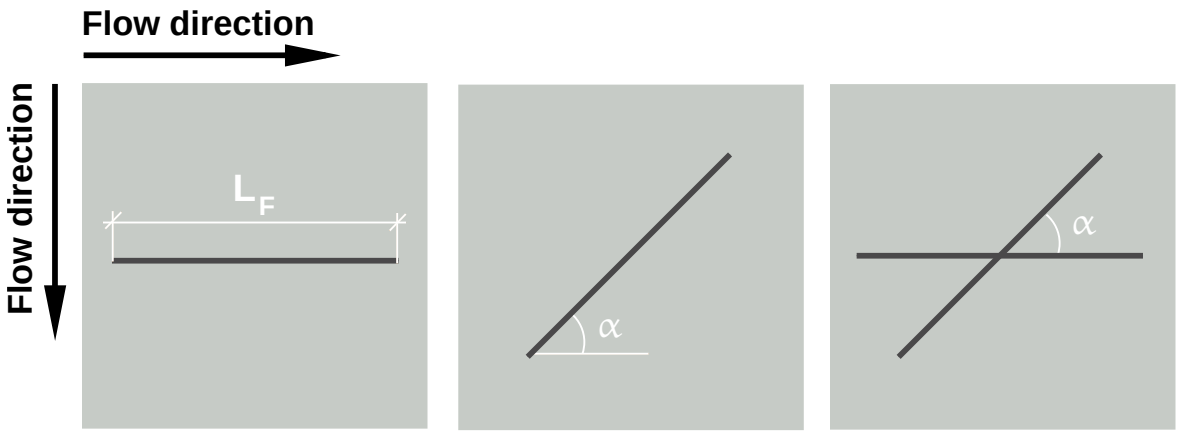


Figure 4.3: Sketches of the three cases of group B. Left: Case B1 (distance to the boundary). Centre: Case B2 (angle to main flow direction). Right: Case B3 (varying angle of intersection).

The *first test case (B1)* is designed to investigate the possibility of identifying a fracture length. The fracture is located in the centre of the domain, and calculations are conducted for flow directions vertically as well as horizontally to the fracture. The relative length of the fracture $L_r$ is defined as the length of the fracture $L_F$ divided by the length of the domain. It varies in the range of $0.5 \leq L_r \leq 1.0$ ($L_F = 0.30,\ 0.40,\ 0.50,\ 0.60\,\mathrm{m}$). Considering two different permeability ratios (see below) and excluding symmetrical port configurations, a total of 100 transport simulations are obtained.

In the *second test case (B2)* the tracer-breakthrough curves of a domain with a single inclined fracture are evaluated. The mid-point of the fracture is fixed in the centre of the domain and the fracture length is constant $L_F = 0.5\,\mathrm{m}$. Here, due to symmetry reasons, only west-east port configurations are considered. The inclination angle $\alpha$ varies in steps of 15° in the range of $15° \leq \alpha \leq 75°$. This yields a total of 130 transport simulations.

Finally, in the *third test case (B3)*, domains containing two fractures, intersected at a certain angle, are assessed. Both fractures have the length $L_F = 0.5\,\mathrm{m}$ and their mid-points are fixed in the centre of the domain. The same port configurations and angles as for test case B2 are considered, yielding a total of 130 transport simulations.

### 4.1.3 Group C: Systematically distributed fractures

The third group of test cases represent domains with systematically distributed fractures in a porous matrix (Figure 4.4). The fractures vary in length and their angle of inclination $\alpha$ relative to the main flow direction is either 0° or 45°. In accordance with the test cases of group B, a fixed fracture permeability of $k_F = 8.33 \cdot 10^{-10}\,\mathrm{m}^2$ is combined with two different matrix permeabilities $k_M = 1.0 \cdot 10^{-13}\,\mathrm{m}^2$ and $k_M = 1.0 \cdot 10^{-12}\,\mathrm{m}^2$.

The *first test case (C1)* represents systems with short fractures ($L_F = 0.10\,\mathrm{m}$) that are not connected with each other. The fracture distance is $d_F = 0.10\,\mathrm{m}$ for both angles of inclination. This yields a slight difference in fracture density of the two systems; $d_2 = 4.2$ or $d_2 = 4.4\,\mathrm{m}^{-1}$ respectively. For the system with $\alpha = 0°$, only the port configurations with the input ports N05 – N07 and W03 – W07 are used. All other configurations correspond to one of the

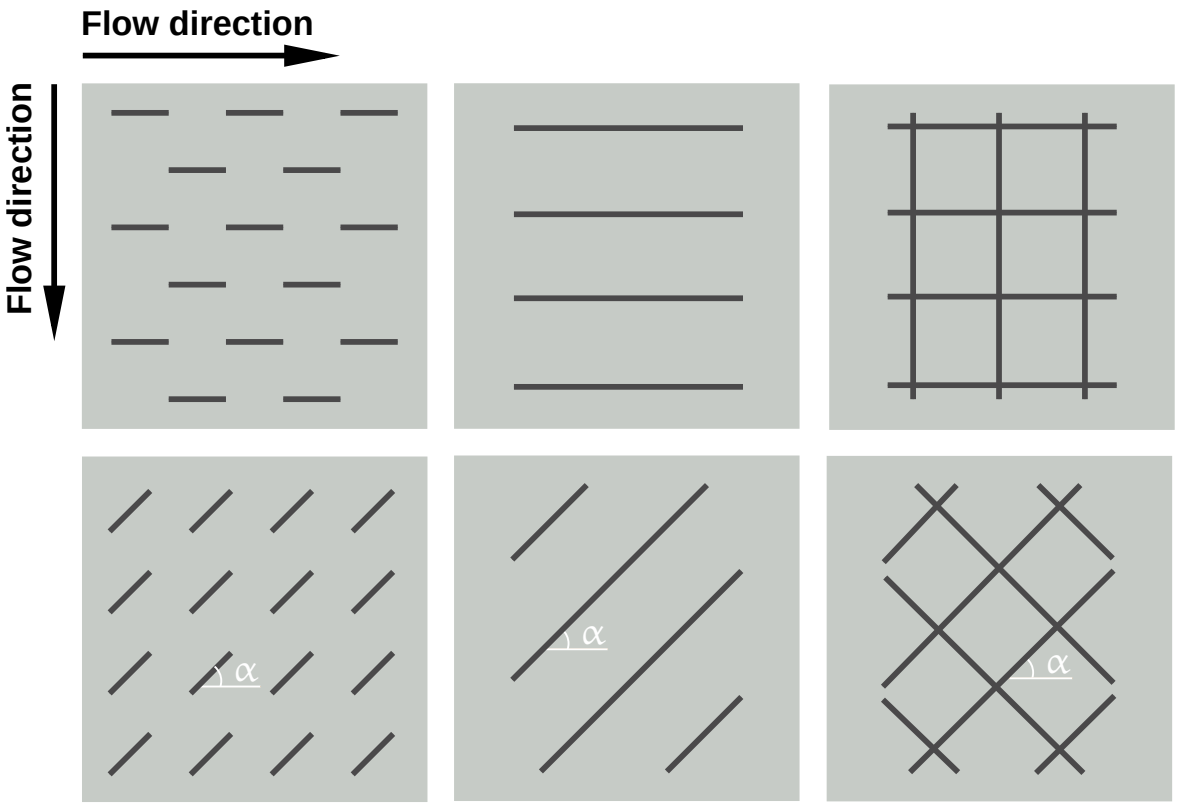


Figure 4.4: Sketches of the three cases of group C. On the top $\alpha = 0°$ and below $\alpha = 45°$. Left: Case C1 (short non-connected fractures). Centre: Case C2 (long non-connected fractures). Right: Case C3 (long connected fractures).

selected ones due to the periodicity of the system. For $\alpha = 45°$, the configurations with the input ports W05 – W07 are used. This yields a total of 22 simulations.

The domains of the *second test case (C2)* contain long fractures, however, still not connected to each other. The distance to the input and the output boundary is constant (0.10 m). The fracture distance is $d_F = 0.15\,\text{m}$ for both angles of inclination which yields fracture densities of $d_2 = 4.4$ and $d_2 = 3.7\,\text{m}^{-1}$ respectively. For the system with $\alpha = 0°$, only the port configurations with the input ports N07 and W05 – W07 are used. For $\alpha = 45°$, the configurations with the input ports W07 – W13 are simulated. In total 22 simulations are conducted.

Finally, the *third test case (C3)* represents domains with a system of intersected long fractures. The distance to the input and the output boundary is constant (0.10 m). The fracture distance is $d_F = 0.15\,\text{m}$ for both orientations. The fracture density is $d_2 = 6.6$ and $d_2 = 7.5\,\text{m}^{-1}$ respectively. For both orientations, the configurations with the input ports W05 – W07 are used. This yields a total of 12 simulations.

## 4.2 Characteristic shapes of tracer-breakthrough curves

Two goals are pursued in this section. First, a discussion of different curve shapes aims at understanding the flow and transport behaviour that leads to certain characteristics of a tracer-

breakthrough curve. The emphasis is put on advective processes. Dispersive and diffusive processes are minimised in the simulations, however, effects of numerical dispersion must be kept in mind. After considering the influence of permeability on the shape of a tracer-breakthrough curve from a homogeneous domain, the influence of structures is discussed considering exemplary tracer-breakthrough curves from the three groups of test cases. In doing so, the discussion is focussed exclusively on the shape of the curve, i.e. qualitative rather than quantitative information is considered. It is not attempted to discuss the shape of each of the curves of the numerous test case configurations, but to improve the understanding of the principles determining the curve shape.

Second, attention is drawn to the problem of non-uniqueness. This aspect of interpretation is considered by comparing the shapes of tracer-breakthrough curves of very different domains.

### 4.2.1 Influence of permeability

Figure 4.5 shows tracer-breakthrough curves of a homogeneous domain with varying permeability $k$, which are simulated using the model set-up described in Section 3.1. The central port is used and periodic boundary conditions are imposed on the boundaries parallel to the main flow direction. Due to the chosen boundary conditions with constant pressures at the in- and at the output ports, the discharge Q varies with different permeabilities $k$. The $y$-axis therefore represents the tracer-mass flux $q_M$ instead of the concentration $c$ in order to obtain comparable curves with a constant area under the curve.

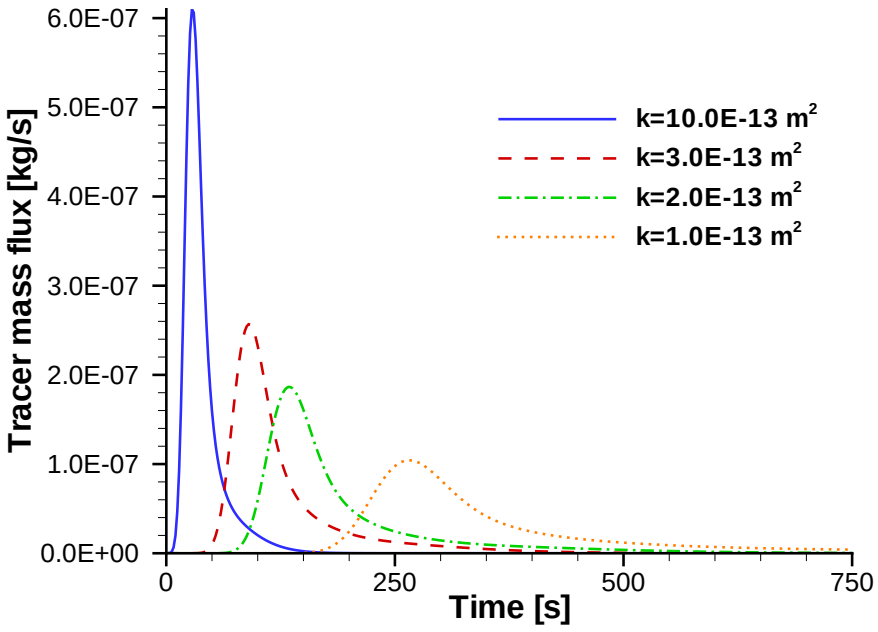


Figure 4.5: Tracer-breakthrough curves of homogeneous domains with varying permeability $k$.

Analysing selected variables that describe the characteristics of these curves, yields the following relationships with the permeability $k$ (Figure 4.6):

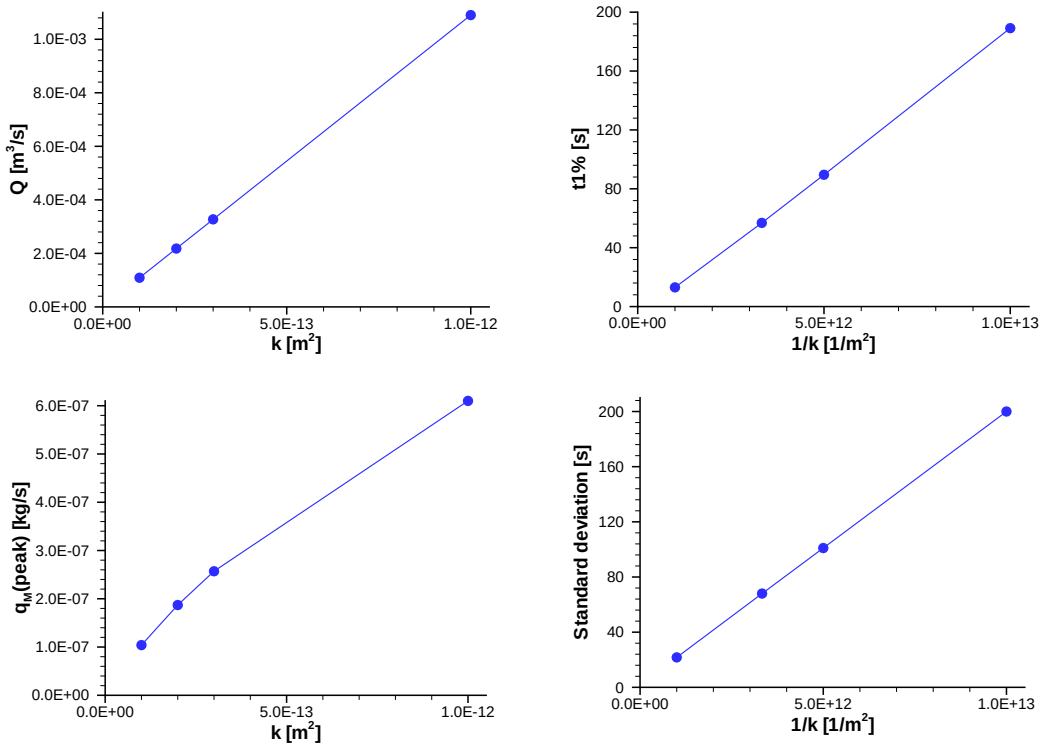


Figure 4.6: Dependence of characteristic variables of tracer-breakthrough curves in the homogeneous domain. Top, left: Discharge, $Q \propto k$. Top, right: Initial arrival time, $t_1\% \propto 1/k$. Bottom, left: Peak tracer-mass flux, $q_{M,peak} \propto 1/k$. Bottom, right: Temporal standard deviation, $\sigma_t \propto 1/k$.

- The discharge Q is observed to increase linearly with increasing permeability k. This is a logical consequence of the DARCY equation (2.9) and the fact that the pressure distribution is equal for all permeabilities k, hence the pressure gradient $\partial p/\partial x_i$ and the flown through area A is independent of the permeability k.

- The increasing discharge Q leads to decreasing travel times of the tracer. The initial arrival time, represented by $t_{1\%}$ (see page 39), is inversely proportional to the permeability k. Due to numerical dispersion, the curve in Figure 4.6 (top, right) deviates from perfect linearity. The larger the permeability k (i.e. the smaller $1/k$) the stronger the underestimation of $t_{1\%}$.

- The peak tracer-mass flux $q_{M,peak}$ increases linearly with increasing permeability k. This relationship can be derived analytically for the transport of a Dirac pulse in a one-dimensional domain. Assuming that the spreading of the curve due to the varying length of the stream lines in the two-dimensional port-port domain is described by the longitudinal dispersivity $\alpha_l$ of the one-dimensional analytical solution, this statement of proportionality is valid for the two-dimensional domain as well. The deviation from exact linearity, observed in Figure 4.6 (bottom, left), is explained by the influence of numerical dispersion on the simulated curves. This effect grows stronger with increasing

flow velocities, causing an increasing underestimation of $q_{M,peak}$ for increasing permeability $k$. Since a linear dependency is observed for the discharge, it can be concluded that the peak concentration $c_{peak}$ is independent of the permeability $k$.

- As the peak tracer-mass flux $q_{M,peak}$ decreases, the temporal standard deviation $\sigma_t$ must increase, due to the fact that the total tracer mass, i.e. the area under the curve, is constant. The temporal standard deviation $\sigma_t$ is observed to be inversely proportional to the permeability $k$. This is the logical consequence of the linear increase of $q_{M,peak}$ with increasing permeability $k$.

The observed behaviour of the simulated tracer-breakthrough curves confirms that the applied numerical model is a good approximation of the analytical solution if the influence of the numerical dispersion is taken into account.

### 4.2.2 Influence of structures

Above, the influence of the permeability on the shape of a tracer-breakthrough curve in a homogeneous domain is discussed. In the following, based on the simulated curves from the three groups of test cases, the discussion deals with the influence of structures on the curve shape.

From the test cases, a very large number of curves are available. In order to draw conclusions what kind of structures and port configurations yield what curve characteristics, the curves are classified according to their shape. It should be underlined that the shape and not the absolute values such as actual arrival time or peak amplitude is of interest. This is important in order to consider that two curves stemming from domains of different effective permeability, yielding differences in arrival time and peak amplitude, can still have the same curve shape characteristics.

It should be mentioned, that substantial effort was put in finding ways of automatically classifying the tracer-breakthrough curves. An automatic procedure would have the advantage that the classification is more objective than if the curves are visually classified. The quality of such automatic classification is strongly dependent on the variables used as input for the classification algorithm. In this case, variables would be required that describe only the curve shape and not the absolute values. The definition of such variables is only possible after normalising the curves so that all absolute characteristics are eliminated. For the purpose of this investigation, it is not expected that an automatic classification algorithm would yield a better result than a simple visual classification. Consequently, the curves are here classified visually.

The only definite criterion for a classification according to the shape is the number of concentration peaks of the curve. All other shape characteristics such as, for example, ”fast increase” or ”long tailing” cannot be clearly defined, since they are strongly dependent on the scale of visualisation. Such characteristics are therefore considered as variations within the groups of the classification according to the number of peaks.

From the total amount of simulated curves, examples are selected for the demonstration of the formation of curves with a certain number of peaks and variations hereof. The curves are shown in Figures 4.7 and 4.8.

#### Curves with one peak

Common to all curves within this group is that the concentration increase is rather rapid in comparison to the concentration decrease after the peak. The variations within this group of curves are therefore mainly concerned with the descending part of the curve after the peak. The concentration may either decrease rather quickly, or the negative gradient of the curve after the peak may be smaller. In both cases the curve is characterised by a long tailing with a very low concentration. This is due to the chosen model set-up, forcing a small part of the tracer to follow very long streamlines. In general, the peak is very distinct and narrow. There are, however, also curves with one very round and flat peak. In Figure 4.7 examples of the described variations are presented.

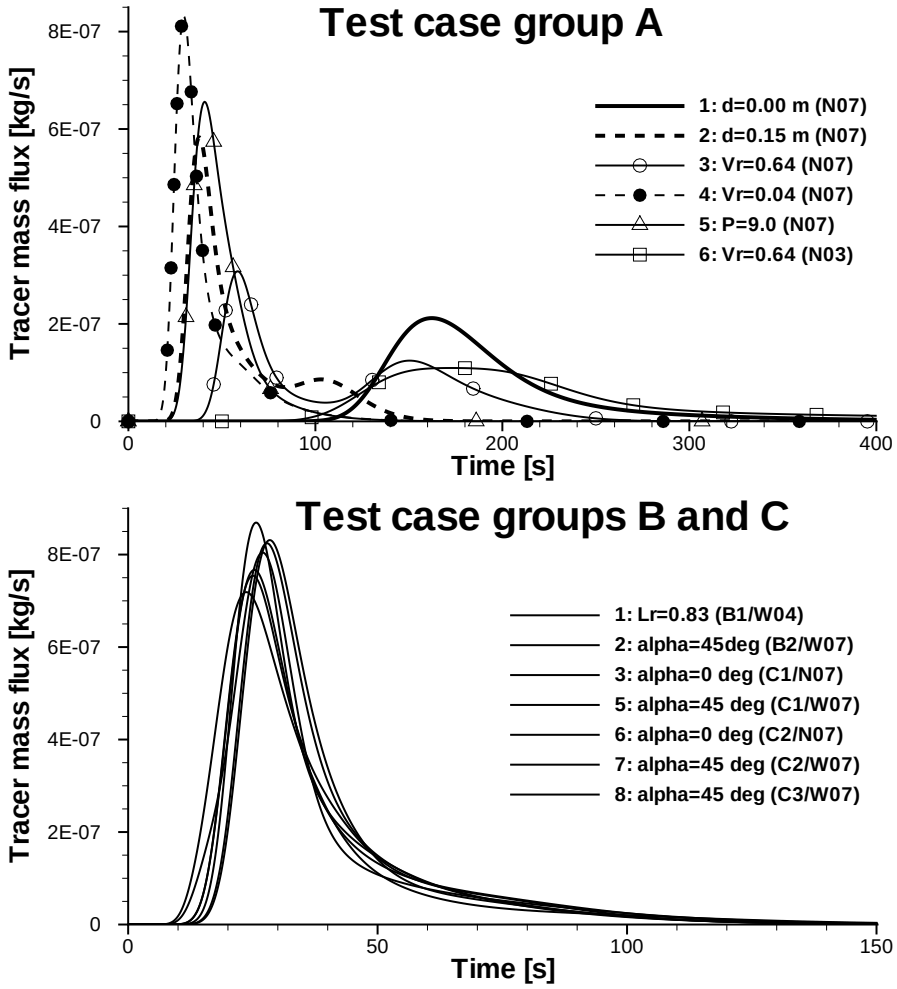


Figure 4.7: Examples of single peak tracer-breakthrough curves. For reasons of comparison, curves 2 and 4 with two peaks are included into the plot of group A. The curves of the test case groups B and C are not differentiated due to their similarity.

Considering first the cases of *group A* (block-shaped structures), curves with one peak are generally found in the following situations:

- For port configurations far away from a structure.
- For configurations where the in- or output port is directly connected to the structure ($d = 0$).
- For most port configurations where the structure is very small, especially if the structure is low permeable.
- For flow perpendicular to a thin layer.

For all these situations the occurrence of a single peak is promoted by a permeability ratio close to one.

From these observations, it can be concluded that a single peak is obtained if the tracer is transported almost exclusively along one flow path only, with weak interference from the structure. Obviously, if ports are far away from the structure, or if the structure is very small (Figure 4.7, top, curve 4), the influence of the structure is not so strong. This is especially true for structures of low permeability, since such structures do not attract the tracer, forcing a part of it to take a detour. The direct contact between an in- or output port and a structure can be considered as a restriction to the spreading of the tracer. If, for example, the structure has a lower permeability than the rest of the domain, the tracer tries to flow around the structure, avoiding resistance, if the structure is not directly connected to the input port. The difference is demonstrated by curves 1 and 2 in Figure 4.7 (top), representing situations with $d = 0$ and $d = 15\,\text{cm}$ respectively. If the main flow direction is perpendicular to a thin layer which has almost the same extent as the model domain, this layer causes only a decrease in effective permeability (Figure 4.7, top, curve 5).

The observed round flat single peak curves, demonstrated by curve 6 in Figure 4.7 (top), are formed due to another reason than the single flow path. Here, the tracer is rather equally distributed over several flow paths. These flow paths, yield slightly different peak arrival times due to varying combinations of length and seepage velocity, the concentration upon arrival is, however, very simular.

For the test cases of *group B* (a few single or intersecting fractures), single peak curves are found in the following situations:

- For port configurations far away from a fracture parallel to the main flow direction, especially if the fracture is short.
- For flow perpendicular or at a large angle to a fracture.
- In accordance with the observations of group A, the influence of a fracture generally decreases for decreasing permeability contrast between fracture and matrix.

The decreasing influence of a fracture with increasing distance is discussed for group A and does not need to be explained again. The shorter the fracture is in flow direction, the lower the connectivity effect of the fracture. A fracture which is oriented perpendicularly to the main flow direction has no influence on the flow, it may even be completely neglected. This is due to the fact that, for flow perpendicular to fractures, the effective permeability is determined as the harmonic mean of the matrix and fracture permeabilities, weighted with the length in flow direction. Due to the small aperture, the significance of a fracture

on the harmonic mean is very weak. Similarly to the behaviour of the domains of group A, a decreasing permeability contrast weakens the significance of fractures. Examples of single peak curves of test case group B are shown in Figure 4.7 (bottom). The curves are not differentiated due to the similarity of the selected curves.

Concerning the test cases of *group C* (systematically distributed fractures), the following situations yield single peak curves:

- Flow perpendicular to fractures.
- Some of the port configurations in the middle of the fracture systems, especially if the fracture orientation is at an angle to the principal flow direction and if the permeability ratio is low.

All of these observations are recognised from the previous cases. It is concluded that for systems of fractures, only in cases where the tracer is not transported through a limited number of fractures, but is distributed over a larger part of the network, single peak curves can be obtained. The tendency to increased spreading is stronger for a low permeability contrast between fractures and matrix. Examples of single peak curves of test case group C are shown in Figure 4.7 (bottom).

#### Curves with multiple peaks

From all curves of the test case configurations, about one third exhibit more than one peak. Accounting for curves with one clear peak and a tendency to a second peak, this share grows to approximately 45%. The relative magnitude of the peak amplitudes varies. In most cases the first peak is the highest. Curves with two peaks of very similar amplitude are observed as well as cases where the second peak arrives very late and is very low compared to the first one. There are also cases where the first peak is lower than the second one, however, often not as distinct as the subsequent higher peak. Some curves even exhibit three peaks or a tendency hereof. Figure 4.8 shows examples of curves with multiple peaks.

The discussion of the single peak curves shows that for all three groups of test cases, the same principles control the flow and transport behaviour. Consequently, the occurrence of curves with multiple peaks is not discussed separately for the three groups. The described variations of curves with multiple peaks are observed in the following situations (curve numbers refer to Figure 4.8):

- A strong permeability contrast increases the probability of obtaining multiple peaks, especially if the tracer is injected into a low permeable region.
- Injection close to a structure boarder often yields a second, usually lower peak. The stronger the permeability contrast is, the larger the difference between the amplitude of the peaks (curve 1 and 2).
- Injection in the vicinity of a single parallel fracture yields two peaks. The closer to the fracture, the higher is the amplitude of the first peak (curve 3 and 4).
- The longer a single parallel fracture is, the more distinct the two peaks (curve 4 and 5). The more direct the connection of two ports by a fracture is, the higher the probability of obtaining a second peak.

- For a large number of short parallel or inclined fractures, at the most a tendency towards a second peak is obtained (curve 6 and 7).
- A system of inclined long fractures yields curves with two peaks only if the injection port is close to a fracture.
- A second cluster of perpendicular fractures, intersecting the first parallel one, has only a weak influence on the curve shape for low permeability contrasts (compare curve 10 and 11). For a stronger contrast, the peak amplitudes are slightly modified (compare curve 8 and 9).

The observed behaviours always follow the same principles, i.e. if there are two or more distinct flow paths multiple peaks are formed. The variations are due to (1) differences in the distribution of the tracer mass between these flow paths and (2) differences in their average seepage velocity. From the observations made it is clear that such distinct flow paths can only form if the permeability contrast in the region of the injection is sufficient. The extention of this region grows with increasing permeability ratio, however, only if the tracer is injected into a lower permeable region. Tracer which is injected directly into a high permeable region is likely to form a single peak only, because the tracer tends to follow the path of least resistance. These, very few, principles are sufficient for the explanation of the behaviours listed above.

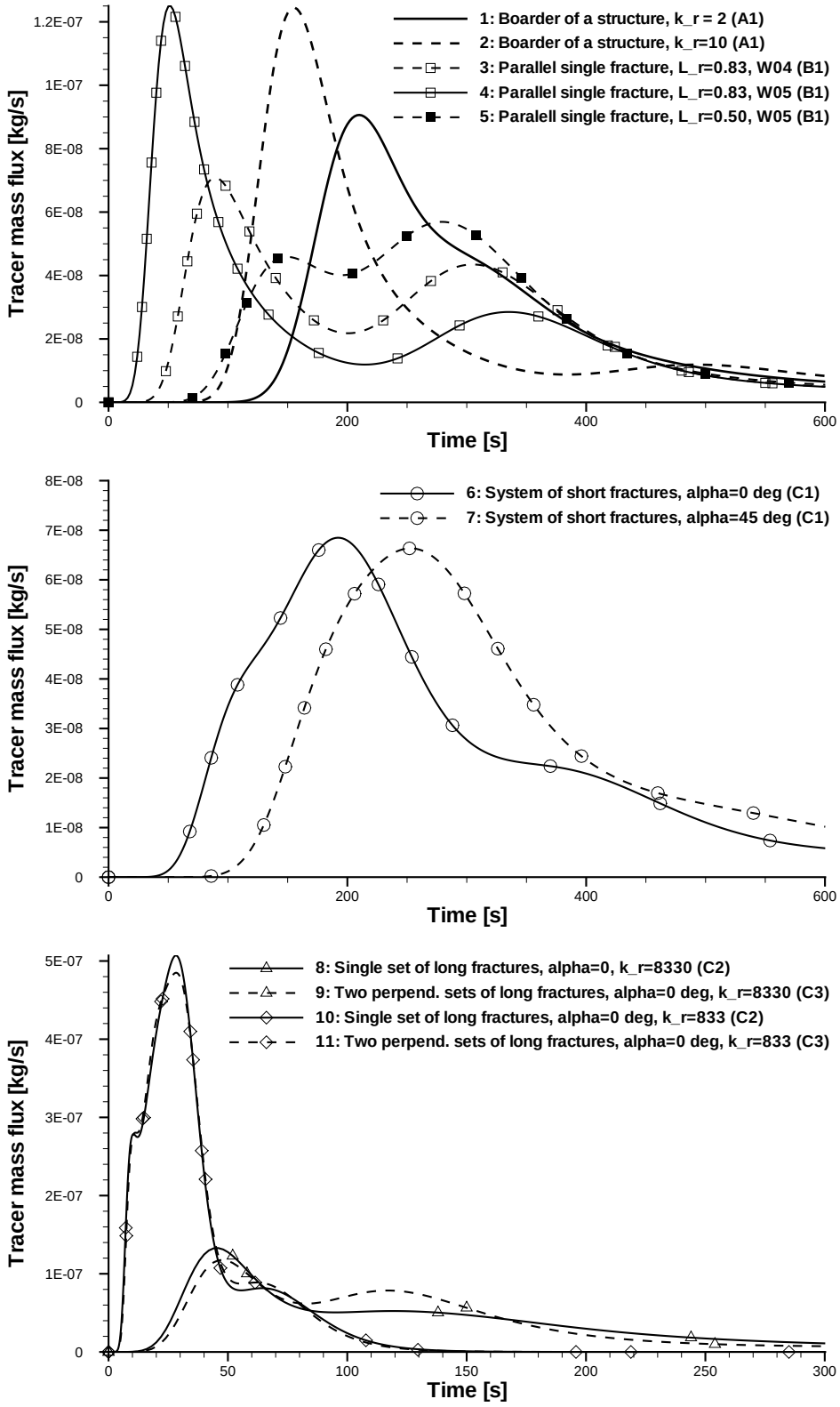


Figure 4.8: Examples of tracer-breakthrough curves with multiple peaks (or tendency hereof).

### 4.2.3 Conclusions

From the presented observations and discussions, the principles of the formation of certain shapes of tracer-breakthrough curves are clear. The main conclusion that must be drawn, is that there are a very large number of combinations of structure geometries and properties that yield a very similar result. In the above discussion, exclusively the shape characteristics are considered, excluding absolute characteristics, such as actual arrival times and peak magnitudes. This approach corresponds to a situation where only one curve is interpreted. The above discussion shows that it is an unsolvable task to reveal a structure or a system of structures based on one curve only. Including other type of information such as observations from exposed walls, general geological knowledge about an area or geophysical measurement results may decrease the uncertainty of a tracer-breakthrough curve interpretation. In most cases, however, a sufficient probability of obtaining a correct result is not obtained. This shows that the ideal procedure, schematically shown in Figure 4.1, is not likely to lead to useful results.

One way of decreasing the degrees of freedom of the problem is to conduct several tracer-breakthrough measurements at different locations, as done in the ”Aquifer Analogue” research project (Section 1.2). In the following sections of this chapter, the possibilities and limitations of identification of certain structures and their properties using multiple distributed port configurations is investigated.

## 4.3 Structure localisation

Determining the characteristics of a domain involves the determination of both the geometry of structures as well as the properties of structures and background material. This chapter deals with the possibilities and limitations of the former task using multiple measured tracer-breakthrough curves from different port configurations. From the previous sections it is clear that the shape of tracer-breakthrough curve can be explained if the structure geometry and the material properties of the structure and the background material are known. Preliminary investigations have shown that it is not necessary to consider the complete curve in order to localise structures, but that the initial arrival of the tracer is a strong indicator. The use of the initial arrival time has the advantage that only the initial part of a curve must be measured or simulated. Two assumptions are made: (1) a tracer-breakthrough curve represents the local region between the in- and the output port and only to a limited extent the rest of the domain and, (2) the part of the tracer that arrives first is the least disturbed by the rest of the domain. These assumptions are of course simplifications of the actual transport behaviour that must be taken into account during interpretation. Since the actual initial arrival time cannot be objectively determined, the arrival time of one percent of the tracer mass $t_{1\%}$ is used instead. The use of $t_{1\%}$ yields slightly delayed arrivals, especially for curves with a high temporal standard deviation, which must be kept in mind when evaluating the data.

The three groups of test cases (A – C) are used for the investigation of the possibilities and limitations of the approach for different types of systems. First, observations from the plots of the initial arrival time are described (Section 4.3.1) and, second, the feasibility of such plots for the localisation of structures is discussed (Section 4.3.2).

### 4.3.1 Description of the $t_{1\%}$-plots

As mentioned above, here the variation of $t_{1\%}$ for different configurations is described and reasons for the observed behaviour are given. For a better understanding of the discussion, it is useful to recall the geometries of the various test cases from Figures 4.2 – 4.4.

#### Group A: Block-shaped structures

In Figure 4.9, plots of $t_{1\%}$ of a selection of representative configurations are shown. The x-axis ranges from port N01 to N07 only, since the permeability distributions are symmetrical. For each configuration, the left boundary of the structure is indicated by a vertical bar.

For all curves, there is a more or less abrupt increase in initial arrival time just before the change from high to low permeability. Within the range of the low permeable structure a constant arrival time is reached only after a slow increase. This means that the tracer-breakthrough curves of ports within the range of a low permeable structure are stronger influenced by a high permeability outside of the structure, than the other way around. For the different configurations, the significance of the abrupt increase varies.

For *test case A1* (Figure 4.9(a) and 4.9(b)), comparing the curves of the distances $d = 0.00\,m$ and $d = 0.15\,m$, it is concluded that the abrupt change is clearer for the distance $d = 0.00$.

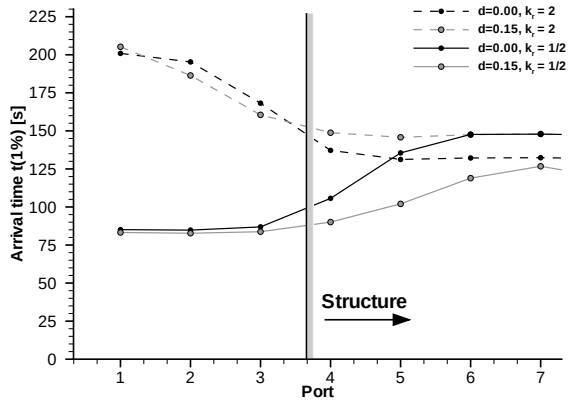


(a) Distance to boundary, $k_1/k_2 = 2$ or $1/2$

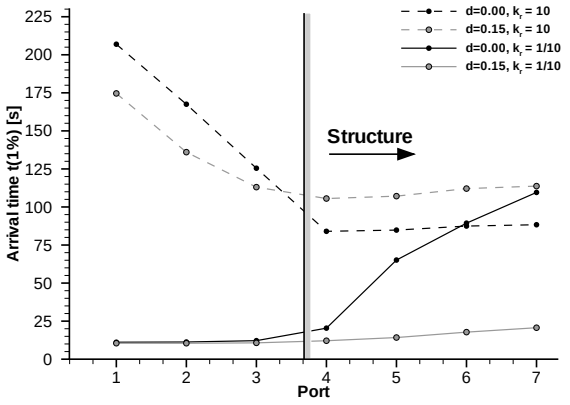


(b) Distance to boundary, $k_1/k_2 = 10$ or $1/10$

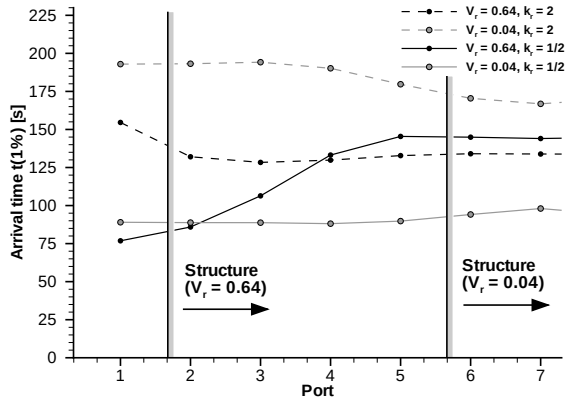


(c) Relative volume, $k_1/k_2 = 2$ or $1/2$

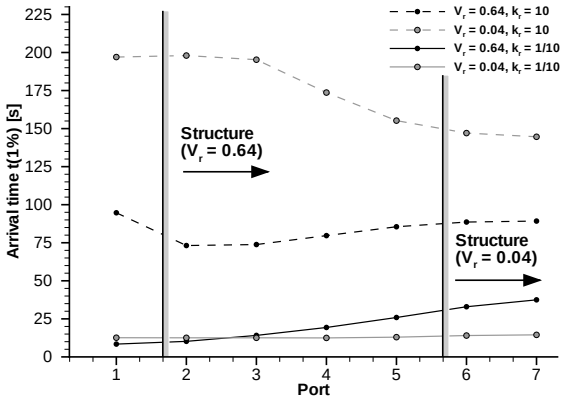


(d) Relative volume, $k_1/k_2 = 10$ or $1/10$

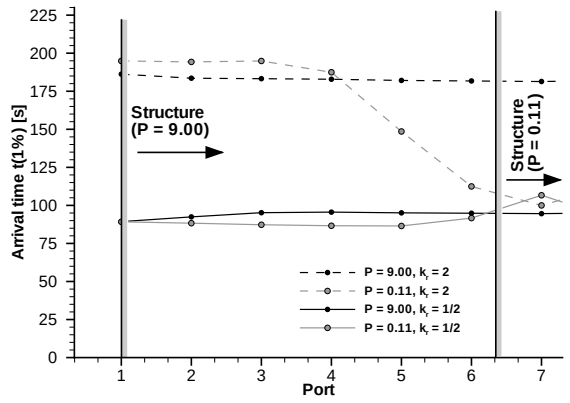


(e) Shape ratio, $k_1/k_2 = 2$ or $1/2$

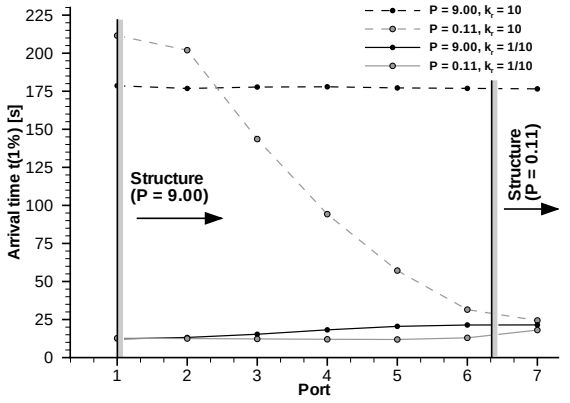


(f) Shape ratio, $k_1/k_2 = 10$ or $1/10$

Figure 4.9: Plots of the initial arrival time (represented by $t_{1\%}$) over the input ports for the selected configurations of the test cases of group A. The bars indicate the left boundaries of the structures. $k_1$ is always the permeability of the structure.

This effect is the strongest for a high permeability contrast. The reason for this behaviour is that the tracer is forced to flow through the structure if it is located directly at the port. If not, and if for example the structure has a low permeability, the tracer can avoid the structure by flowing around it, causing less difference in arrival time for ports within and outside of the width of the structure.

The comparison of the different relative volumes $V_r = 0.64$ and $0.04$ from *test case A2* (Figures 4.9(c) and 4.9(d)), clearly shows that structures of very small relative volumes are better detected if it has a permeability that is higher than the surrounding area, especially for a large permeability contrast. Small structures of low permeability are very easily flown around, and the interference with the flow field is weak. It is also observed that, for large permeability contrasts, even large structures of low permeability are strongly influenced by the surrounding permeability.

From the Figures 4.9(e) and 4.9(f), *test case A3*, it is concluded that a very thin and long ($P = 0.11$) structure causes a change in arrival time both for structures of higher and lower permeability as well as for weak and strong permeability contrast. For wide and short ($P = 9.00$) structures, there is only a very slight bend of the curve.

#### Group B: Single fractures

Figure 4.10 presents the variation of $t_{1\%}$ over non-symmetrical west-east port configurations. In the two most upper figures, the dashed line indicates the position of the fracture. In all plots, the curves are labelled with the value of the considered variable ($L_r$ or $\alpha$). In order to see the influence of the fracture(s) clearly for both permeability contrasts, different time scales are used. Concepts such as early arrival or steep gradient always refer to the individual scale of the plots.

Figures 4.10(a) and 4.10(b) of *test case B1* show the influence of a fracture of varying relative length $L_r$. For the central port configuration (W07-E07), at the same level as the fracture, the initial tracer arrival always occurs very early. The longer the fracture, the earlier the arrival. For a high permeability contrast, the arrival time increases first slowly and later more rapidly with increasing distance between in- and output port and the fracture. For the lower permeability contrast, the gradient of the arrival time curve is steeper than for the higher contrast, and a constant time is reached closer to the fracture. This indicates a stronger influence of the fracture for a higher permeability contrast.

For *test case B2* (Figure 4.10(c) and 4.10(d)), all 13 west-east configurations are considered since the domain contains an inclined fracture which means that e.g. the ports W01 and W13 are not symmetrical with respect to the location of the fracture. It is, however, interesting to see that the $t_{1\%}$-plots are symmetrical. This means, that it does not make a difference if the in- or the output port is closer to the fracture, i.e. simulation from west to east yields the same result as in the opposite direction. For both permeability contrasts, a decreasing influence of the fracture for an increasing angle to the main flow direction is observed. The decrease in arrival time for the outer ports for angles of $\alpha = 30^o$, $45^o$, and $60^o$ is due to the fact, that either the in- or output port is relatively close to the fracture for these angles. For example, the tracer that crosses the northern boundary, simultaneously enters the domain across the south boundary (periodic boundary conditions) and reaches the output port quickly via the inclined fracture. This behaviour is less distinct for a lower permeability contrast, where the direct flow path between the two ports is faster than the detour across the boundary and along the fracture due to the higher matrix permeability. In principle, the influence of increasing inclination angle is similar to the effect of decreasing relative length.

*Test case B3* (Figure 4.10(e) and 4.10(f)) shows the combined effect of test case B1 ($L_r = 0.5$) and B2. Especially for the port configuration W07–E07, the initial tracer arrival seems to be dominated by the parallel fracture, since nearly no variation is observed for different intersection angles. The initial arrival of this port configuration occurs earlier than both for test case B1 ($L_r = 0.5$) and the earliest arrival of B2 ($\alpha = 15^o$). Considering the port configurations further away from the centre, the variations for different intersection angles are very small as well. The observed insensitivity to variation of the intersection angle is even more significant for the smaller permeability contrast.

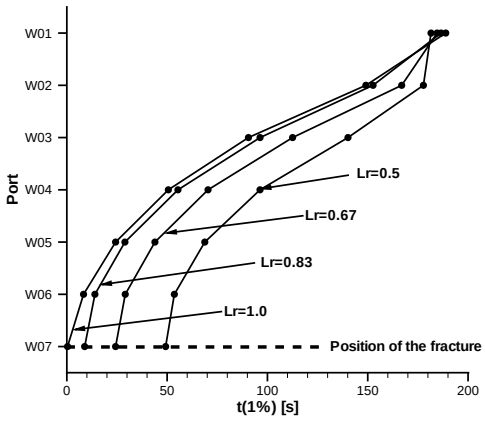


(a) Relative length, $k_F/k_M = 8330$

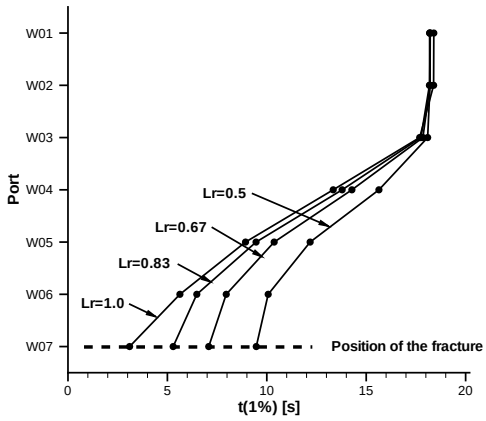


(b) Relative length, $k_F/k_M = 833$

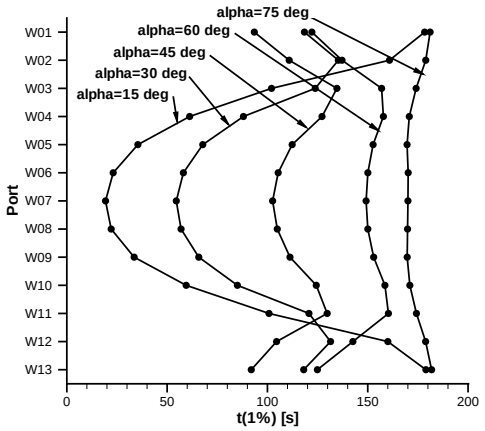


(c) Inclination angle, $k_F/k_M = 8330$

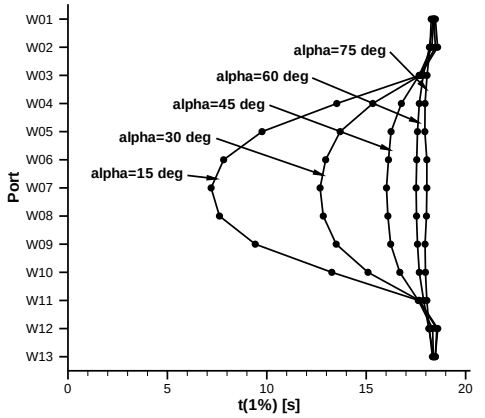


(d) Inclination angle, $k_F/k_M = 833$

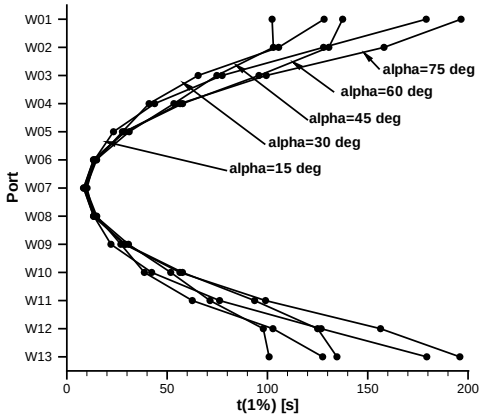


(e) Intersection angle, $k_F/k_M = 8330$

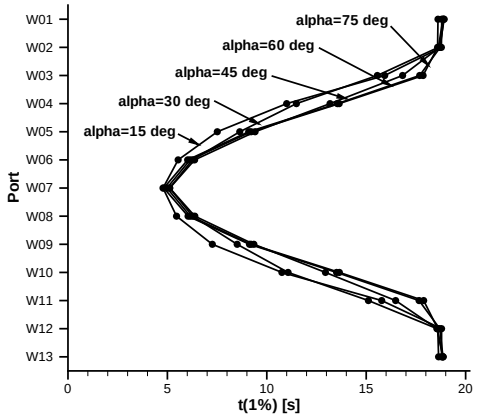


(f) Intersection angle, $k_F/k_M = 833$

Figure 4.10: Plots of the initial arrival time represented by $t_{1\%}$ over the input ports for the selected configurations of the test cases of group B. Note that the scales of the left and the right plots are different.

#### Group C: Systematically distributed fractures

Figure 4.11 presents the variation of $t_{1\%}$ over non-symmetrical west-east port configurations. The fracture systems are indicated at their actual position relative to the ports. Dashed lines in a plot always represent the inclined system of fractures. In order to see the influence of the fractures clearly for both permeability contrasts, different time scales are used. Concepts such as early arrival or steep gradient always refer to the individual scale of the plots.

First, considering *test case C1* (Figures 4.11(a) and 4.11(b)), the two curves for the parallel and the inclined systems are observed to be rather similar. For $\alpha = 0^o$ the fastest arrival occurs at the port configuration with the longest total fracture length between the ports (W06–E08). This corresponds to the observations for test case B1. For the inclined system with $\alpha = 45^o$ the earliest arrival occurs both at port configuration W05–E09 and W06–E08. This behaviour is the same as observed in test case B2, i.e. it is irrelevant if the in- or the output port has a certain distance to a fracture. The result is a smoother shape of the curve than for the parallel fracture system. The chosen scale of the left and the right figure differs by a factor of 10 in correspondence with the variation of the permeability ratio ($k_F/k_M$), allowing a comparison of the two figures. It is observed that, despite the difference in permeability contrast, the shape of the curves is very simular, only a somewhat stronger fracture influence is recorded for the stronger contrast.

In principle, the behaviour of *test case C2* (Figures 4.11(c) and 4.11(d)) corresponds to the previous observations. The minimum time is obtained for port configurations close to a fracture and the course of the curve of the inclined system is smoother than for the parallel one.

Finally, *test case C3* (Figures 4.11(e) and 4.11(f)) shows the variation of the initial arrival time for systems with two perpendicular sets of fractures. It is very interesting to see that for a strong permeability contrast, the curves of the parallel ($\alpha = 0^o$) and of the inclined ($\alpha = 45^o$) systems are very similar. Comparing the curve of the parallel system of this test case with the corresponding curve of test case C2, it is observed that fractures perpendicular to the main flow direction have no significant effect on the initial arrival of the tracer. The influence of the fractures of the inclined system decreases significantly as the permeability contrast decreases.

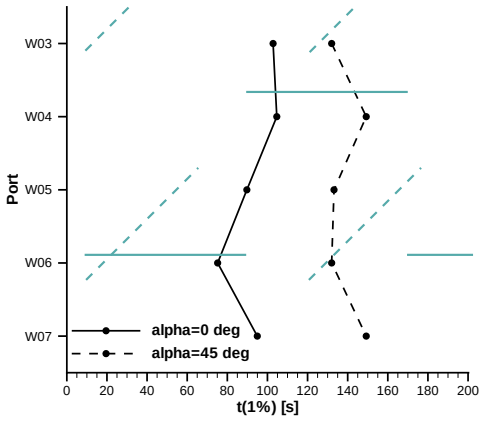


(a) Short fractures, $k_F/k_M = 8330$

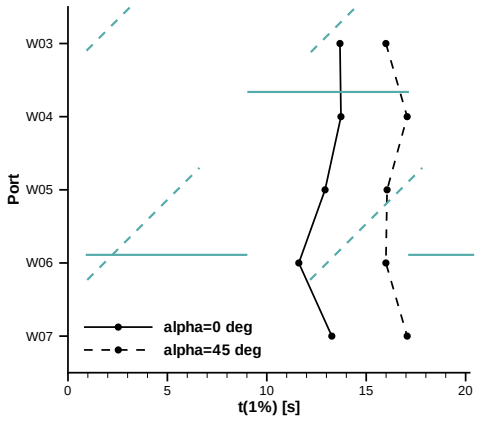


(b) Short fractures, $k_F/k_M = 833$

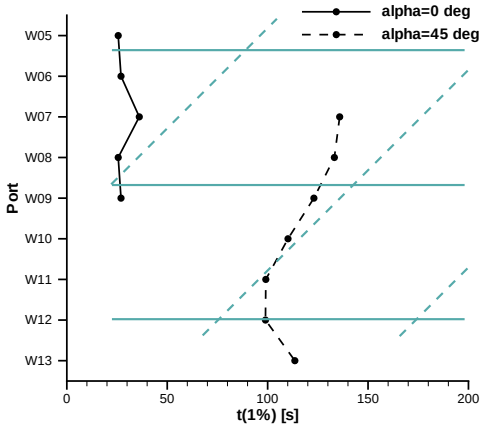


(c) Long fractures, $k_F/k_M = 8330$

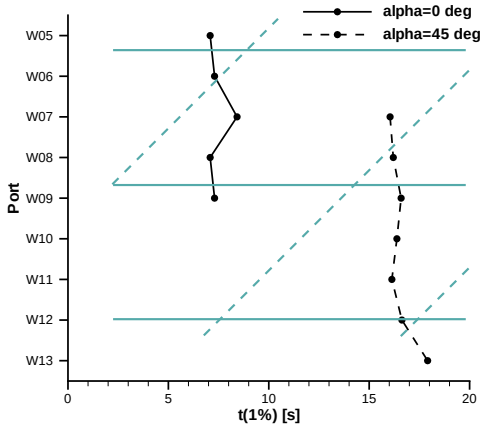


(d) Long fractures, $k_F/k_M = 833$

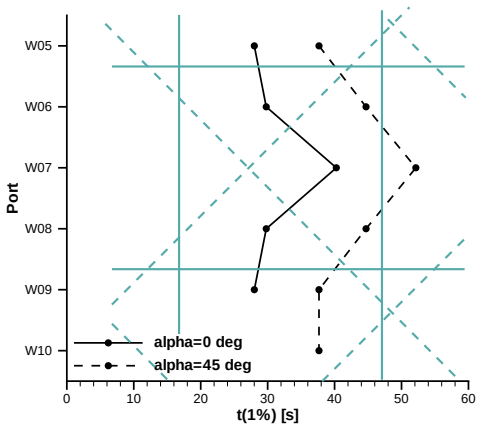


(e) Two sets of fractures, $k_F/k_M = 8330$

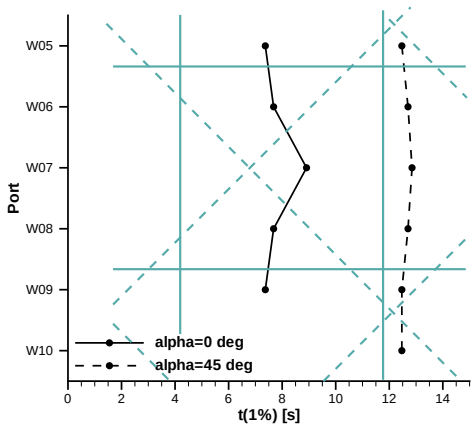


(f) Two sets of fractures, $k_F/k_M = 833$

Figure 4.11: Plots of the initial arrival time represented by $t_{1\%}$ over the input ports for the selected configurations of the test cases of group C. Note the different scales of the left and the right plots and of the two most lower plots compared to the upper ones.

### 4.3.2 Possibilities and limitations of structure localisation

The previous discussion shows that it is relatively easy to understand why different behaviours are observed for certain *known* structure geometries and locations. However, in order to use the $t_{1\%}$-plots for the localisation of *unknown* structures, it must be considered that

- only one plot is available. No other plots, except for simulated ones, with known structures that can be used for a comparative interpretation are available.
- more than one structure system may yield the same result, i.e. the $t_{1\%}$-plots are not unique.

In the following, the $t_{1\%}$-plots of the three groups of test cases (A – C) are discussed regarding their feasibility for localisation of unknown structures.

The plots of block-shaped systems (group A) differ from the plots of fractured systems through the occurrence of a plateau, i.e. a range of constant $t_{1\%}$, which is not found within group B and C. However, if the shape of a high permeable block is very narrow and long in flow direction (P=0.11), the similarity of the plot with the one of a single fracture is very strong. These two situations cannot be differentiated. However, apart from this extreme case a block-shaped structure can be differentiated from a single fracture or a system of fractures. A $t_{1\%}$-plot of a system of structures is separable from a system with one single structure by the repeating character of the curve.

Common to all three groups of test cases is the fact that a thin structure is not identifiable if the main flow direction is perpendicular to the structure. Neither a layer nor a fracture can be identified in case of perpendicular flow. This means that is is essential to conduct measurements in at least two directions. If a certain orientation can be expected, based on other information, it is a good approach to choose one of the measurement axes to be parallel to the main structure orientation.

Considering the plots of domains of group A with *block-shaped structures* (Figure 4.9), the boundary of a structure is indicated by a sudden increase in $t_{1\%}$ just before the boundary when moving from a high to a lower permeable region. Except for extremely small or narrow structures (parallel to the main flow direction) with a permeability that is lower than the background permeability, the identifiability of the structure boarder using $t_{1\%}$ is very good. However, the stronger the permeability contrast is, the stronger the influence of the high permeable region on the low permeable one. This means that the point of $t_{1\%}$-increase is shifted closer to the permeability boundary or even into the lower permeable region. In order to detect the two- or three-dimensional shape of this type of fractures the number of port configuration directions must correspond to the number of dimensions.

Comparing the plots of group B containing *a few single fractures* (Figure 4.10), it is concluded that it is not possible to determine the length of a fracture using the initial arrival time (case B1). A direct connection between in- and output port yields a very short arrival of the tracer, however, the term short is relative and not useful if only one curve is available. The question if a fracture is inclined or not (case B2) can be answered by using one port configuration direction parallel to the assumed fracture orientation and one direction perpendicular hereof. The degree of inclination, however, can only be determined if several directions are considered and in this way a minimum arrival time for a certain angle is

found. Two intersected fractures (case B3) require the same port configuration directions for their identification as for one single fracture. These two directions yield a plot with a very short minimum initial arrival time in the direction of the parallel fracture and a longer minimum time in the other direction. Similar to one inclined fracture, the angle of intersection can only be determined if the direction of the port configurations is stepwise rotated. In this case one local minimum arrival time is found for each fracture direction. For the investigated permeability contrasts, no significant difference in identifiability is observed.

Concerning *systematically distributed fracture systems* as represented by the domains of group C (Figure 4.11), it is not possible to distinguish a system of short fractures (case C1) from a system of long fractures (case C2) for the same reasons as for case B1. In analogy with case B2, the question if a system is inclined or not and what the degree of inclination is can only be answered if several port configuration directions are considered. For two perpendicular sets of fractures (case C3), systems with the inclination angle $\alpha = 0^o$ and $\alpha = 45^o$ cannot be distinguished, even if two perpendicular measurement directions are used. A stepwise rotation is required where the lowest local minima represent the directions of the fractures. The use of two perpendicular directions, one in the direction of one set of fractures, allows systems with one or two sets of fractures to be differentiated.

### 4.3.3 Conclusions

From the above observations it can be concluded that in many cases, it is a useful approach to determine structure geometry and location based on plots of the initial arrival time. It is, however, important to realise that in certain situations the approach fails, due to non-uniqueness or other reasons mentioned above.

Crucial to the quality of the identification is the density of port configurations and the number of measuring directions used for the localisation. The higher the density and the number of directions, the more accurate the determination of structure geometries. In real cases the number of measurements is often limited due to practical and financial reasons. The experience from the presented test cases can be used to support the planning and design of the experimental set-up to be used for the tracer measurements.

Certain situations of non-uniqueness are mentioned above, e.g. a single fracture and a thin high permeable layer. On the one hand, these two structures cannot be clearly differentiated from each other. On the other hand, it can be argued that if the behaviour, caused by two different types of structures, is similar, it might not be necessary to know exactly what kind of structure caused it. The requirements that a structure identification must meet, may vary depending on the problem. The proposed approach should be considered as one important component amongst many possible information sources. By combining different knowledge of a domain, certain geometries and locations might be excluded apriori and others might be very plausible.

It is suggested that in addition to using the initial tracer arrival for localisation, the shape of the complete curve should be analysed in order to verify the conclusions drawn from the behaviour of the initial tracer arrival.

## 4.4 Approximation of permeabilities

Apart from determining the location of the structure, a crucial task is the approximation of the flow and transport properties of the material within the domain. Since this investigation is focused on advective transport, the property of interest is the permeability.

The defined test cases contain either domains with two different matrix permeabilities or domains with one matrix and one fracture permeability. The available data from each simulated measurement consist of (1) the discharge and (2) the tracer-breakthrough curve. Hence, an approach is required that can approximate the permeabilities within these types of domains with the help of the mentioned available data.

It should be underlined that the aim is to *approximate* the permeabilities and not to exactly determine them. Due to the integral character of the available information, an exact determination cannot be expected.

### 4.4.1 Approach

From the simulated measurements the discharge as well as the tracer-breakthrough curve for each of the port configurations are known. Using the discharge for the determination of the permeabilities is excluded due to the following reasons:

- In addition to the discharge a specific cross-sectional area and the associated pressure gradient at that cross-section is required. This information is not possible to obtain from a real port-port measurement.
- The integral character of the discharge is very strong.

As a consequence, it is decided to utilise the information that is contained in the tracer-breakthrough curve. The approximation is based on the initial arrival time of the tracer (represented by $t_{1\%}$), which is assumed to be primarily dependent on the local permeability between two ports and only secondarily by the global permeability distribution. It is assumed that this mass fraction travels along the shortest flow path from the injection port to the output port. For homogeneous conditions, neglecting dispersive and diffusive processes, this is a valid approach since the first tracer to arrive must have travelled along the shortest distance between the ports. For heterogeneous domains, this is a strong simplification. If, for example, a low permeable structure is located between the two ports, as illustrated in Figure 4.12, the tracer may travel faster around the structure than through it as indicated by the dashed ($D'$) and the solid ($D$) line, respectively. The flow between two ports is always, to a varying degree, the result of the permeability in the total domain, and not only of the permeability between the ports. This is reflected by the fact that a disproportional fraction of the flow will pass through high permeable regions, which if the cross-section is narrow, will lead to increased velocities. Moreover, it is assumed that the dispersive and diffusive influence on the tracer pulse may be neglected. These assumptions are simplifications of the actual process. By applying the approach to the test cases it is investigated if a satisfactory approximation can be obtained.

Below, the equations used for the approximation are shown considering domains of the type contained in test case group A (block-shaped structures). In theory, the same approach

may be applied to the other two groups of test cases. The feasibility of the approach to the various test cases is tested in Sections 4.4.2 and 4.4.3.

In Figure 4.12, the notations of the distances and permeabilities of the equations below are explained.

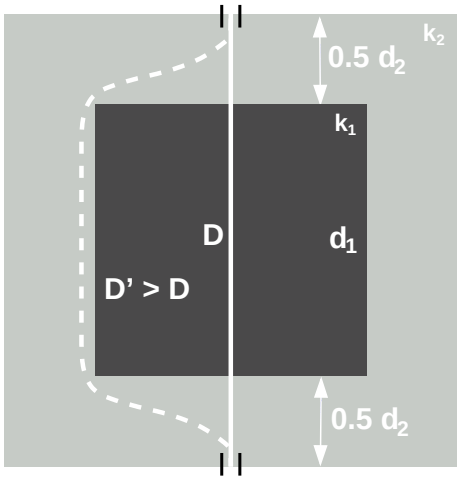


Figure 4.12: Notations for the approximation of the domain permeabilities.

From the equations

$$D = \nu t_{1\%} \tag{4.3}$$

and

$$\nu = \frac{k_e}{n_e \mu} \frac{\Delta p}{D} \tag{4.4}$$

the following equation for the effective permeability $k_e$ between two ports is obtained:

$$k_e = \frac{D^2 n_e \mu}{\Delta p t_{1\%}} \,. \tag{4.5}$$

Here, D is the direct distance between the two ports, i.e. for the three groups of test cases $D = 0.6\,\mathrm{m}$. If the direct distance between two ports passes through an area of one single permeability, this area is assumed to have the same permeability as the effective one. For the case when the direct port connection passes areas with different properties, the effective permeability is assumed to be the harmonic mean of the individual ones:

$$\frac{D}{k_e} = \sum_{i=1}^{n} \frac{d_i}{k_i} \tag{4.6}$$

Here, $d_i$ is the length of the corresponding permeability areas in flow direction.

### 4.4.2 Application to domains containing block-shaped structures

Below, the feasibility of the approach is discussed for each of the test cases A1 - A3 for different permeability ratios. The discussion is based on the graphs presented in the Figures 4.13 – 4.15. In each of the graphs, three curves are shown:

- The dotted line represents the background permeability $k_2$ outside of the structure. It is determined according to (4.5), using $t_{1\%}$ from the port configuration N01-S13, which is located the furthest away from the structure.
- The solid line represents the permeability $k_1$ of the structure, determined according to (4.6). Hereby, $k_2$ as determined in (4.5) (dotted line) is used.
- The dashed line also represents the permeability $k_1$ of the structure, however, determined using the true value of $k_2$.

In all graphs, the calculated value of the permeability is normalised by dividing with the true value, hence, an accurate approximation is found close to 1.0. If the ratio is larger, the permeability is overestimated and vice versa. The graphs are the result of the simulations with the combinations of permeabilities as presented in Table 4.1 on page 63. The references a – d according to Table 4.1 are used in the discussion below, hence, in test case A1a the block structure (A) has a certain distance to the boundary (1) and is half as permeable as the surrounding area (a).

Prior to applying the approach to the test cases, the quality of the approximation for homogeneous domains of varying permeability is assessed. An accuracy of 90–95% of the actual permeability is obtained. An underestimation of this size for the test case domains is therefore not considered as significant.

#### Test case A1: Distance to boundary

In test case A1, the relative volume and the shape of the structure is fixed, whereas the distance to the input port varies. The discussion below is based on Figure 4.13.

**Background permeability $k_2$**
All four graphs indicate that the value of the determined $k_2$ can be considered to be independent of the distance $d$. For all configurations, the approach yields a very good approximation of $k_2$ with deviations in the range of approximately $0.82 < k_{approx} < 1.11$.

The overestimation occurs for the cases A1a and A1c, where the structure is low-permeable compared to the background material. This causes channelling of the flow to the areas outside of the structure and consequently increased velocities, leading to decreased arrival times and finally overestimated permeabilities. The underestimation is obtained for the test cases A1b and A1d with a high permeable structure. It is the result of the fact that the tracer is attracted to the higher permeable structure, causing the actually followed flow path to be longer than the direct distance $D$ and therefore the initial arrival is delayed. For the stronger permeability contrast (A1d) the underestimation is less significant as the high permeability of the structure increases the discharge, i.e. the velocities, in the total domain. The significance of the underestimation decreases as the distance of the structure from the boundary increases.

**Structure permeability $k_1$**
The result of the determination of $k_1$ proves to be less accurate and relatively sensitive to variations in $t_{1\%}$ and to the value of the previously determined $k_2$. In contrast to $k_2$, it is dependent on the distance $d$ from the boundary. When discussing the determination of $k_1$,

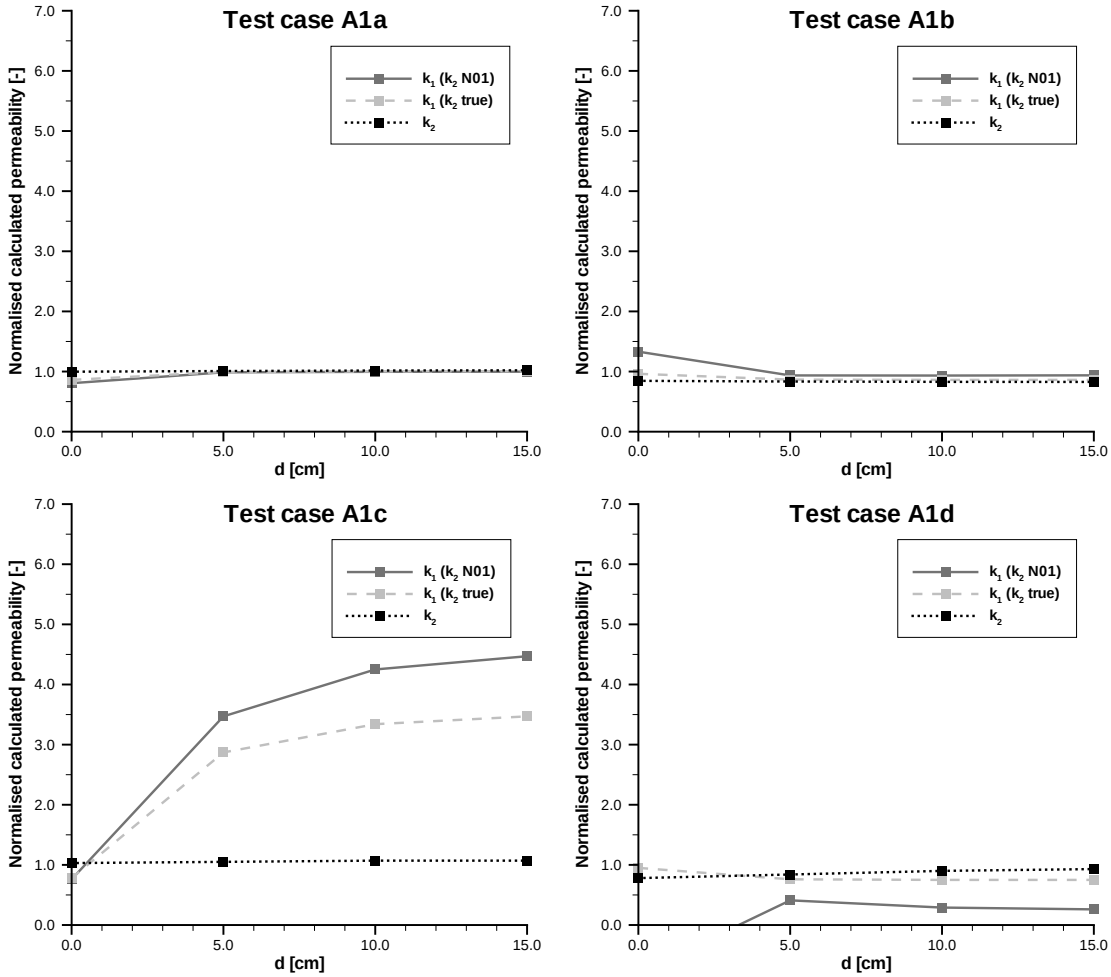


Figure 4.13: Derived permeabilities for test case A1 (distance to boundary d). Top, left: A1a, $k_1/k_2 = 1/2$. Top, right: A1b, $k_1/k_2 = 2$. Bottom, left: A1c, $k_1/k_2 = 1/10$. Bottom, right: A1d, $k_1/k_2 = 10$.

it is interesting to compare the result based on the true value of $k_2$ (dashed line) with the result based on the approximated value of $k_2$ (solid line), derived from $t_{1\%}$ from the port configuration N01-S13. In this way, the reason for a deviation from the true $k_1$ is better understood. The following observations are made:

- For small permeability ratios (A1a and A1b), the determination of $k_1$ is very good except for $d = 0\,m$. In test case A1a there is an underestimation of $\approx 15\%$ for $d = 0\,m$. This is mainly considered to result from the use of $t_{1\%}$ instead of the true initial arrival time, causing an underestimation of the permeability. As the distance to the boundary increases, the flow is no longer forced to totally pass through the low permeable structure. Therefore the underestimation of the permeability is compensated by an increased discharge, i.e. higher average domain velocity. In test case A1b, for $d = 0\,m$, $k_1$ is overestimated by $\approx 30\%$. Comparing this result with the one calculated using the true value of $k_2$ clearly shows, that the reason for this deviation is the sensitivity to $k_2$

(see also test case A1d, $d = 0\,m$).

- For large permeability ratios, there are generally large deviations. In test case A1c, there is a slight underestimation for $d = 0\,m$ due to the reason discussed for test case A1a. As $d$ increases, the value of $k_1$ is increasingly overestimated due to the fact that the tracer follows the much faster flow path around the structure yielding shorter travel times. Considering the examples shown here, this means that if a ratio of $k_1/k_2 = 1/2$ is determined, the result can be assumed to be accurate, whereas for larger determined ratios the calculated permeability of the structure must be reduced. In test case A1d, for $d < 0.05\,m$, the approach yields negative values. Again the deviation of $k_2$ from its true values causes this behaviour. Obtaining a negative value for this configuration is on the one hand a failure of the approach. On the other hand, it can be seen as an indication of large permeability contrasts. For $d > 0.05\,m$, there is a relatively strong underestimation of about $60-75\%$, likewise due to the inaccuracy of $k_2$. This must be considered by increasing the value of $k_1$ if a strong permeability contrast is obtained.

#### Test case A2: Relative volume

In test case A2, the relative volume $V_r$ is varied for a centred structure with a fixed shape ratio ($P = w/h = 1.0$). The discussion below is based on Figure 4.14.

**Background permeability $k_2$**
The approximation of $k_2$ is generally better for small relative volumes than for large ones, due to less influence from the structure. The slight underestimation of $k_2$, obtained for small relative volumes, is due to that fact that $t_{1\%}$ overestimates the true initial arrival time, just as in test case A1a and A1c.

For larger relative volumes, there is always a certain degree of overestimation. For test case A2b and A2d, this is the logical consequence of the increasing influence of the high permeable structure. For test cases A2a and A2c, the overestimation of $k_2$ is explained by the disproportional part of the discharge travelling outside of the heterogeneity, where the resistance is lower, leading to higher velocities in this region.

**Structure permeability $k_1$**
Similar to test case A1, the value of $k_1$ is relatively sensitive to deviations of $k_2$ from the true value, which leads to large deviations especially for strong permeability contrasts.

- For a low permeability contrast (test case A2a–b), the maximum overestimation is 50% for small relative volumes for both configurations. This overestimation is due to the slight underestimation of $k_2$. For larger relative volumes, the approximation result improves. However, for case A2b $k_1$ is underestimated by a maximum of approximately 25%, which is explained by the influence of the lower surrounding permeability $k_2$ and the fact that $t_{1\%}$ overestimates the initial arrival time.

- For a stronger permeability contrast, the deviations are more conspicuous as clearly shown for the test cases A2c–d. In both cases, small relative volumes yield strong deviations, in test case A2d even negative values are obtained. The result is improved if the correct value of $k_2$ is used, however, still eminent inaccuracies are obtained due to

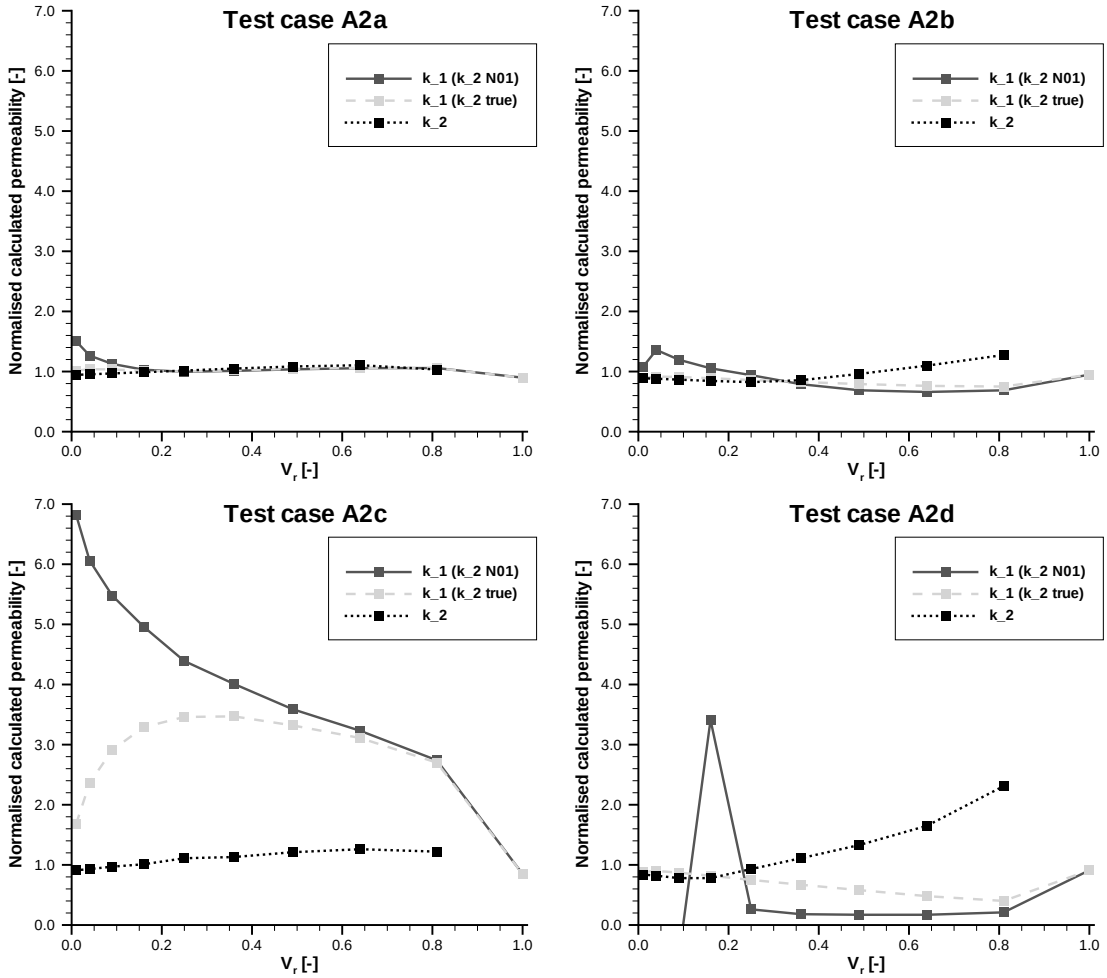


Figure 4.14: Derived permeabilities for test case A2 (relative volume $V_r$). Top, left: A2a, $k_1/k_2 = 1/2$. Top, right: A2b, $k_1/k_2 = 2$. Bottom, left: A2c, $k_1/k_2 = 1/10$. Bottom, right: A2d, $k_1/k_2 = 10$.

the influence of $k_2$. Similar to the situation in the test cases A1c-d, the calculated values must be corrected if large permeability contrasts are obtained.

#### Test case A3: Shape

In test case A3, the shape ratio $P = width/height$, is varied for a centred structure with a constant relative volume of $V_r = 0.09$. This is a rather small relative volume, which must be kept in mind during the discussion below. A small value of P means that the structure is very narrow perpendicular to the flow and very long parallel to the flow (see Figure 4.2). The discussion below is based on Figure 4.15.

**Background permeability $k_2$**
As expected from the experience from the previous test cases, the determination of $k_2$ is generally very accurate and not sensitive to the shape of the structure. For both the test

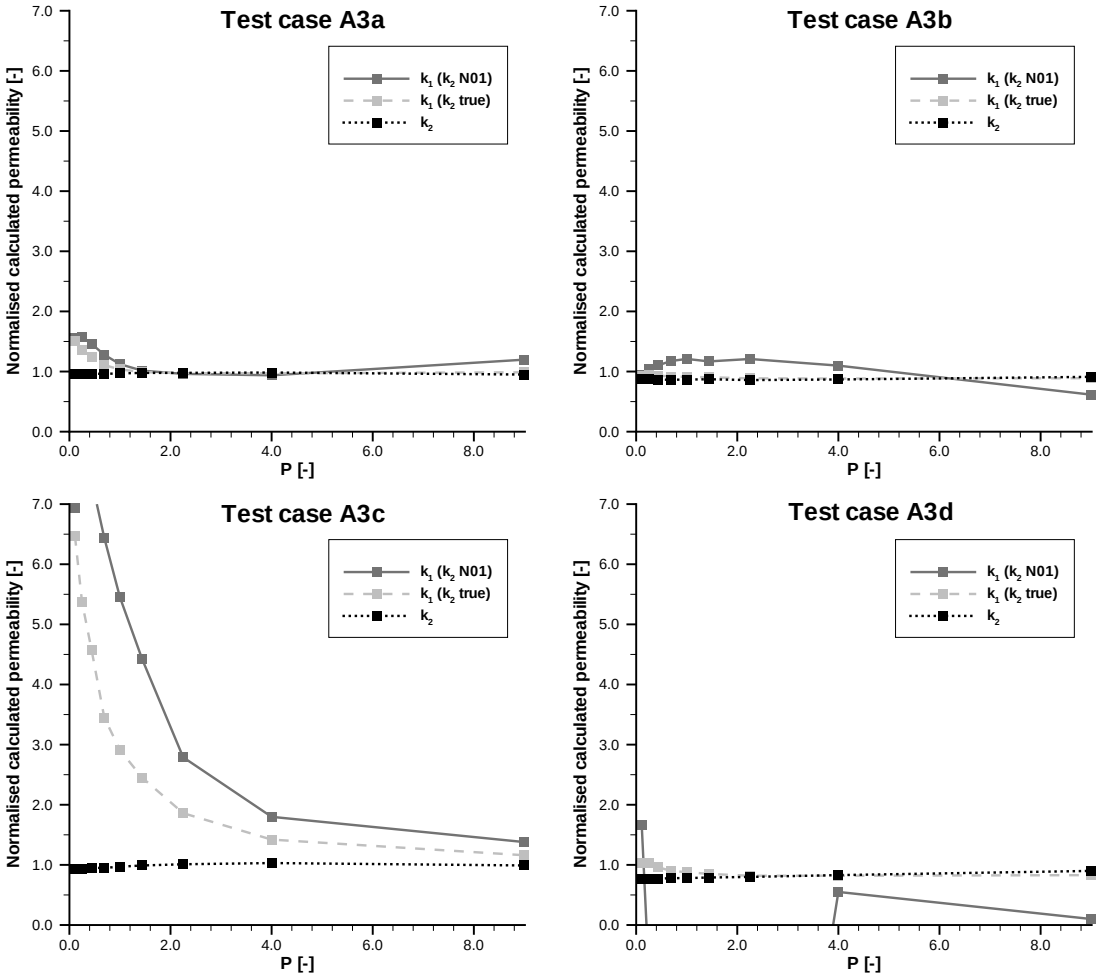


Figure 4.15: Derived permeabilities for test case A3 (shape ratio $P = width/height$). Top, left: A3a, $k_1/k_2 = 1/2$. Top, right: A3b, $k_1/k_2 = 2$. Bottom, left: A3c, $k_1/k_2 = 1/10$. Bottom, right: A3d, $k_1/k_2 = 10$.

cases A3b and A3d, however, a slight underestimation with a maximum of approximately 23% (for A3d) is observed. As the tracer leaves the input port it is attracted towards the higher permeable structure and therefore the shortest flow path is prolonged.

**Structure permeability $k_1$**

For $k_1$, the accuracy of the approximation depends on the shape of the structure as well as on the deviations of $k_2$ from its true value.

- For test case A3a and especially for A3c, for small shape ratios (long and thin in flow direction), there is a strong overestimation of $k_1$, even if the true value of $k_2$ is used. Due to the small width, the tracer can very easily, without a long detour, flow past the low permeable structure. Naturally, this yields a faster arrival than if the tracer would be forced to flow through the structure. This effect is amplified for stronger permeability contrasts. As the width increases, the accuracy improves, however, a slight overestimation remains. This must be accounted for as the permeabilities are determined.

- For the test cases A3b and A3d, there are clear deviations, especially for small shape ratios, mainly due to the difference of $k_2$ from its true value. This even leads to negative values for strong permeability contrasts. As suggested for the previous cases the graphs presented here must be considered when interpreting the calculated permeabilities.

### 4.4.3 Application to fractured porous domains

In order to test the applicability to fractured porous domains, first the simplest test case is used, namely B1. This domain contains one single fracture of varying length (Figure 4.3, left).

**Matrix permeability $k_M$**
It is known from the investigation concerning the location of structures, that a fracture which is perpendicular to the main flow direction has only a negligible influence on the discharge and on the tracer-breakthrough curve. It is therefore possible to determine the matrix permeability in this type of domain. The approximation of the matrix permeability using $t_{1\%}$ of the N07-S07 port configuration of all variations of test case B1 yields normalised values in the range of $0.95 < k_{approx} \leq 1.00$. This is better than using a port configuration located far away but parallel to the fracture. Using port configuration W01-E13 of the variations of test case B1 results in an accuracy in the range of $0.90 < k_{approx} \leq 0.93$, indicating a slight influence of the high permeable fracture, attracting the tracer and provoking a detour from the direct path between the two ports. For port configurations closer to the fracture, the highly permeable fracture causes a strong overestimation of the matrix permeability. For a long fracture and a strong permeability contrast, the overestimation is as high as 20 times the true value. The consequence is that the proposed approach cannot be applied to a system of fractures with a small fracture distance and more than one main orientation.

**Fracture permeability $k_F$**
Applying the approach to determine the fracture permeability proves to be less successful. The approximated fracture permeability is strongly underestimated by one to several orders of magnitude, even though the true value of the matrix permeability is used. Two main reasons are recognised:

- The initial arrival time of a tracer pulse travelling through a fracture that connects or nearly connects two ports is extremely short. In the test case B1 the values are in the range of less than one second to approximately 50 s. Logically, the shortest arrival time occurs for the two domains where the relative length of the fracture is $L_r = 1.0$. Here, because the number is very small, a slight change in travel time causes a strong change in the approximated permeability. This means that the system is extremely sensitive to any type of influence, such as measurement uncertainty in real cases and numerical inaccuracy for simulations.

- Since the domain is porous, the tracer can travel not only through the fracture but also through the matrix close to the fracture. This is seen as a delay in the initial arrival for decreasing permeability contrast between fracture and matrix.

From these observations it is clear that testing the approach on more complex fractured porous domains is not probable to lead to a useful result. It is therefore refrained from applying the approach to the remaining test cases of group B and C.

### 4.4.4 Conclusions

The application of the proposed approach to the test cases of *group A*, shows that it is possible to approximate the permeabilities within a domain of this type, considering a few restrictions. The best result is obtained for the background permeability outside of the structure $k_2$, because it can be determined directly, without involving the permeability of the structure $k_1$. The results of the calculation of the structure permeability prove to be less accurate. The first reason for this behaviour is that the flow field in the vicinity of the structure is strongly influenced by the structure and therefore, in many cases, the shortest flow path for the tracer is not the direct distance between the ports. The second reason is that the calculations involve the harmonic mean of the two permeabilities, leading to a very high sensitivity to deviations of $k_2$ from its true value. In general, the accuracy is better for smaller permeability contrasts. Despite the partly very strong deviations, the approach works, however, under the condition that the characteristics of the graphs shown here are considered. In cases where strong permeability contrasts are obtained, one must always assume that this contrast is underestimated.

For fractured porous domains, as represented by test case *group B and C* the approach has only a very limited applicability. The matrix permeability can be determined if all fractures have the same orientation and if there are measurement configurations perpendicular to these fractures. Using parallel port configurations may lead to under- as well as overestimation of the matrix permeability, depending on the distance to a fracture. Due to the extreme flow and transport situation close to and within a fracture, the proposed approach fails to determine the permeability of a fracture.

I should be underlined that the approach is only used for approximation of permeabilities. A more accurate determination demands the verification of the assumed permeability distribution by numerical simulation and successive adjustment of the material properties.

## 4.5 Application to artificial data sets

In the previous section, the three groups of test cases are used to gain experience concerning the possibilities and limitations of both localisation of structures and approximation of their permeability. The aim of this section is to further test the feasibility of the approach by applying it to artificial data sets, and in this way to simulate the circumstances in a real situation. Tracer-breakthrough curves for two different types of characteristic structure distributions are simulated by one person whereas another person, without knowledge about the structures contained in the domain, applies the proposed approach with the aim to identify the structures. The procedure follows the scheme presented below.

1. **Forward simulations**
   The forward simulations are performed by a person, who is not involved in the subsequent evaluation of the curves. First, two cases with different structure distributions are defined. The first case represents a domain of type A containing block-shaped structures. The second case is of type B with a few single or intersected fractures. Domains of type C with a system of fractures are excluded due to the less successful results for the test cases C1 – C3. Numerical models with the same set-up (Section 3.1) as used for the simulations in the previous sections, are set up for each of the cases applying periodic boundary conditions in order to obtain comparable tracer-breakthrough curves from all 26 ports. These simulated curves are from now on denoted the ”measured” curves since, for the evaluation, the structure distribution is unknown, just as if the curves would be the result of actual measurements.

2. **Evaluation**
   The evaluation of the measured curves is performed for each case by a person without knowledge about the true structure distributions. The outer shape of the domains, the boundary conditions and the measurement configurations are given, which corresponds to the situation in a real case. In addition, the porosities are given which means that the actual permeability can be approximated and not just the ratio between permeability and porosity. Similarly to the test cases, it is also known that the diffusive and dispersive effects are minimised. Based on the ”measured” tracer-breakthrough curves the structures are localised and their properties are approximated.

3. **Verification**
   The approximated structure distributions are verified by setting up numerical models, based on the evaluation results. New tracer-breakthrough curves are simulated and compared to the ”measured” ones. If the curves are considered to be sufficiently similar, the true structure distributions are revealed and the applicability of the method is assessed. If the compared curves differ significantly the procedure is repeated in order to further improve the result. It should be underlined that only if a limited number of iterations lead to a satisfying identification result, the proposed approach can be considered as feasible.

This scheme is not a perfect representation of a real situation, however, important experience is gained that can be used in a real case.

### 4.5.1 Evaluation of case I

The first case is concerned with a domain of type A containing block-shaped structures. The aim is to assess if the exact location and permeabilities can be determined.

#### Analysis of tracer-breakthrough curves

First, the shapes of the complete tracer-breakthrough curves are discussed in order to get an impression of the transport behaviour. Here, the discussion of characteristic curve shapes in Section 4.2 is a useful support. The following visually identified clusters of curves are listed in order of their initial arrival:

1. The first curves to arrive have the highest peaks. There is little variation in initial arrival time and in most cases the curve tailing is weak.
2. The second cluster of curves arrives somewhat later and have a more pronounced tailing. The peaks are lower than for the first cluster.
3. The third group of curves arrives only slightly later than the second cluster, however, the peaks are significantly lower and the curves have a strong tendency towards a second peak.
4. Cluster four contains curves with two clear low peaks, where the first peak is higher than the second one.
5. Finally, the fifth cluster is the latest, however, the peaks have approximately the same magnitude as for the third cluster.

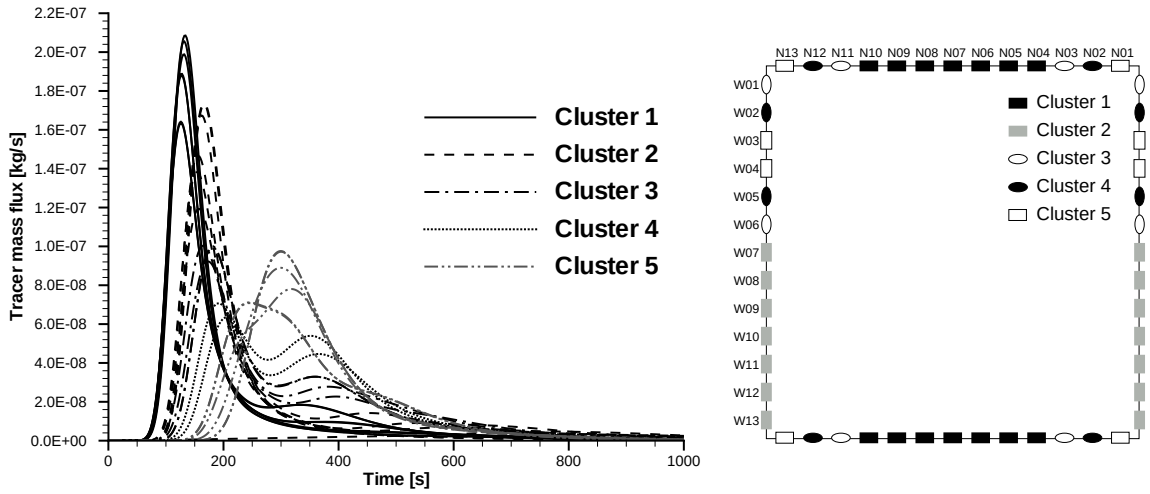


Figure 4.16: Left: "Measured" tracer-breakthrough curves of case I, visually classified according to arrival time and shape. Right: Ports marked according to the classification result.

By marking the ports according to cluster number, as done in Figure 4.16, a pattern is revealed that supports the evaluation procedure. In the *north-south direction*, the curves of

cluster one are associated to the seven most central ports. Because of the fast arrival and the high peaks, this indicates a region of high permeability. The most outer ports in this direction have a similar shape (cluster 5) but a significantly later arrival, suggesting a region of lower permeability. Between these two regions, curves with two peaks (cluster 4) or a tendency hereof (cluster 3) and intermediate arrival times are found, a behaviour which can be expected where a sudden change in permeability is located.

Considering the *west-east direction* the curves with the second earliest arrival are associated to the seven lowest port configurations, suggesting that a higher permeable structure is located here. From the observations from both directions, a high permeable square structure is assumed in the lower central part of the domain. A more exact location is expected when the initial arrival time is used.

#### Localisation based on $t_{1\%}$

For the more accurate localisation of the expected structure, the arrival times $t_{1\%}$ for each of the input ports are plotted as shown in Figure 4.17 (left). An early arrival indicates a high permeability and vice versa. The behaviour of the two curves confirms the assumed structure location. The course of the north-south curve is symmetrical and the arrival time of port configurations N04-S10 to N10-S04 is approximately constant. This and the extremely abrupt decrease from ports N01-S13 to N04-S10 and from ports N13-S01 to N10-S04 indicate a situation, where a structure has direct contact to a port. A structure with a high permeability ranging from configuration N04-S10 to N10-S04 is assumed. The extension in the other direction is approximated from the curve of the west-east port configurations. The course of this curve is smoother with the maximum arrival at port configuration W04-E10, indicating the lowest effective permeability, and a range of short arrival time between port configurations W07-E07 and W13-E01, indicating a region of high permeability. Together, the two curves lead to the assumed structure distribution presented in Figure 4.17 (right) with $k_1 > k_2$. The rectangular structure geometry is determined by two corner points with the co-ordinates [0.15, 0.00] and [0.45, 0.30], yielding a relative volume of $V_r = 0.25$.

#### Approximation of the permeability

The background permeability should be calculated based on the initial arrival time of a configuration which is as distant as possible from the structure. Consequently, the two port configurations W03-E11 and W04-E10 are chosen as indicated in Figure 4.17. Using (4.5), a permeability of $k_2 \approx 9.3 \cdot 10^{-14}\,m^2$ is obtained. According to the discussion in Section 4.4, this result is considered to be rather reliable, since the interfering structure is quite far away and since the approximation of the background permeability is generally relatively accurate. From the plots to the right in Figure 4.14, for $V_r = 0.25$ it can be expected that the derived value corresponds to approximately 90% of the true value for both weak and strong permeability contrasts. Consequently, the value of $k_2$ is approximated to $1.0 \cdot 10^{-13}\,m^2$.

The structure permeability $k_1$ is approximated based on the port configurations W10-E04 and W11-E03, since they are located approximately in the assumed centre of the structure. Because the distance to the output ports in north-south direction is $d = 0$, the use of the central north-south ports would yield a strong deviation of the permeability $k_1$, especially if

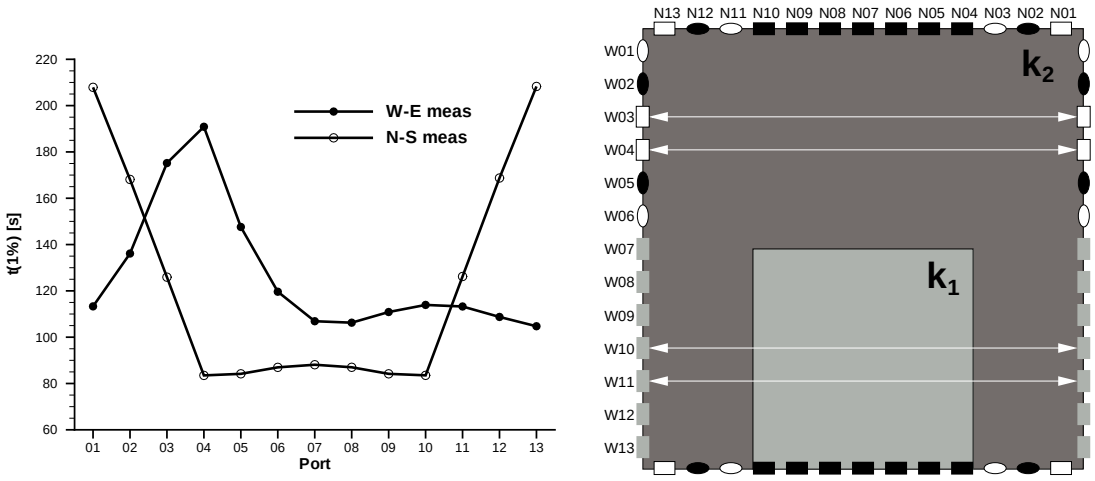


Figure 4.17: Left: "Measured" arrival times $t_{1\%}$ for the port configurations of case I. The x-axis represents the number of the input port. Right: Assumed structure distribution for case I. The port configurations marked with arrows are used for the approximation of the permeabilities.

the permeability contrast is high, as shown in Figure 4.13 (right). Applying (4.6), yields $k_1 \approx 3.8 \cdot 10^{-13}\,m^2$, which is a relatively high permeability contrast ($\approx 4$). Based on the experience from the test cases of group A, it must be assumed that the true contrast is even higher. From the two plots to the right in Figure 4.14, the accuracy of the approximation of $k_1$ for a contrast of 2 (top) and 10 (bottom) for a relative volume of $V_r = 0.25$ is read. The correction of the approximated value is here oriented to the the plot with the stronger contrast. It is observed that the curve based on the approximated value of $k_2$ ($k_1$ ($k_2$ N01)) is instable for $V_r < 0.25$. This makes the correction sensitive and uncertain, as the true value of $V_r$ is unknown. For $V_r = 0.25$ and a permeability contrast of 10 the estimated value of $k_1$ amounts only to $\approx 30\%$ of the true value for $k_1$ ($k_2$ N01). For $V_r = 0.20$ the corresponding value is an overestimation by a factor 1.9. Additionally, a comparison with the approximation of $k_1$ using the true value of $k_2$ makes clear that there is also a strong sensitivity to the value of $k_2$. In this difficult situation it is decided to test if a value of $k_1 = 1.0 \cdot 10^{-12}\,m^2$ yields reasonable results. This combination of permeabilities yields a contrast of 10.

#### Verification of the assumed structure distribution

In order to verify the assumed permeability distribution, a model is set-up and tracer-breakthrough curves are simulated for the same port configurations as for the measurements. The type of structure distribution investigated here, is very well defined without fuzziness and small disturbances, as would be the case in nature. It is therefore expected, that the agreement between the "measured" and the simulated curves is very good if the right structure distribution is assumed. In Figure 4.18, the "measured" and the simulated data are confronted.

The plots of the initial arrival time, the discharge as well as the tracer-breakthrough curves show that the simulated data agree very well with the "measured" curves. The simu-

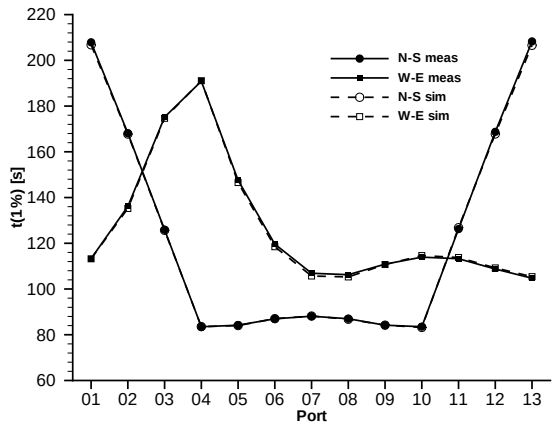


(a) Initial arrival times.

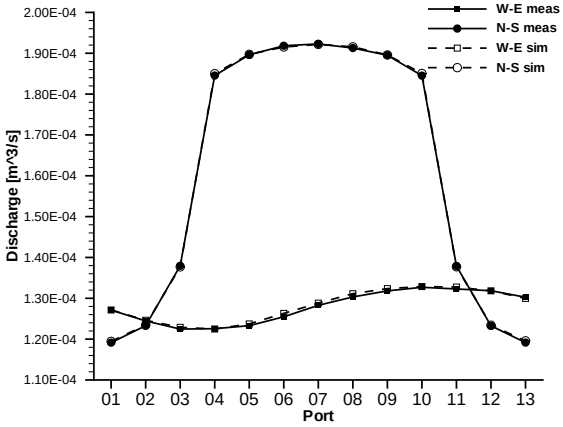


(b) Volume discharge.

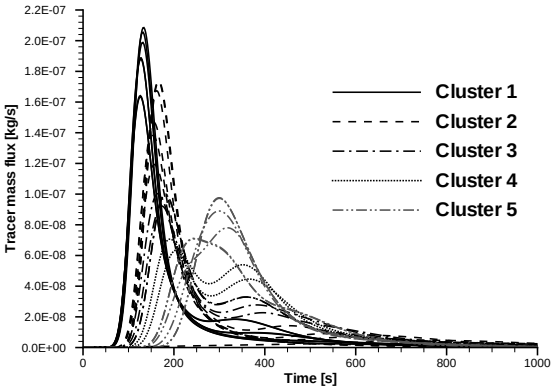


(c) ″Measured″ tracer-breakthrough curves.

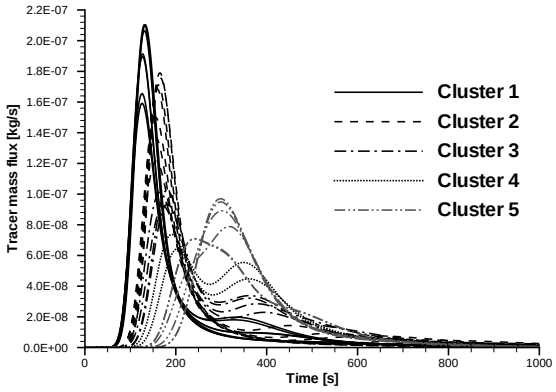


(d) Simulated tracer-breakthrough curves.

Figure 4.18: Comparison of ″measured″ and simulated results of case I.

lated tracer-breakthrough curves are plotted with the same line pattern as the corresponding "measured" curve. Revealing the true structure distribution and comparing it with the assumed one, confirms a perfect match in geometry as well as permeability.

#### Conclusions for case I

The application of the proposed approach to an artificial domain, which contains block structures, confirms the conclusion drawn for the test cases, that it is possible to identify the location and the properties of a block-shaped structure. It is true that an artificial example is idealised and that a real case must be assumed to be more complex with additional small-scale heterogeneities, which would lead to emphasised macro-dispersion. Still, this artificial case shows that it is a feasible method for the approximation of the distribution of such structures and their properties.

### 4.5.2 Evaluation of case II

The second case contains a few single or intersecting fractures. From the study of the test cases of group B it is known, that the spatial range of influence of a fracture is large, due to the strong permeability contrast between fractures and matrix. This renders the structure identification more difficult than for the previous case, both concerning the localisation and the approximation of the permeabilities.

#### Analysis of the tracer-breakthrough curves

First, the properties of the complete tracer-breakthrough curves are discussed. In Figure 4.19, the "measured" tracer-breakthrough curves are shown. Due to a strong similarity of the north-south curves and strong differences of the west-east curves a classification of the curves into clusters is not considered to be useful for the identification procedure.

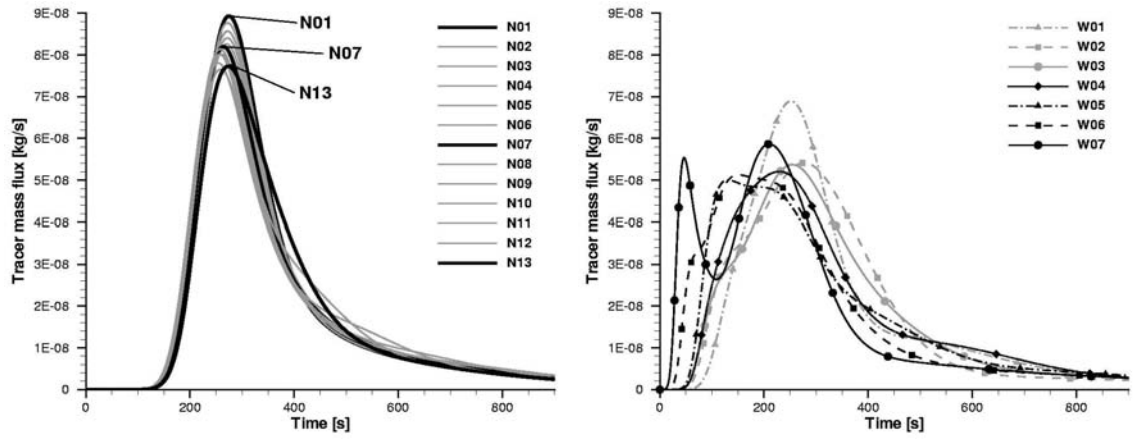


Figure 4.19: "Measured" tracer-breakthrough curves of case II. Left: North-south port configurations. Due to the similarity of the curves, not all are differentiated. Right: West-east port configurations. Due to symmetry reasons only configurations W01 – W07 are shown.

The curves of the *north-south port configurations* are all very similar, both concerning the initial arrival time and the shape of the curve. The peak mass flux decreases from port configuration N01-S13 (highest) to N12-S02 (lowest) and increases slightly again to N13-S01, however, not at a constant rate. The peak arrival time shows only a slight variation.

In contrast to the curves of the north-south port configurations, the variations of the curves of the *west-east configurations* are very significant. There is perfect symmetry, which means that, for example, the curve of configuration W01-E13 is identical with the curve of configuration W13-E01. Only the central configuration W07-E07 is unique. This curve has the earliest initial arrival time and two clear peaks, the second peak being slightly higher than the first one. The curve of configuration W06-E08 arrives slightly later and has a tendency towards three peaks, where the second one is the highest and the first one is the lowest, possibly corresponding to the first peak of the curve of configuration W07-E07. The curve of configuration W05-E09 is the third to arrive and it has a tendency towards two peaks, possibly corresponding to the two last peaks of the curve of configuration W06-E08. Additionally, the mass flux decrease occurs very slowly, almost indicating a very late third peak. For the curves of the remaining configurations, the emphasis is successively shifted towards the indication of the second peak. The curve of configuration W01-E13 has the latest arrival and the shape of the curve is very similar to a curve of a homogeneous domain, except for a late tendency towards a second peak. Such tendency is also observed for the curve of configuration W04-E10. All curves arrive earlier and have lower peaks than the curves of the north-south configurations.

The significant variations and multi-peak curves of the west-east direction, on the one hand, and the small variations of the curves of the north-south direction, on the other hand, suggest that there are fractures with their main orientation in west-east direction. Due to the symmetry it is concluded that the fracture pattern is identical on both sides of the port configuration W07-E07. The various peaks of a curve can be the combined result of tracer travelling through (1) fracture(s) close to the port configuration, (2) fracture(s) further away from the port configuration, and (3) the matrix. Additional information is, however, required before further conclusions can be drawn.

#### Localisation based on $t_{1\%}$

The discussion of the initial arrival times of the curves is expected to reveal additional knowledge about the location of the fractures and about the domain properties. Figure 4.20 shows the variation of $t_{1\%}$ for the north-south as well as for the west-east port configurations.

The observed limited variations of the curves of the *north-south* configurations are concurrent with a relatively smooth course of the $t_{1\%}$ curve. The minimum arrival time is obtained for port configuration N11-S03. The curve is not symmetrical, but there is a relatively fast decrease towards the minimum from the west and a rather slow increase from the minimum towards the east.

The values of $t_{1\%}$ of the *west-east* configurations are symmetrical, clearly lower than for the other configurations and show strong variations. The arrival time increases rather suddenly between the central and the neighbouring port configurations. Following this increase, there is almost a plateau between the port configurations W04-E10 and W03-E11.

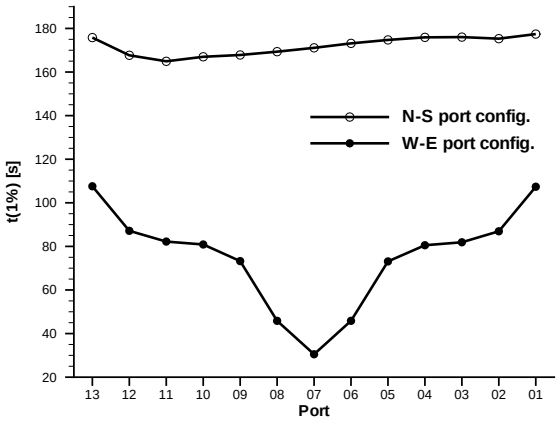


Figure 4.20: "Measured" initial arrival times of case II.

Further away from the centre the time increase grows stronger again.

The fact that only minor variations in arrival time are observed for the north-south configurations supports the assumption that possible fractures are not oriented in north-south direction, or if they are, they are very short causing only minor variations. The small variations could also be the result of slightly inclined fractures with a more west-east oriented direction.

Concerning the west-east direction, first, it is assumed that there is one central fracture between the ports W07 and E07, causing the narrow first peak of configuration W07-E07 and the first low peak of configuration W06-E08. Because the initial arrival of the central configuration is very short, the fracture must either be very long or have a very short distance to at least one of the ports. Unfortunately, it is not possible to use the perpendicular port configurations for the approximation of the length of the assumed fracture (Section 4.3.2). Second, fractures are expected further away from the centre, possibly around configuration W05-E09 and W09-E05, since the curves of these port configurations show a rather high first peak. Such structures would explain the plateau of the $t_{1\%}$ plot, even though it must be underlined that the approximation of the location of the assumed structures is not very accurate. Since the initial arrival of the port configurations away from the centre is not as early as for the centre configuration, these assumed fractures are likely to be shorter than the central one and/or inclined. Due to the observations of the north-south direction, inclined fractures are assumed with their west-east centre around port configuration N09-S05.

The assumed fracture locations are shown in Figure 4.21.

#### Approximation of the permeability

Based on the assumed fracture distribution, port configuration N03-S11 and N04-S10 are used to determine the matrix permeability. According to (4.5), an average value of $t_{1\%}$ of 176 s yields an approximated matrix permeability of $k_M \approx 1.0 \cdot 10^{-13}\,m^2$. Since the influence of fractures seems to be weak in the north-south direction, it is assumed that this value is reliable.

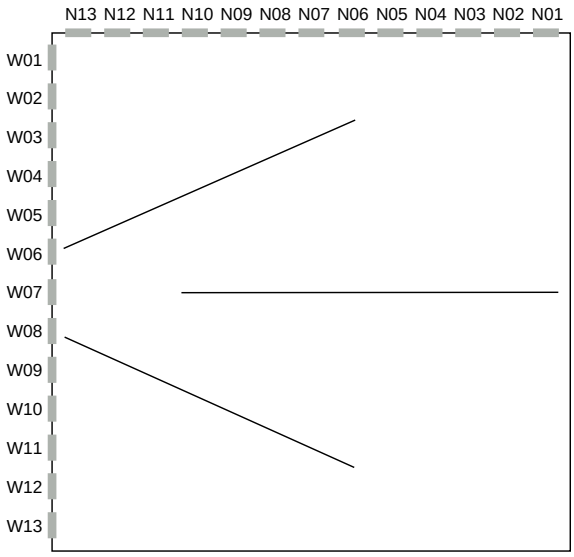


Figure 4.21: Initial assumption of the fracture distribution of case II.

As concluded in Section 4.4.3, it is not possible to use the initial arrival time for the approximation of fracture permeability. There is, however, one observation that indicates a reduced permeability contrast between fractures and matrix. Test case B2 showed that the range of influence of a fracture, perpendicular to its orientation, decreases for decreasing permeability contrast. Since the shape of the $t_{1\%}$-plot of the west-east configurations is rather sharp around the central port a contrast corresponding to a somewhat reduced value (5000) of the higher one of the contrasts used in the test cases (8330) is used as orientation, leading to an approximated fracture permeability of $k_F = 5.0 \cdot 10^{-10}\,m^2$. As a first approximation, all fractures are assumed to have the same permeability. The fact that the approximation of the fracture permeability is not very reliable makes the identification of the fracture distribution very complex, since a large number of degrees of freedom remains.

#### Verification of the assumed structure distribution

The simulations of all port configurations are first conducted using the fracture distribution (Figure 4.21) and the properties discussed above. Since the agreement between the "measured" and the simulated results are not satisfactory for this constellation, the procedure is repeated until the result has reached a certain level of improvement. During this iterative procedure numerous combinations of the following variations are tested:

- the lengths of the fractures,
- the orientation of the non-central fractures,
- the horizontal and the vertical position of the fractures,
- the permeability of the fractures and,
- the permeability of the matrix.

Trying principally different fracture distributions is not considered as useful, since the purpose of the application to the artificial cases is to test if the proposed identification procedure can be used to obtain a reliable first approximation of the structure distribution.

The discussion of structure identification for the test cases is based on the initial arrival time of the tracer. Consequently, the objective of the optimisation of the simulated results is to minimise the difference of the plots of this variable. Despite the large number of iterations a satisfactory agreement between "measured" and simulated data is not obtained. It is refrained from discussing the results of each of the trial runs and the changes made for each step. Only the best fitted simulated results are shown together with the "measured data" in Figure 4.22. The figure shows initial arrival times, discharges, and tracer-breakthrough curves.

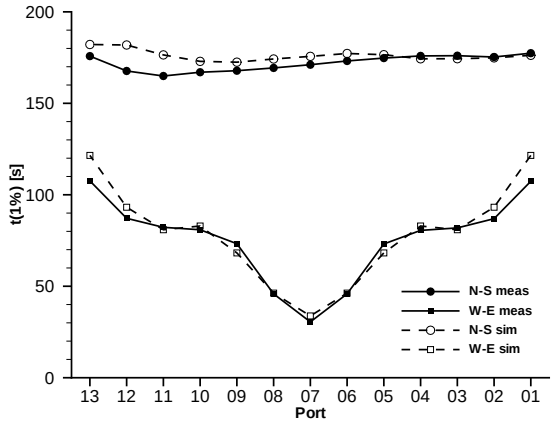


(a) Initial arrival times.

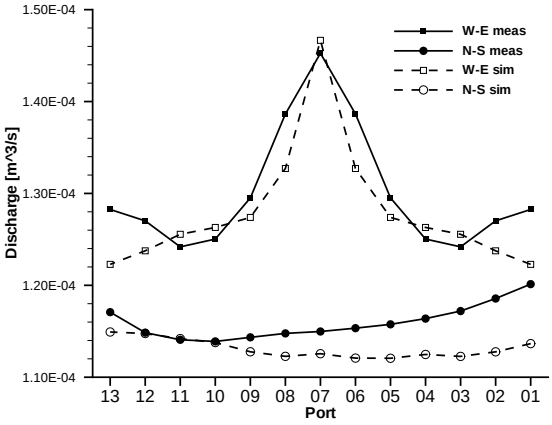


(b) Volume discharge.

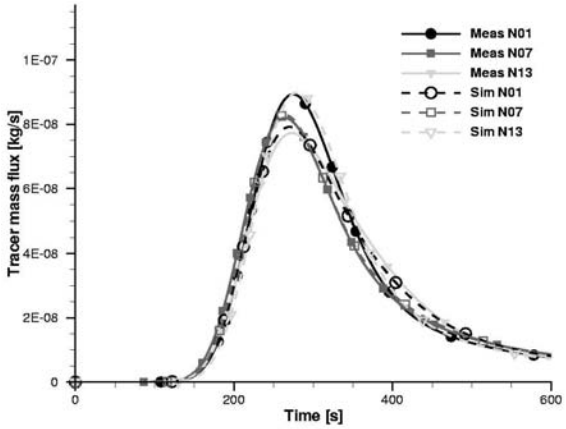


(c) Selected tracer-breakthrough curves of the north-south port configurations.

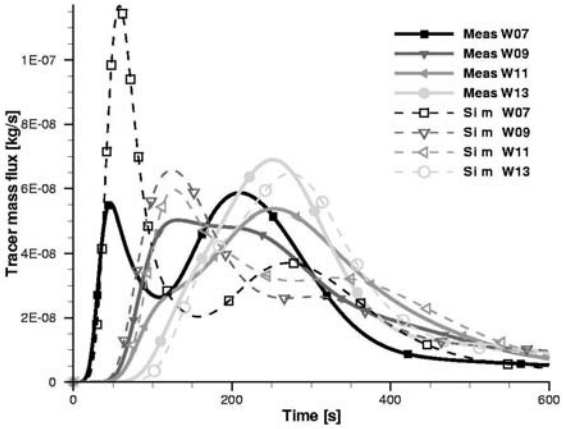


(d) Selected tracer-breakthrough curves of the west-east port configurations.

Figure 4.22: Comparison of "measured" and simulated results of case II.

The best fit is obtained for the initial arrival times. This is expected since the objective of the iteration is to minimise the difference between the plots of this variable. However, it must be underlined that the principle variations of the values of the north-south port configurations are not very well captured. On a different time scale, this would be more obvious.

Concerning the discharge values in general, on the one hand, the "measured" and the simulated ones are rather similar. For the individual port configurations, on the other hand, there are differences that may not be neglected.

The strongest deviations are obtained for the tracer-breakthrough curves of the west-east port configurations. In most cases, the first peak is too high. Only the most outer curve, W13-E01, has an acceptable agreement with the measured curve. Concerning the curves of the north-south curves, the agreement is better, especially for configuration N07-S07.

Finally, in Figure 4.23 the true fracture distribution is revealed (left). The approximated fracture distribution which yields the best fit is shown on the right hand side in the same figure. Table 4.2 shows the true and the approximated permeabilities for matrix and fractures.

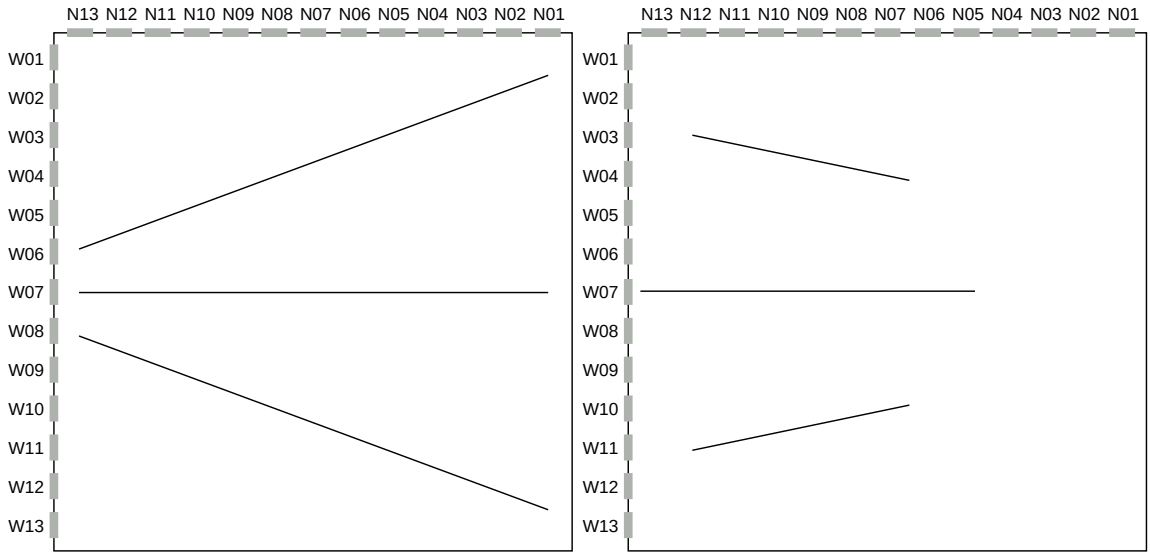


Figure 4.23: True (left) and approximated (right) fracture distributions of case II.

Table 4.2: True and approximated permeabilities of case II.

| | Matrix permeability $k_M$ | Fracture permeability $k_F$ | |
|---|---|---|---|
| True | $1.0 \cdot 10^{-13}$ | $2.1 \cdot 10^{-10}$ | $m^2$ |
| Approximated | $1.0 \cdot 10^{-13}$ | $5.0 \cdot 10^{-10}$ | $m^2$ |

The first thing that becomes apparent when the true distribution is revealed, is that the *initially assumed* location of the fractures as shown in Figure 4.21 is very close to the true distribution. The initially assumed fractures are, however, shorter and the angle of incidence

of the two inclined fractures is larger. Concerning the permeabilities, the true and the assumed matrix permeabilities are equal. The assumed fracture permeability is overestimated by a factor of 2.4. It should, however, be recalled that during the initial approximation procedure the fracture permeability was assumed to be rather low because of the shape of the $t_{1\%}$-plot in west-east direction. The true value confirms that this was a correct observation. The rather accurate initial approximation of the location as well as the permeabilities is considered as an indication of the feasibility of using the initial arrival time of the tracer for structure identification in this type of systems.

On the contrary, the changes made in structure location and geometry during the verification, finally leading to the distribution shown in Figure 4.23 (right), indicate that it is not an easy task to achieve an accurate identification. Due to the large number of degrees of freedom, hence non-uniqueness, it can very easily happen that changes are made in the wrong direction. This might in the end yield an approximation which is actually less accurate than the first assumption. However, despite the deviations in fracture orientation, length and permeability, the fundamental characteristics, such as number of fractures and approximate location, of the true and the finally approximated fracture distributions are rather similar.

#### Conclusions for case II

The results of the identification of the fracture distribution in case II show that the proposed approach for structure identification is a useful support for approximating the distribution and material properties of systems containg a few single fractures. Despite deviations, the fundamental characteristics are approximated correctly. The exact distribution, though, with a correct fracture permeability, is not found. The failure of determining either the fracture permeability or the fracture length accurately is considered as the main disadvantage of the approach. If a method is found that can determine at least one of these two properties, thus reducing the degrees of freedom, the accuracy of the approximation would increase significantly.

## 4.6 Application to a real case

In the previous sections, the possibilities and limitations of structure identification is investigated, first, based on a number of test cases of different characteristics and, second, based on two artificial cases. For the first artificial case (block-shaped structures), very satisfying results are obtained, whereas for the second case (a few single or intersecting fractures), the approach is less successful. In this section, the approach is applied to a real case.

Within the framework of the "Aquifer Analogue" research project conclusions about the inner structure of a fissured sandstone block were drawn, based on port-port tracer measurements (Section 1.2). The aim of this section is to verify these conclusions. For this purpose, the approach that is tested and discussed in the previous sections of this chapter is used. First, the permeability distribution is approximated from the clustered tracer-breakthrough curves. Second, a numerical model is set up and used for the simulation of the tracer measurements. The simulation results are compared with the measurements in order to assess the validity of the assumed structure distribution.

### 4.6.1 Experimental set-up and measurements

Within the framework of the "Aquifer Analogue" research project, which is introduced in Section 1.2, port-port tracer measurements were conducted on an air saturated fissured sandstone block with the dimensions $60 \times 60 \times 60\,\mathrm{cm}$ (Figure 1.2). During a measurement a pressure difference of $0.5\,\mathrm{bar}$ was imposed on two opposite ports whereas the other ones were closed. After steady state had been reached, a defined amount of tracer (helium) was injected at the input port and the concentration at the output port was recorded. This procedure was repeated for all direct port-port connections. On each side of the block, a raster of measurement ports was located with $4 \times 4$ ports and one central port, additionally. Due to technical problems, the central ports did not yield reliable results, hence, a total number of 48 ($4 \times 4 \times 3$) measurements were available for the subsequent evaluation.

The basic concept of this approach is to consider groups of similar curves instead of single ones. In this way, the most significant structures are revealed, however, at the cost of suppressing local variations in the material properties.

First, the set of curves was divided into subsets according to measuring configuration, i.e. the location of the ports relative to the block boundaries. This was necessary in order to assure comparability between the tracer-breakthrough curves for the further evaluation. In Figure 4.24 the three configurations are shown together with the associated measured tracer-breakthrough curves.

Second, for each subset, Principal Component Analysis (PCA) was used in order to determine appropriate variables for the subsequent classification of the tracer-breakthrough curves. Such variables are, for example, discharge, initial arrival time or the arrival time of certain percentages of the injected tracer mass. By means of PCA, a large set of variables is reduced to a limited number of nearly uncorrelated variables which describe most of the variance contained in the data set. A detailed discussion on theory and application of PCA is given in, for example, JOLLIFFE (1986[31]) and JACKSON (1991[30]).

Third, based on the selected variables, a classification of the tracer-breakthrough curves was conducted using Cluster Analysis. The aim of this method is to form groups of objects

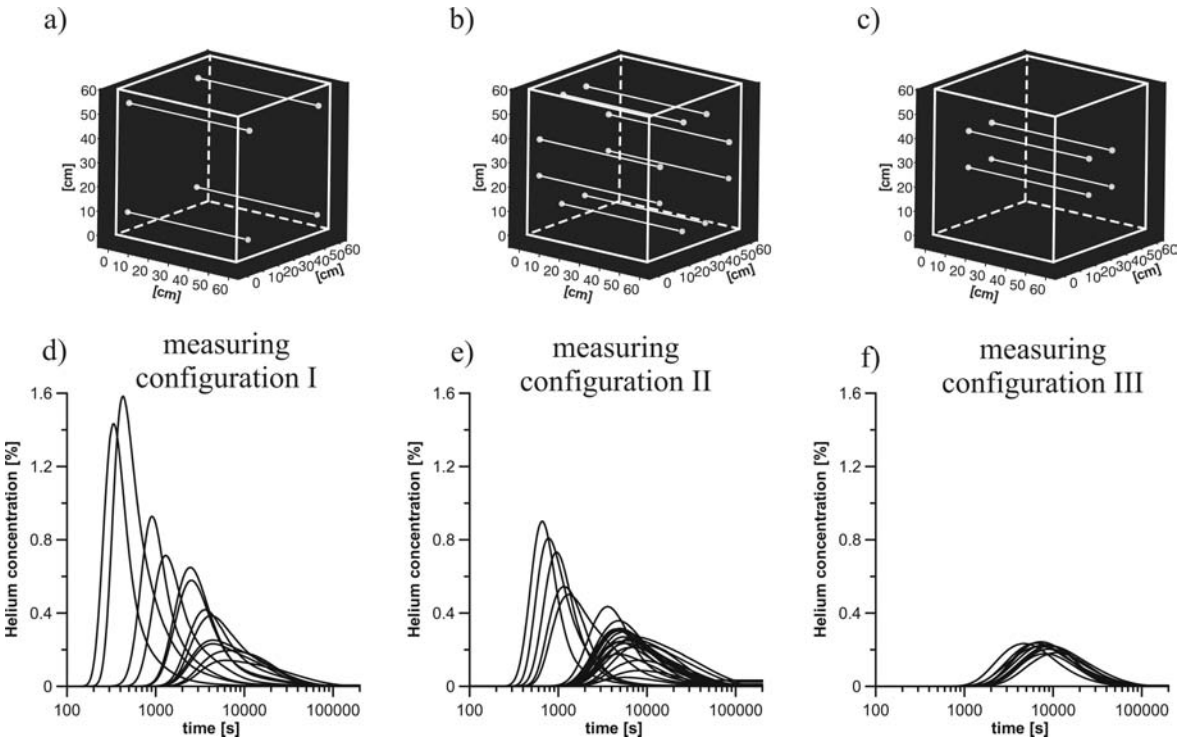


Figure 4.24: Illustration of the division of the complete set of tracer-breakthrough curves according to port configuration, i.e. the location of the ports relative to the block boundaries. Figures (a) - (c) indicate the three possible configurations for one of three spatial directions. Figures (d) - (f) shows the measured tracer-breakthrough curves which are associated to each of the configurations. (BRAUCHLER, 2005[13]).

that are as similar as possible whereas the objects in different groups are as different as possible. A detailed discussion on possible algorithms and applications can be found in, for example, KAUFMAN & ROUSSEEUW (1990[33]) and WILKS (1995[65]).

By evaluating the characteristics of each cluster of curves and by associating these characteristics with the location of the measurement ports, conclusions about the inner structure of the block were drawn. It was concluded that the system is determined mainly by two quasi-homogeneous horizontal layers of different permeability where the upper layer is more permeable than the lower one. Additionally, it was assumed that there is no significant influence of high permeable fractures.

The work described above was conducted by staff of the Center for Applied Geoscience, University of Tübingen, Germany. A detailed description of the measurements as well as the evaluation methods and results is found in BRAUCHLER (2005[13]) and DIETRICH ET AL. (2005[18]).

### 4.6.2 Approximation of geometry and properties of the assumed structures

As stated above, it is assumed that the sandstone block consists of two quasi-homogeneous layers, where the upper layer is more permeable than the lower one. Plots of the distribution

of the measured discharge (not shown here), as well as a priori knowledge, confirm this assumption and additionally indicate that the boundary between the two layers is slightly inclined. In order to enable slightly different characteristics within the identified lower layer to be considered, a third middle layer is introduced, as indicated in Figure 4.25.

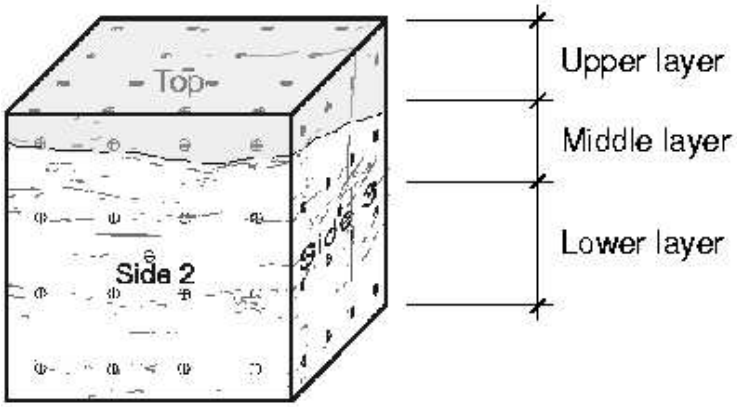


Figure 4.25: View of the block sample, indicating the approximate layer boundaries and port locations (modified from BRAUCHLER (2005[13])).

The measured tracer-breakthrough curves, averaged over each identified cluster, are shown in Figure 4.26. For each measurement configuration (I – III, Figures 4.24 a – c) BRAUCHLER (2005[13]) identified three clusters (1 – 3). The characteristics and the spatial

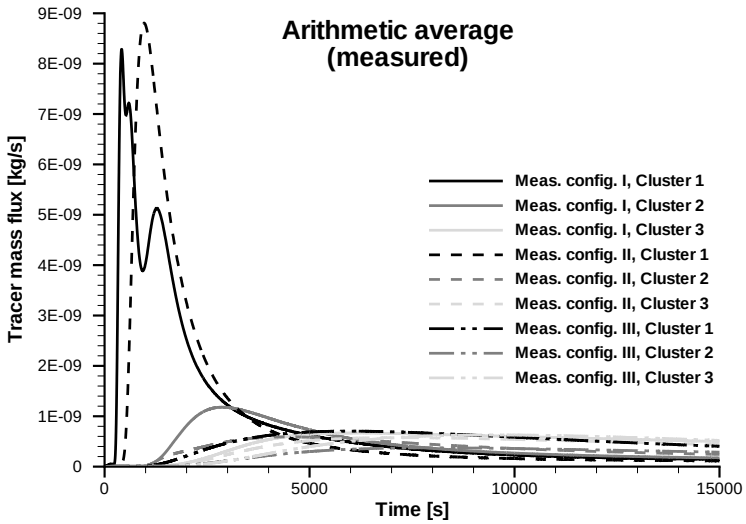


Figure 4.26: The measured tracer-breakthrough curves, averaged over each cluster (1 – 3) for each of the three possible measuring configurations (I – III).

allocation of these clusters are presented in Table 4.3, referring to the layers indicated in Figure 4.25. It is very evident that the curves of the upper layer originate from significantly different flow conditions, compared to all the other averaged curves. Moreover, the curves that are measured in the direction from bottom to top are generally the slowest and the

Table 4.3: Characteristics of each of the identified clusters and their spatial allocation for each of the three measuring configurations.

| Cluster | Allocation | Arrival | Peak | Spreading |
|---|---|---|---|---|
| Measuring configuration I (corner ports) | | | | |
| 1 | Upper layer | very early | clear, high | narrow |
| 2 | Lower layer | late | clear, intermediate | wide |
| 3 | Bottom-top | very late | flat, low | very wide |
| Measuring configuration II (outer middle ports) | | | | |
| 1 | Upper layer | early | clear, high | very narrow |
| 2 | Middle/lower layer | late | flat, low | wide |
| 3 | Bottom-top | very late | flat, low | very wide |
| Measuring configuration III (middle ports) | | | | |
| 1 | Lower layer | late | flat, low | very wide |
| 2 | Middle layer | latest | flat, very low | widest |
| 3 | Bottom-top | latest | flat, very low | very wide |

most widely distributed in time, except for the curve of the middle layer for the middle port configuration, which has a late initial arrival and the widest spreading of all six curves.

Using the average arrival time $t_{1\%}$ of each of the clusters and assumptions for the effective porosities (0.23 for the upper and 0.12 for the middle and the lower layers (BENGELSDORF, 1997[8]; MÜLLER, 1996[42])) yields a first approximation of the permeabilities as listed in Table 4.4. Instead of listing the notation of the clusters, the location of the ports on the block is used, e.g. "upper layer". From the approximated permeability values, three

Table 4.4: First approximation of the permeabilities ($m^2$) of each of the identified clusters.

| Allocation | Meas. config. I | Meas. config. II | Meas. config. III |
|---|---|---|---|
| Upper layer | $8.9 \cdot 10^{-14}$ | $5.0 \cdot 10^{-14}$ | |
| Middle layer | | $1.6 \cdot 10^{-14}$ | $8.4 \cdot 10^{-15}$ |
| Lower layer | $1.7 \cdot 10^{-14}$ | | $1.3 \cdot 10^{-14}$ |
| Bottom-top | $1.1 \cdot 10^{-14}$ | $1.0 \cdot 10^{-14}$ | $8.3 \cdot 10^{-15}$ |

observations can be made:

- The difference in permeability between the upper and the middle/lower layers is just less than one order of magnitude.
- There seems to be a tendency towards a lower approximated permeability further away from the boundaries.
- The harmonic mean of the horizontal permeabilities of the layers is higher than the approximated permeability from bottom to top, indicating anisotropy.

The first observation indicates a strong contrast in permeability between the layers. The second observation is due to two competing effects occurring as the ports approach a boundary: (1) the total discharge decreases slightly; and (2) the effective velocity increases because the area through which half of the discharge flows decreases. Since the second effect is stronger, the initial arrival time of a tracer-breakthrough curve measured close to a boundary is less than if the boundaries are far away. This behaviour is also discussed in Section 3.2.2. The observed anisotropy is reasonable, as the permeability perpendicular to the bedding is usually lower than in the horizontal direction.

### 4.6.3 Verification of the assumed structure distribution

Based on the known outer geometry and the experimental set-up in combination with the approximated structure distribution and structure properties, a numerical model is set up for the verification of the assumptions.

#### Boundary conditions

At the in- and the output ports, constant pressures are imposed, whereas the rest of the block surface is impervious to flow and transport. A tracer pulse is injected by keeping a certain tracer-mass flux constant during one time step. In Figure 4.27, a mesh for one of the port configurations is shown. The assumed layered structure as well as the refinement around the ports can be clearly seen.

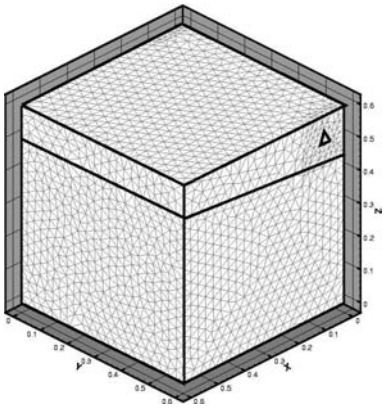

| Fluid properties | | | |
|---|---|---|---|
| $\mu$ | $1.81 \cdot 10^{-5}$ | | $kg\,m^{-1}\,s^{-1}$ |
| $D_{m,e}$ | $6.8 \cdot 10^{-6}$ | | $m^2\,s^{-1}$ |
| **Matrix properties** | | | |
| | *Upper layer* | *Middle/Lower layer* | |
| $k_{x,y}$ | $5.5 \cdot 10^{-14}$ | $8.9 \cdot 10^{-15}$ | $m^2$ |
| $k_z$ | $3.7 \cdot 10^{-14}$ | $6.4 \cdot 10^{-15}$ | $m^2$ |
| $n_e$ | 0.23 | 0.12 | - |
| $\alpha_l$ | $1.5 \cdot 10^{-2}$ | | m |
| $\alpha_t$ | $1.5 \cdot 10^{-3}$ | | m |

Figure 4.27: Model set-up. Left: Example of a generated mesh with refinement in the vicinity of a port. Right: Used model fluid and matrix properties of the assumed structures. The anisotropy ratio between the horizontal and the vertical direction is 1.5.

#### Fluid properties

The dynamic viscosity $\mu$ of air at 20°C and 101.3 kPa is $1.81 \cdot 10^{-5} kg\,m^{-1}\,s^{-1}$ and is kept constant during the simulation. The compressibility due to pressure changes is considered in the model by applying the universal gas law for an ideal gas.

The molecular diffusion coefficient $D_m = 7.0 \cdot 10^{-5} m^2 s^{-1}$ is valid for helium and air at low pressures and a temperature of 20°C (REID ET AL., 1987[53]). There are different approaches to determining the *effective* diffusion coefficient $D_{m,e}$, considering the reduced diffusive flux due to the porous medium, as discussed by, for example, CUNNINGHAM (1980[16]), BIRKHÖLZER (1994[11]), and MCDERMOTT (1999[40]). Based on these approaches, an effective diffusion coefficient of $D_{m,e} = 6.8 \cdot 10^{-6} m^2 s^{-1}$ is used for both layers.

#### Matrix properties

The approximated permeabilities as presented in Table 4.4 are only to be considered a first but relatively accurate approximation of the permeabilities of the assumed structures. Resulting from a few initial flow calibration runs of the model, the values presented in the table to the right in Figure 4.27 are used for all further simulations.

The effective porosity $n_e$ is set to 0.23 for the upper and 0.12 for the lower layer, as already mentioned in Section 4.6.2. The longitudinal and the transversal dispersivities are set to $\alpha_l = 1.5 \cdot 10^{-2} m$ and $\alpha_t = 1.5 \cdot 10^{-3} m$.

### 4.6.4 Discussion of the results

Here, first, the observations from the flow and the transport simulations in comparison with the measurements are presented. These observations are then interpreted and conclusions about the inner structure of the block sample is drawn.

#### Flow simulation

In Table 4.5, the ratios between the simulated and the measured discharges are presented. The approximation of the discharges of all corner configurations (configuration I) and of the

Table 4.5: Ratios of $Q_{sim}/Q_{meas}$.

| Allocation | Meas. config. I | Meas. config. II | Meas. config. III |
|---|---|---|---|
| Upper layer | 1.00 | 0.76 | |
| Middle layer | | 1.34 | 1.41 |
| Lower layer | 0.99 | | 0.71 |
| Bottom-top | 1.01 | 0.99 | 1.11 |

bottom-top clusters are very accurate (the maximum deviation is 11%). For the other clusters, under- as well as overestimation of the discharges is obtained. The absolute deviations of the middle ports (configuration III) are relatively small in comparison to the deviations of all ports and are therefore not considered significant. The same accounts for the outer middle ports (configuration II) of the lower layer. The only deviation which cannot be neglected is the one from the outer middle ports (configuration II) of the upper layer. Here, there is a clear underestimation of the measured discharge. Increasing the permeability would, however, lead to an overestimation of the discharge of the upper layer of the corner ports (configuration I). Therefore, the chosen permeability distribution is accepted and used for the transport simulation.

### Transport simulation

The quality of the transport simulations is judged by comparing the measured and the simulated tracer-breakthrough curves as well as the arrival times $t_{1\%}$. In Figure 4.28, the averaged measured tracer-breakthrough curves are plotted together with the individual curves of each port configuration. The ratios of the arrival times are presented in Table 4.6.

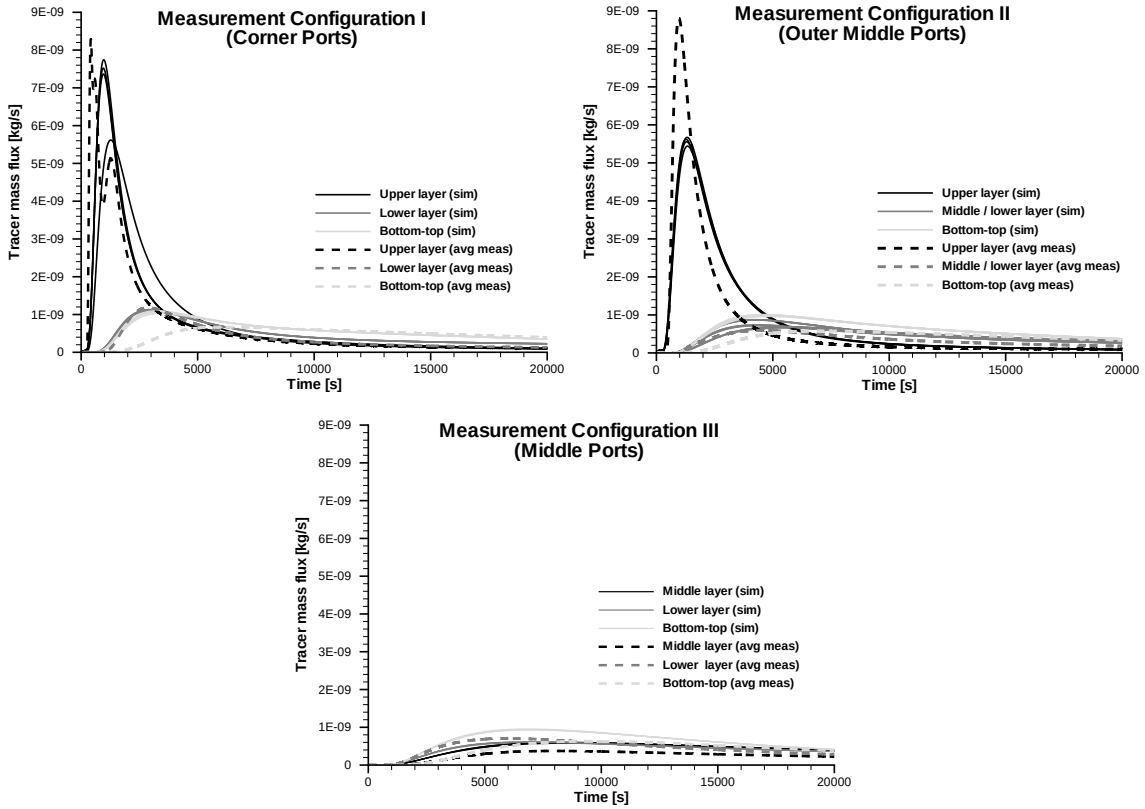


Figure 4.28: Comparison of average measured tracer-breakthrough curves with all individual simulated curves for each measurement configuration.

Table 4.6: Ratios of $t_{1\%}(\text{sim})/t_{1\%}(\text{avg. meas})$.

| Allocation | Meas. config. I | Meas. config. II | Meas. config. III |
|---|---|---|---|
| Upper layer | 1.41 | 1.17 | |
| Middle layer | | 0.88 | 0.64 |
| Lower layer | 0.86 | | 1.07 |
| Bottom-top | 0.57 | 0.64 | 0.63 |

The first impression from Table 4.6 is that the simulated curves in the upper layer arrive too late whereas the other curves arrive too early (except for the lower layer, configuration III). A visual comparison of the average measured curves and the individual simulated ones, however, leads to the conclusion that the initial tracer arrival time in general coincides very

well. The reason for the deviations in $t_{1\%}$ are due to the shape of the curves, i.e. the initial arrival time of the simulated curves of the upper layer is very accurate but they are not as steep as the averaged measured ones. This leads to differences in the arrival time of 1% of the injected tracer.

Considering the *corner port configuration (I)*, the curves of the upper layer have a very accurate initial arrival time, but the increase of the tracer-mass flux is not strong enough, leading to a smaller and delayed peak. At later times, the tailing fits well. As regards the curves of the lower layer, the initial arrival comes slightly too early, whereas the shape of the curves is very accurately reproduced. The simulated bottom-top curves definitely arrive too early but, as the simulation continues, the characteristic strong tailing is satisfactorily described.

The characteristics of the *outer middle port curves (II)* are very similar to the ones for the corner ports. The observations are therefore not repeated.

For the *middle port configuration (III)*, there is a satisfactory agreement for the curves of the lower layer. The simulated curves of the other two clusters arrive too early and are steeper than the averaged measured cluster curves. This is most significant for the bottom-top simulations.

#### Interpretation of the simulation results

Interpreting the observations made for the simulated discharges and tracer-breakthrough curves in the previous parts of this section leads to conclusions concerning the inner structure of the investigated fissured sandstone block.

The simulated corner port curves (configuration I) of the *upper layer* are observed to reproduce the measured discharge very accurately, whereas the discharge of the outer middle ports (configuration II) is underestimated. This suggests that the real layer is not as homogeneous as initially assumed. As for the shape of the simulated curves, the initial arrival time is very close to the average measured curves, whereas the tracer-mass flux increase is not steep enough.

A fundamental model investigation, illustrated in Figure 4.29, is conducted in order to investigate the influence of thin low-permeable layers on the discharge and the shape of the tracer-breakthrough curve. For this purpose, a two-dimensional model with three different permeability distributions is set-up: (1) homogeneous, isotropic ($k_1$), (2) heterogeneous with low-permeable layers ($k_1$, $k_2$), and (3) homogeneous, anisotropic ($k_x = k_1,\ k_z$). The permeability in z-direction of the homogeneous, anisotropic domain is calculated as

$$k_z = \frac{Q_{\text{transversal to structures}}}{Q_{\text{homogeneous}}} \cdot k_1 \,. \tag{4.7}$$

This simple investigation shows that thin layers of low-permeable material, parallel to the main flow direction, cause only a slight decrease in discharge but significantly steeper tracer-breakthrough curves with higher peaks, compared to a homogeneous domain. It is possible that the upper layer contains structures such as fractures filled with consolidated material or clay, causing this type of behaviour.

The fit of the discharges and the curves of the *lower layer* is very good for the corner as well as for the outer middle ports (configurations I and II). For the middle ports (configura-

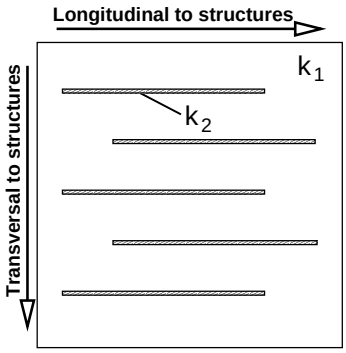


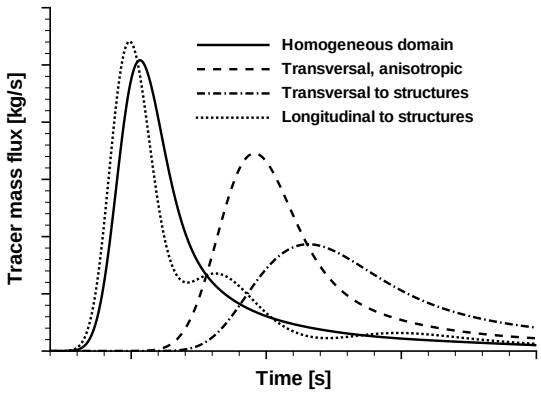


| Permeabilities | ($m^2$) |
|---|---|
| $k_1$ | $1.0 \cdot 10^{-13}$ |
| $k_2$ | $1.0 \cdot 10^{-14}$ |
| $k_z$ (Hom., anisotr.) | $5.4 \cdot 10^{-14}$ |

| Simulated discharges | ($m^3 s^{-1}$) |
|---|---|
| Homogeneous domain | $1.09 \cdot 10^{-4}$ |
| Transversal, anisotropic | $0.70 \cdot 10^{-4}$ |
| Transversal to structures | $0.59 \cdot 10^{-4}$ |
| Longitudinal to structures | $1.03 \cdot 10^{-4}$ |

Figure 4.29: Results of a fundamental investigation of the influence of low-permeable thin layers on flow and transport. The anisotropy factor for the homogeneous, anisotropic case is determined as $Q_{\text{homogeneous}}/Q_{\text{transv. to structures}}$.

tion III), the curves of the lower part are very well approximated, whereas the simulations of the middle layer have a slightly overestimated discharge. This leads to an arrival which is too early and peaks which are too high for the latter curves. It is possible that the middle layer represents a region of lower effective permeability, which causes this behaviour. Since these deviations are not very significant, the two-layer structure is accepted.

The largest deviations are obtained for the *bottom-top* simulations. The applied anisotropy factor of 1.5 yields a very good approximation of the discharge. However, the simulated tracer-breakthrough curves arrive too early and have peaks which are too high. The fundamental investigation of the influence of low-permeable thin layers, mentioned for the upper layer (see Figure 4.29), shows that flow and transport perpendicular to such layers are strongly influenced by the structures. Using an anisotropy factor, determined by the ratio of the measured discharges, to represent the structures reproduces neither the discharge nor the tracer-breakthrough curves perpendicular to the structures correctly. The effect of the real layers is stronger. The implementation of these thin layers of low permeability into the upper layer would improve the shape of the tracer-breakthrough curves in the bottom-top direction. The middle layer may contain such structures as well.

### 4.6.5 Conclusions

The application of the discussed procedure for identification of structures to a real case shows that it is a useful approach in order to obtain a first approximation of the geometry and properties of structures.

The discussed procedure is applied here on a laboratory-scale sample with very well defined dimensions and a regular raster of measurement ports. The measurements are con-

ducted under controlled conditions in a laboratory. These circumstances are very advantageous for the procedure. Additionally, due to the characteristics of the sample, i.e. layered structure without significant influence of single permeable fractures, the identified clusters of tracer-breakthrough curves yield a rather clear picture of the sample structure and its properties.

The conditions are not always as favourable, especially if measurements are conducted in the field. At present, an experimental set-up on a field block of a larger scale is being prepared. This involves carrying out measurements under less controlled conditions and the existence of significant fractures within the domain. With a 7-spot star-shaped configuration of vertical bore holes and packers within the bore holes, a large set of tracer-breakthrough curves can be obtained. By applying the discussed identification procedure on this data set, its feasibility can be tested further.

## 4.7 Synopsis

This chapter deals with the possibilities and limitations of identifying structure distributions and material properties in domains of different type. The structure identification is based on a large number of tracer measurements that are obtained from port-port configurations of varying location.

First, the behaviour of tracer-breakthrough curves, depending on domain properties such as effective permeability, permeability contrast, structure type, structure shape, and structure location, is investigated. Useful knowledge about the processes that yield a certain curve shape is gained. The investigation is based on three groups of test cases of varying type: (A) block-shaped structures, (B) a few single or intersecting fractures, and (C) systematically distributed fractures.

Second, an approach for approximating the location and the geometry of structures is developed. Based on the three groups of test cases (A – C), it is concluded that the initial arrival time of the tracer can be used for structure localisation. It is discussed in which situations the approach yields reliable information and which type of structures or system of structures can only be localised under certain conditions. In general, the possibilities of approximating the structure geometry of fractures are limited. The exact orientation can only be determined if the tracer measurements are conducted parallel and in the vicinity of the fracture. The fracture length is not possible to approximate on the basis of the initial tracer arrival time. The experience gained is very useful for the planning and design of experimental set-ups to be used for tracer measurements for structure identification.

Third, it is shown that the initial tracer arrival time can be used for determining the permeability of block-shaped structures. Apart from certain special situations reliable results are obtained. For systems containing fractures, it is shown that the matrix permeability can be rather accurately approximated under certain conditions. The approximation of the fracture permeability fails due to the strong sensitivity of the results to variations in the initial tracer arrival time.

Fourth, the developed identification approach is tested by applying it to two artificial cases of different type. For each of the two cases, only "measurement" results, "experimental" set-up and domain character is known, corresponding to the situation in a real case. The first case is known to contain block-shaped structures. The identification result corresponds exactly to the true permeability distribution which is a very satisfying result. In a real case it must be taken into account that the accuracy is not as high, however, a reliable approximation can be expected. The second artificial domain is known to contain a few possibly intersecting fractures. An identification of the fundamental characteristics of the system is achieved, however, with a rather poor accuracy. Due to the failure of approximating fracture lengths and permeabilities, too many degrees of freedom remains yielding a problem with non-unique solutions.

Finally, the identification approach is applied to a real case. The domain consists of a cubic block of fissured sandstone on which a large number of tracer measurements were conducted. It is concluded that the block consists of two nearly horizontal layers of different permeability and that low-permeable thin horizontal structures, possibly filled fractures, exist. The identified structure distribution is verified using a numerical model. The agreement between the measured and the simulated tracer-breakthrough curves as well as the

discharges is very good. This confirms that the developed identification approach is very useful for domains that are determined mainly by block-shaped structures.

# 5 Final remarks

This dissertation deals with issues that are relevant for the interpretation of measured or simulated process information of heterogeneous porous domains. Arising from the framework of the presented research work, the discussion is focused on process information in the form of tracer-breakthrough curves. Due to the same reason, the investigations are conducted for domains on a laboratory scale.

The shape of tracer-breakthrough curves is determined by the physical processes that take place when a fluid is transported through a porous medium. These processes are, on the one hand, controlled by the distribution of geological *structures* and their material properties. On the other hand, on the considered scale, it must always be taken into account that the flow and transport processes are biased by the influence of the domain *boundaries*. For each of these two central themes, a number of identified problems are investigated by means of numerical simulation. The results are analysed and discussed with regard to interpretation of measured or simulated process information. In the following, the main issues and the most relevant conclusions for each of these two themes are summarised. Finally, an outlook is given with suggestions for possible further research.

#### Influence of boundaries on flow and transport processes

Three main issues are identified as relevant for understanding the influence of impervious boundaries on tracer-breakthrough curves and the associated discharges. The first is investigated for a homogenous domain, without disturbance of structures. The two last ones are investigated for strongly heterogeneous domains with fracture distributions of certain statistical properties.

- *What is the fundamental influence of impervious boundaries on certain characteristic variables of tracer-breakthrough curves?*
  It is shown that the the discharge decreases as a port configuration is shifted closer to a boundary. Due to the velocity distribution, however, initial and peak arrivals occur earlier. As expected, the significance of the boundary influence clearly decreases as the distance to the boundary increases, however, not linearly. An interesting conclusion is that the tracer-breakthrough curve reacts more sensitively to varying boundary distance than the discharge.

- *How significant is the influence of the boundaries compared to that of structures?*
  Considering the average behaviour of tracer-breakthrough curves, it is concluded that the influence of boundaries, on the one hand, and structures, on the other hand, is in the same order of magnitude concerning relevant flow and transport variables. Consequently, the boundary influence is an essential factor that determines the system behaviour significantly.

- *Does the sensitivity to structure and material parameter changes vary with the distance to a boundary?*
  The sensitivity of a system is quantified by the standard deviation of certain selected flow and transport variables. It is concluded that the sensitivity of these variables increases if a domain is limited by impervious boundaries.

The investigations show that general statements concerning the influence of boundaries on the flow and transport behaviour can only be made in exceptional cases for domains with very simple structure distributions. For more complex domains, boundary effects must be investigated individually in order to exclude unfavourable experimental or numerical set-ups and in order to interpret measured or simulated data correctly. The work presented demonstrates new ways of analysing different aspects of the boundary influence.

#### Possibilities and limitations of structure identification

Two aspects of structure identification on the basis of tracer-breakthrough curves are investigated. First, based on defined test cases, the *possibilities* of identifying the geometry of structures and determining their material properties are shown. Second, it is also shown that, even for such simple geometries, there are *limitations* in both localising structures and determining their material properties. The presented work consists of investigations on two different levels of available information:

- On the first level, both *structure distribution and tracer-breakthrough curves* are given. It is shown, that the explanation of the shape of tracer-breakthrough curves is fairly straightforward when the underlying structure distribution is known. A new approach for structure identification which is based on the shape and the initial arrival time of several tracer-breakthrough curves that are measured at different locations is developed . With this approach, block-shaped structures can be approximated with satisfying accuracy if certain restrictions and rules of interpretation are considered. For systems containing fractures, the identification is restricted to localising the structures and in some cases determining the material properties of the matrix. It is recognised that several combinations of geometries and material properties yield the same process information, hence, the problem of non-uniqueness is inevitable.

- On the second level, the new structure identification approach is tested on unknown artificial as well as real domains for which *only tracer-breakthrough curves* and the experimetal set-up are given. Is concluded that for domains which contain block-shaped structures, structure identification based on tracer-breakthrough curves is a successful approach. This conclusion is valid for both the artificial and the real domains. The results of the identification of a distribution of a few single fractures show that the proposed assessment approach is a useful support for approximating the distribution and material properties of systems containing a few single fractures. Despite deviations, the fundamental characteristics are approximated correctly. The exact distribution, though, with a correct fracture permeability, is not detected.

It can be concluded that the newly developed approach constitutes an important and helpful tool for identifying structure distributions. It should, however, be underlined that the most accurate identification result is achieved if all available information is considered.

### Outlook

The research work presented in this thesis shows that on the laboratory-scale the influence of impervious boundaries on flow and transport must be taken into account. If measurements are conducted at varying distance from the domain boundaries, the obtained data are not directly comparable. This can be a major disadvantage, especially if a statistical evaluation of the data is to be conducted, requiring a sufficiently large number of comparable measurements. In this situation, a normalisation procedure that eliminates disturbance due to boundaries, while maintaining data variations due to domain properties would be very beneficial. Within the framework of the "Aquifer Analogue" research project first steps towards the development of such a procedure were taken. Further development of a normalisation method would constitute a useful support for the evaluation of experimental data.

From the discussion of possibilities and limitations of identification of structures and their material properties it is concluded that process information in the form of tracer-breakthrough curves is a useful identification support. The investigations presented in this thesis are based on simulations of flow and transport in artificial domains with very clearly defined structure geometries. Additionally, by minimising dispersive and diffusive effects, the conditions are further simplified compared to a real case. In order to improve the reliability of the proposed approach, it should be investigated how more natural conditions influence the results. Additional applications of the proposed approach on real domains are required as well, in order to test its feasibility.

# Bibliography


[1] G.B. Baecher, N.A. Lanney, and H.H. Einstein. Statistical description of rock properties and sampling, 1977. 5C 1–8. 2.1

[2] I. Balberg, B. Berkowitz, and Drachsler G.E. Application of a percolation model to flow in fractured hard rocks. *Journal of Geophysical Research*, 96B(10 015-10 021), 1991. 2.1

[3] G.I. Barenblatt, I.P. Zheltov, and I.N. Kochina. Basic concepts in the theory of seepage of homogeneous liquids in fissured rocks (strata). *PMM: Journal of Applied Mathematics and Mechanics, Vol. 24*, pages 1286–1303, 1960. 2.2

[4] P. Bastian, K. Birken, S. Lang, Johannsen K., N. Neuß, and C. Wieners. UG: A flexible software toolbox for solving partial differential equations. *Computing and Visualization in Science*, pages 27–40, 1997. 2.4.4

[5] P. Bastian, Z. Chen, R.E. Ewing, R. Helmig, H. Jakobs, and V. Reichenberger. Numerical simulation of flow in fractured porous media. In Z. Chen, R.E. Ewing, and Shi, editors, *Numerical treatment of multiphase flows in porous media*, Lecture notes in physics, pages 1 – 18. Springer-Verlag, Berlin, Heidelberg, 1999. 2.4.3

[6] J. Bear. *Dynamics of Fluids in Porous Media*. (Environmental Science Series). American Elsevier Publ. Comp., New York, 1972. 2.3.1, 2.8, 2.3.2, 2.3.2, 2.3.2

[7] J. Bear. Modeling flow and contaminant transport in fractured rocks. Chapter 1.1.: Introduction. In *Flow and Contaminant Transport in Fractured Rock / Ed. by J.Bear*, pages 1–10. Academic Press, San Diego u.a., 1993. 2.2, 1

[8] K. Bengelsdorf. Fazies- und Reservoirgeologie im Stubensandstein von Pliezhausen-Rübgarten. Diplomarbeit, Geowissenschaftliche Fakultät der Eberhard-Karls-Universität Tübingen, 1997. 4.6.2

[9] B. Berkowitz. Analysis of fracture network connectivity using percolation theory. *Mathematical Geology*, 27:467–483, 1995. 2.1

[10] B. Berkowitz. Characterizing flow and transport in fractured geological media: A review. *Advances in Water Resources*, 25:861–884, 2002. 2.4.1

[11] J. Birkhölzer. *Numerische Untersuchungen zur Mehrkontinuumsmodellierung von Stofftransportvorgängen in Kluftgrundwasserleitern*. (Technische Hochschule Aachen / Lehrstuhl und Institut für Wasserbau und Wasserwirtschaft: Mitteilungen; 93) (Zugl.: Aachen, T.H., Diss.). Eigenverlag, Aachen, 1994. 4.6.3

[12] O. Bour and P. Davy. Connectivity of random fault networks following a power law fault length distribution. *Water Resources Research*, 33(7):1567 – 1583, 1997. 2.1

[13] R. Brauchler. *Characterization of fractured porous media using multivariate statistics and hydraulic travel time tomography*. Geowissenschaftliche Fakultät der Eberhard-Karls-Universität Tübingen / Tübinger Geowissenschaftliche Arbeiten (TGA) C 87 (Zugl.: Tübingen, Univ., Diss., 2004). Tübingen, 2005. 4.24, 4.6.1, 4.25, 4.6.2

[14] S.R. Brown. Fluid flow through rock joints: The effect of surface roughness. *Journal of Geophysical Research*, 92(B2):1337 – 1347, 1987. 2.1

[15] O. Cirpka. *Numerische Methoden zur Simulation des reaktiven Mehrkomponententransports im Grundwasser*. (Mitteilungen / Institut für Wasserbau, Universität Stuttgart; H. 95) (Zugl.: Stuttgart, Univ., Diss., 1997). Eigenverlag, Stuttgart, 1997. 2.3.3

[16] R.E. Cunningham and R.J.J. Williams. *Diffusion in gases and porous media*. Plenum press, New York and London, 1980. 4.6.3

[17] W.S. Dershowitz and H.H. Einstein. Characterizing rock joint geometry with joint system models. *Rock Mechanics and Rock Engineering*, 21:21 – 51, 1988. 2.1

[18] P. Dietrich, R. Helmig, H. Hötzl, J. Köngeter, M. Sauter, and G. Teutsch. *Flow and transport in fractured porous media*. Springer, Heidelberg, Germany, 2005. 1.2, 1.2, 2.2, 3, 4, 4.6.1

[19] P.A. Domenico and F.W. Schwartz. *Physical and chemical hydrogeology*. John Wiley & Sons, New York, Chicester, Brisbane, Toronto, Singapore, 1990. 2.1

[20] J.-R. Dreuzy, P. Davy, and O. Boer. Hydraulic properties of two-dimensional random fracture networks following power law distributions of length and aperture. *Water Resources Research*, 38(12):12–1 – 12–9, 2002. 2.1, 2.1

[21] H. Eichel. Investigation of boundary influences on flow and transport in porous media. Diplomarbeit, Institut für Wasserbau, Lehrstuhl für Hydromechanik und Hydrosystemmodellierung, Universität Stuttgart, 2002. 3.1

[22] N.I. Fisher, T. Lewis, and B.J.J. Embleton. *Statistical analysis of spherical data*. Cambridge University Press, 2 edition, 1993. 2.1

[23] A. Fuchs. *Optimierte Delaunay-Triangulierungen zur Vernetzung getrimmter NURBS-Körper*. Institut für Mathematische Methoden in den Ingenieurwissenschaften, Numerik und geometrische Modellierung, Universität Stuttgart / Berichte aus der Mathematik (Zugl.: Stuttgart, Univ., Diss., 1999). Shaker Verlag, Aachen, 1999. 2.4.2

[24] L.W. Gelhar. *Stochastic Subsurface Hydrology*. Wiley, Prentice Hall, 1993. 4

[25] P. Grathwohl. *Diffusion in natural porous media: contaminant transport, sorption/desorption and dissolution kinetics*. Kluwer Academic Publishers, 1998. 2.3.3

[26] R. Helmig. *Theorie und Numerik der Mehrphasenströmung in geklüftet-porösen Medien*. (Institut für Strömungsmechanik und Elektronisches Rechnen im Bauwesen Hannover, Bericht; 34) (Zugl.: Hannover, Univ., Diss., 1993). Eigenverlag, Hannover, 1993. 2.2, 2.7

[27] R. Helmig. *Multiphase flow and transport processes in the subsurface*. Springer-Verlag, Heidelberg, 1997. 2.4.3, 2.4.4

[28] R. Helmig, H. Class, R. Huber, H. Sheta, R. Ewing, R. Hinkelmann, H. Jakobs, and P. Bastian. Architecture of the modular program system MUFTE-UG for simulating multiphase flow and transport processes in heterogeneous porous media. *Mathematical Geology*, 2, 1998. 2.4.4

[29] Ch. Hirsch. *Numerical computation of internal and external flows*, volume 2: Computational methods for inviscid and viscous flows. John Wiley & Sons Ltd., Chichester, England, 1984. 2.4.3

[30] J.E. Jackson. *A user's guide to principal components*. Wiley series in probability and mathematical statistics. John Wiley & Sons, Inc., New York, 1991. 4.6.1

[31] I.T. Jolliffe. *Principal component analysis*. Springer series in statistics. Springer Verlag, New York, 1986. 4.6.1

[32] W. Käss. *Geohydrologische Markierungstechnik*. (Lehrbuch der Hydrogeologie; 9). Borntraeger, Berlin Stuttgart, 1992. 1.1, 4, (document)

[33] L. Kaufman and P.J. Rousseeuw. *Finding groups in data. An introduction to cluster analysis*. Wiley series in probability and mathematical statistics. John Wiley & Sons, Inc., New York, 1990. 4.6.1

[34] W. Kinzelbach. *Numerische Methoden zur Modellierung des Transports von Schadstoffen im Grundwasser*. R. Oldenburg Verlag, München Wien, 1992. 2. Auflage. 2.3.2, 2.3.3, 2.4.3

[35] O. Kolditz. *Strömung, Stoff– und Wärmetransport im Kluftgestein*. Gebr. Borntraeger, Berlin – Stuttgart, 1997. 2.1

[36] K.-P. Kröhn. *Simulation von Transportvorgängen im klüftigen Gestein mit der Methode der Finite Elemente*. (Institut für Strömungsmechanik und Elektronisches Rechnen im Bauwesen Hannover, Bericht; 29) (Zugl.: Hannover, Univ., Diss., 1990). Eigenverlag, Hannover, 1991. 1, 2.7

[37] J.C.S. Long. *Investigation of equivalent porous medium permeability in networks of discontinuous fractures*. PhD thesis, Berkeley, 1983. 2.4.2

[38] J.C.S. Long and D.M. Billaux. From field data to fracture network modeling: An example incorporating spatial structure. *Water Resources Research*, 23(7):1201–1216, 1987. 2.4.2

[39] G. Matthess and K. Ubell. *Lehrbuch der Hydrogeologie*. Gebrüder Borntraeger, Berlin, Stuttgart, 1983. 2.1

[40] C.I. McDermott. *New experimental and modelling techniques to investigate the fractured porous system*. Tübinger Geowissenschaftliche Arbeiten (tga) c 51, Geowissenschaftliche Fakultät der Eberhard-Karls-Universität Tübingen, 1999. 4.6.3

[41] L. Moreno and C.F. Tsang. Multiple-peak response to tracer injection tests in single fractures: a numerical study. *Water Resources Research*, 27(8):2143 – 2150, 1991. 2.1

[42] T. Müller. Teil B: Bestimmung der Gesteins- und Kluftgeometrie eines Stubensandsteinhorizontes. Diplomarbeit, Geologisches Institut, Lehrstuhl für Angewandte Geologie, Universität Karlsruhe (TH), 1997. 4.6.2

[43] H. Murawski. *Geologisches Wörterbuch*. dtv, Ferdinand Enke Verlag, Stuttgart, 10th edition, 1998. 2.1

[44] L. Neunhäuserer. *Diskretisierungsansätze zur Modellierung von Strömungs- und Transportprozessen in geklüftet-porösen Medien*. (Mitteilungen / Institut für Wasserbau, Universität Stuttgart; H. 119) (Zugl.: Stuttgart, Univ., Diss., 2003). Eigenverlag, Stuttgart, 2003. 2.4.3

[45] A. Nur. The origin of tensile fracture lineaments. *Journal of Structural Geology*, 4:31–40, 1982. 2.1

[46] S. O. Ochs, R. Hinkelmann, L. Neunhäuserer, M. Süß, R. Helmig, S. Gebauer, and R. Kornhuber. Adaptive methods for the equidimensional modelling of flow and transport processes in fractured aquifers. In *5th International Conference on Hydro-Science & -Engineering*, Warsaw, Poland, 2002. 2.13

[47] N. Odling. The development of network properties in natural fracture patterns: An example from the Devonian sandstones of western Norway. In L.R. Myer, C.-F. Tsang, N.G. Cook, and R.E. Goodman, editors, *Fractured and jointed rock masses*, Proceedings of the conference on fractured and jointed rock masses, Lake Tahoe / California / USA / 3 – 5 June 1992, 1995. A.A. Balkema / Rotterdam / Brookfield. 2.1

[48] N.E. Odling, P. Gillespie, B. Bourgine, C. Castaing, J-P. Chilès, N.P. Christenson, E. Fillion, A. Genter, C. Olsen, L. Thrane, R. Trice, E. Aarseth, J.J. Walsh, and J. Watterson. Variation in fracture system geometry and their implications for fluid flow in fractured hydrocarbon reservoirs. *Petroleum Geoscience*, 5:373 – 384, 1999. 2.1

[49] Y. Park, J. Dreuzy, and K. Lee. Transport and intersection mixing in random fracture networks with power law length distributions. *Water Resources Research*, 37(10):2493 – 2501, 2001. 2.1

[50] N.J. Price. *Fault and joint development in brittle and semi-brittle rock*. Permagon Press, Oxford, England, 1966. 2.1

[51] Nelson R.A. *Geologic analysis of naturally fractured reservoirs*. Butterworth-Heinemann, Boston, 2001. 1.1

[52] M.V. Rats and S.N. Chernyashov. Statistical aspects of the problem on the permeability of the jointy rocks. In *Hydrologie des roches fissurées = Hydrology of Fractured Rocks.*

*Dubrovnik Symposium 1965. Organisé par l'Unesco. Vol. 1*, (International Association of Scientific Hydrology; 73), pages 227–236. Unesco, Paris, 1967. 2.2

[53] R.C. Reid, J.M. Prausnitz, and B.E. Poling. *The properties of gases and liquids*. McGrawHill, 1987. 2.3.3, 4.6.3

[54] E.S. Romm. *Flow characteristics of fractured rocks (in Russian)*. Nedra, Moscow, 1966. 2.4.1

[55] Y. Rubin. Prediction of tracer plume migration in disordered porous media by the method of conditional probabilities. *Water Resources Research*, 27(6):1291 – 1308, 1991. 4

[56] M. Sahimi. *Flow and transport in porous fractured media and fractured rock: From classical methods to modern approaches*. VHC Verlagsgesellschaft, Weinheim, 1995. 2.3.3

[57] A.E. Scheidegger. General theory of dispersion in porous media. *Journal of Geophysical Research*, 66(10):3273–3278, 1961. 2.3.3

[58] A. Silberhorn-Hemminger. *Modellierung von Kluftaquifersystemen: Geostatistische Analyse und deterministisch-stochastische Kluftgenerierung*. (Mitteilungen / Institut für Wasserbau, Universität Stuttgart; H. 114) (Zugl.: Stuttgart, Univ., Diss., 2002). Eigenverlag, Stuttgart, 2002. 1.1, 2.1, 2.2, 2.1, 2.1, 2.3, 2.4, 2.5, 2.6, 2.9, 2.11, 2.4.2, 2.12

[59] D.T. Snow. Anisotropic permeability of fractured media. *Water Resources Research*, 5(6):1273–1289, 1969. 2.4.1

[60] D. Stauffer and A. Aharony. *Introduction to percolation theory*. Taylor & Francis, London Washington DC, 1991. 2.1

[61] Y.W. Tsang and C.F. Tsang. Channel model of flow through fractured media. *Water Resources Research*, 23(3):467–479, 1987. 2.4.1

[62] (U.S) Committee on Fracture Characterization and Fluid Flow. *Rock fractures and fluid flow: contemporary understanding and applications*. National Academy Press, Washington, D.C., 1996. 1.1, 1.1, (document)

[63] E. Wallbrecher. *Tektonische und gefügeanalytische Arbeitsweisen*. Enke Verlag, Stuttgart, 1986. 2.1

[64] F. White. *Fluid mechanics*. McGraw-Hill, USA, 4th edition, 1999. 2.4.1

[65] D.S. Wilks. *Statistical methods in the atmospheric sciences*. Academic Press, Inc., 1995. 4.6.1

[66] J. Wollrath. *Ein Strömungs- und Transportmodell für klüftiges Gestein und Untersuchungen zu homogenen Ersatzsystemen*. (Institut für Strömungsmechanik und Elektronisches Rechnen im Bauwesen Hannover, Bericht; 28) (Zugl.: Hannover, Univ., Diss., 1990). Eigenverlag, Hannover, 1990. 2.4.1, 2.4.2

# Zusammenfassung

## Einleitung

Geklüftete geologische Formationen sind von Relevanz für viele hydrogeologische Fragestellungen die sowohl wirtschaftlich als auch für den Umweltschutz eine wichtige Rolle spielen. Beispiele hierfür sind Grundwassergewinnung, Nutzung von geothermischer Energie oder Sicherheit von unterirdischen Lagerstätten für Abfall.

Die im Untergrund vorherrschenden geologischen Eigenschaften sind das Ergebnis natürlicher Prozesse, die zu einer komplexen Verteilung von klein- und großskaligen Strukturen wie z. B. Schichten, Linsen, Kluftzonen, Einzelklüften und Mikroklüften führen können. Die physikalischen Prozesse, die beim Transport eines Fluids im Untergrund stattfinden, werden sehr stark von diesen Strukturen kontrolliert. Die Lösung von Aufgaben der oben genannten Fragestellungen erfordert, dass sowohl ein gutes Verständnis der Strömungs- und Transportprozesse als auch Methoden zur Bestimmung von Strukturgeometrien und Materialeigenschaften vorhanden sind.

Es ist notwendig alle zur Verfügung stehenden Informationen zu verwenden um ein möglichst genaues Bild von einem Untersuchungsgebiet zu erzielen. Diese Arbeit befasst sich mit der Interpretation von sogenannten „Tracermessungen". Bei der Durchführung solcher Messungen wird ein Markierstoff der Strömung an einer Stelle zugeführt und der Konzentrationsverlauf an einer anderen Stelle gemessen. Mithilfe der Eigenschaften der sich ergebenden Durchbruchskurve können Rückschlüsse auf die geologische Struktur eines Gebietes gezogen werden. Während für die Auswertung von Messergebnissen von quasihomogenen Gebieten etablierte Methoden bestehen (z. B. KÄSS, 1992[32]), ist die Interpretation von Durchbruchskurven von stark heterogenen Gebieten, wie z. B. geklüfteten porösen Systemen, noch eine Herausforderung (U.S. NATIONAL RESEARCH COUNCIL, 1996[62]).

Die hier vorgestellten Arbeiten wurden im Rahmen des von der Deutschen Forschungsgemeinschaft (DFG) finanzierten Verbundprojektes „Festgesteins-Aquiferanalog: Experimente und Modellierung" durchgeführt. Hieraus ergeben sich die in dieser Arbeit gewählte Untersuchungsskala sowie der verwendete Modellaufbau. In Abbildung 1 ist der im Projekt untersuchte Sandsteinblock dargestellt.

Tracermessungen liefern indirekte Information. Dies bedeutet, dass die gesuchte Strukturinformation nicht direkt abgelesen werden kann, sondern dass die gemessene Durchbruchskurve interpretiert werden muss um auf Strukturgeometrien und Materialeigenschaften eines Gebiets schließen zu können. Der Konzentrationsverlauf ist das Ergebnis kombinierter Effekte der Strömungs- und Transportprozesse. Folglich wird die Form der Durchbruchskurve auch von den Anfangs- und Randbedingungen beeinflusst. Die Signifikanz des Randeinflusses hängt vor allem vom Abstand zum Rand, von der Art der Rand-

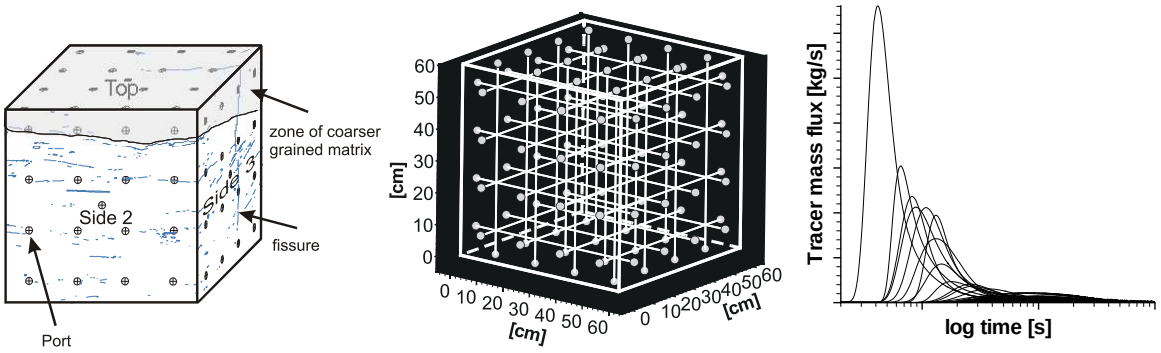


Abbildung 1: Der untersuchte kubische Block besteht aus luftgesättigtem Sandstein und hat eine Kantenlänge von 60 cm (R. BRAUCHLER, Zentrum für Angewandte Geowissenschaften, Universität Tübingen). Links: Block mit „Messports“ und Strukturen. Mitte: Verwendete, direkte Port-Konfigurationen. Rechts: Gemessene Durchbruchskurven.

bedingungen und von den Gebietseigenschaften ab.

Vor diesem Hintergrund lassen sich die zwei Schwerpunkte dieser Arbeit ableiten:

- Untersuchung der Möglichkeiten und Einschränkungen der Strukturidentifikation basierend auf Durchbruchskurven.
- Untersuchung des Einflusses von Rändern auf Tracermessungen.

Im Folgenden wird zunächst der für die Untersuchungen verwendete Modellaufbau vorgestellt. Anschließend werden die Vorgehensweise der Untersuchungen, die Diskussion der Ergebnisse und die Schlussfolgerungen der beiden Schwerpunkte zusammengefasst. Schließlich wird kurz auf mögliche weiterführende Untersuchungen eingegangen. Die englischsprachigen Querverweise beziehen sich auf den Hauptteil dieser Arbeit.

## Modellaufbau

Die hier durchgeführten Untersuchungen erfordern einen flexiblen Modellaufbau, der die Simulation von Strömung und Transport unter variierenden Bedingungen zulässt (Section 3.1):

- Homogene und heterogene Gebiete (Teilgebiete mit abweichender Permeabilität, einzelne Klüfte oder Kluftsysteme).
- Verschiedene Port-Konfigurationen mit unterschiedlichem Abstand zum Gebietsrand.
- Unterschiedliche Randbedingungen (einschließlich periodischer Randbedingungen).

Wie in Abbildung 2 zu sehen ist, hat das zwei-dimensionale Modellgebiet die Abmessungen $60 \times 60$ cm. Entlang der vier Ränder sind jeweils 13 Messports verteilt. Während eines Simulationslaufes sind nur zwei Ports (z. B. W10 und E04) offen für Strömung und Transport. Unterschiedliche konstante Drücke am In- bzw. Output-Port induzieren eine Strömung im

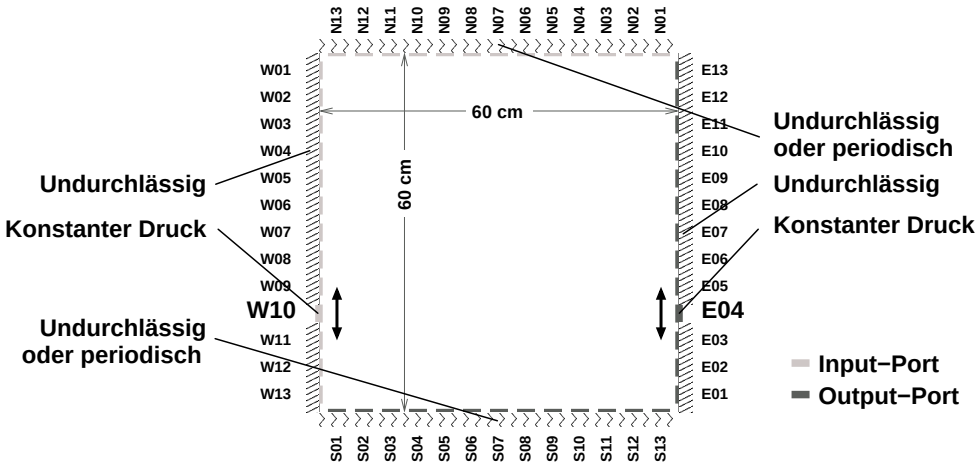


Abbildung 2: Skizze des Modellaufbaus. Die Randbedingungen der Strömung sind beispielhaft für eine der möglichen Port-Konfigurationen (W10-E04) gezeigt.

System. Je nach Zweck der Simulation sind alle andere Ränder *entweder* undurchlässig *oder* die Ränder ohne offenen Port (z. B. Nord und Süd) werden als eine periodische Fortsetzung des Modells angenommen.

Bei der Transportsimulation unterscheiden sich nur die Bedingungen an den beiden offenen Ports. Am Input-Port wird der Tracermassenfluss während des ersten Zeitschrittes konstant gehalten um anschließend zu Null gesetzt zu werden. Am Output-Port wird der Konzentrationsgradient zu Null gesetzt, welches die Bestimmung der Durchbruchskurve an dieser Stelle ermöglicht.

Die Simulationen werden mit dem Modellsystem MUFTE-UG (Section 2.4.4) durchgeführt. Für die Generierung von Finite-Volumen-Netzen wird der Netzgenerator ART benutzt. Kluftsysteme werden mit dem Kluftgenerator FRAC3D erzeugt (Section 2.4.2).

## Untersuchung des Einflusses von Rändern auf Strömungs- und Transportprozesse

Mess- oder Simulationsergebnisse, die von einem räumlich begrenzten Gebiet stammen, sind immer in gewissem Maße von Rändern beeinflusst. Diese Arbeit befasst sich mit dem Einfluss von Undurchlässigen Rändern auf Strömungs- und Transportprozesse (Chapter 3). Folgende Fragestellungen werden untersucht und diskutiert:

- Was ist der prinzipielle Einfluss von undurchlässigen Rändern auf relevanten Strömungs- und Transportvariablen (Section 3.2)?
- Wie signifikant ist der Einfluss der Ränder im Vergleich zu dem der im Gebiet vorhandenen Strukturen? Muss der Randeinfluss wirklich berücksichtigt werden oder wird das Systemverhalten durch die Strukturen dominiert (Section 3.3)?
- Variiert die Sensitivität der Durchbruchskurve gegenüber Struktur- und Parameterveränderungen mit dem Abstand zum Rand (Section 3.4)?

Um die erste Frage zu beantworten werden Durchbruchskurven verschiedener Port-Konfigurationen mit variierendem Randabstand simuliert. Die lateralen Ränder des homogenen, isotropen Gebietes sind undurchlässig. Relevante Strömungs- und Transportvariablen werden verglichen und diskutiert. Zusammenfassend kann festgestellt werden, dass für den verwendeten Modellaufbau, die Ränder einen nicht zu vernachlässigenden Einfluss darstellen, sowohl bezüglich der Strömung als auch des Transports. Es werden keine lineare Zusammenhänge zwischen Strömungs- und Transportvariablen auf der einen Seite und Randabstand auf der anderen Seite festgestellt. Die Ränder wirken als ein Widerstand zur Strömung, was in einen abnehmenden Durchfluss näher am Rand resultiert. Anders als zunächst erwartet, werden auch die Anfangs- und Peakankunftszeiten der Durchbruchskurve kürzer. Dieses Verhalten kann durch die Geschwindigkeitsverteilung im Gebiet erklärt werden. Die Durchbruchskurve reagiert sensitiver als der Durchfluss auf Änderungen des Randabstandes.

Für die Untersuchungen der zweiten und dritten Frage werden Kluftsysteme unterschiedlicher statistischen Eigenschaften generiert. Fünf Ensembles, die sich durch die Parameter Kluftlänge, Kluftdichte und die Anzahl der Kluftscharen unterscheiden, werden erzeugt (Section 3.3.2). Für diese Gebiete werden jeweils für alle 26 möglichen direkten Port-Konfigurationen (jeweils 13 in Nord/Süd- und Ost/West-Richtung) Durchbruchskurven mit undurchlässigen bzw. periodischen lateralen Rändern simuliert. Für jede Kombination von Kluftensemblen und Randbedingungen werden für relevante Strömungs- und Transportvariablen der Mittelwert, die Standardabweichung und die Extremwerte ermittelt. Die ausgewählten Variablen sind: Durchfluss Q, mittlere Aufenthaltszeit $t_{eff}$, Peakkonzentration $c_{peak}$ und zeitliche Varianz $\sigma_t^2$. Die Datenreihen dieser Variablen werden normalisiert um einen direkten Vergleich zu erlauben (Equation 3.2). Der Mittelwert beschreibt das allgemeine Verhalten einer Variable während die Standardabweichung die Variation einer Variable repräsentiert. Die maximalen und minimalen Werte der Variablen werden durch die Extremwerte erfasst.

Um die zweite Frage zu beantworten werden die Durchbruchskurven des homogenenen Gebietes, das durch undurchlässigen Rändern begrenzt wird, mit Durchbruchskurven der Kluftsysteme, die mit periodischen Randbedingungen simuliert wurden, verglichen. Somit können Variationen, die nur aufgrund von Randeinfluss zustande kommen, den Variationen, die ausschließlich von Heterogenitäten verursacht werden, gegenübergestellt werden. In Abbildung 3 sind für die Variablen Durchfluss Q und Peakkonzentration $c_{peak}$ Mittelwert, Standardabweichung und Extremwerte des homogenen Falls und der heterogenen Ensembles aufgetragen. Im Allgemeinen ist die Größe der Standardabweichung der Kluftensembles vergleichbar mit dem Wertebereich der Variablen des homogenen Falles. Das Verhältnis ist nicht durchgehend größer oder kleiner als eins. Was die Extremwerte betrifft beschreiben sie, mit sehr wenigen Ausnahmen, einen weiteren Wertebereich als für den homogenen Fall. Aus diesem Verhalten wird gefolgert, dass der Einfluss der Ränder mindestens in der gleichen Größenordnung wie der Einfluss der Klüfte ist. Folglich muss, für den untersuchten Modellaufbau, der Randeinfluss berücksichtigt werden.

Für die Untersuchung der dritten Frage werden Simulationsergenisse der heterogenen Ensembles mit undurchlässigen bzw. periodischen Rändern verglichen. Die Größe der Standardabweichung wird als Maß für die Sensitivität gegenüber Strukturvariationen verwendet. In Abbildung 4 sind Mittelwerte und Standardabweichungen dargestellt. Die Auswer-

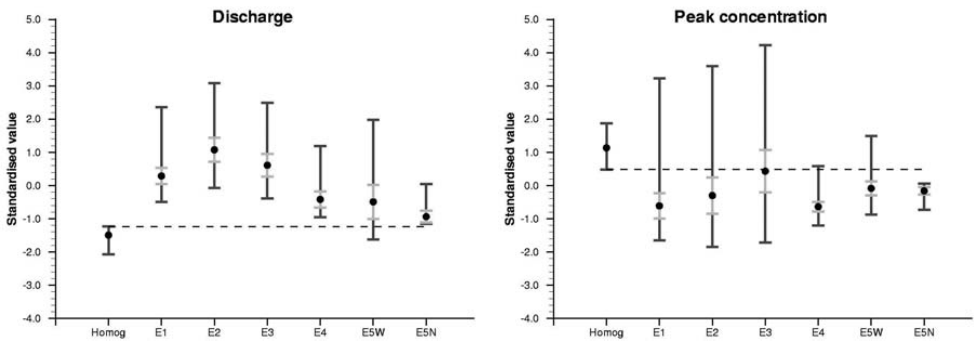


Abbildung 3: Ausgewählte Ergebnisse des homogenen Gebietes mit undurchlässigen Rändern und der heterogenen Ensembles mit periodischen Randbedingungen. Mittelwerte in Kombination mit Extremwerten und Standardabweichung (symmetrisch um den Mittelwert verteilt). Die gestrichelte Linie repräsentiert die mittlere Port-Konfiguration (W07-E07) des homogenen Gebietes.

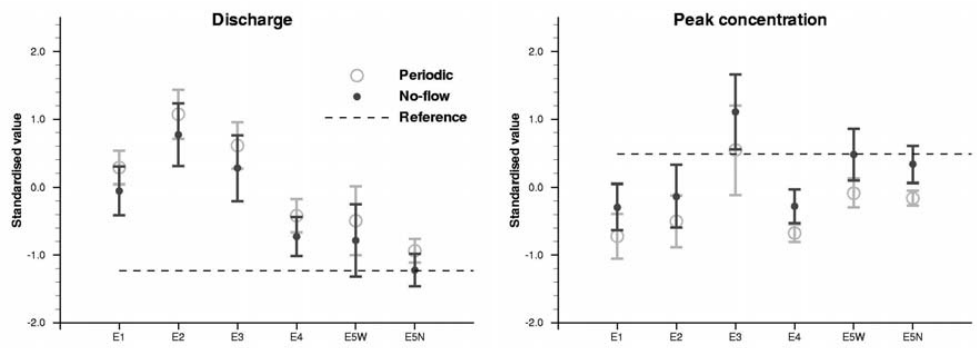


Abbildung 4: Mittelwerte und Standardabweichungen der Kluftensembles für unterschiedliche Randbedingungen.

tung zeigt, dass eine generelle Zunahme der Standardabweichung beobachtet werden kann, wenn das Gebiet durch undurchlässigen Rändern begrenzt wird. Dies gilt insbesondere für schlecht verbundene Kluftsysteme. Eine Vernachlässigung des Randeinflusses könnte zu einem ungünstigen Modellaufbau und Interpretationsfehlern führen. In Übereinstimmung mit den oben vorgestellten Ergebnissen, wird hiermit gezeigt, dass der Einfluss von Rändern auf Mess- oder Simulationsergebnisse stets ein wichtiger Teilaspekt bei der Planung und Auswertung von Messungen und Simulationen ist.

Insgesamt zeigen die Untersuchungen, dass allgemeingültige Aussagen bezüglich des Randeinflusses nur für sehr einfache Gebiete möglich sind. Komplexere Gebiete verlangen eine besondere Beachtung des Randeinflusses um einen ungünstigen experimentellen oder numerische Aufbau zu vermeiden und um gemessene und simulierte Daten korrekt zu interpretieren. Die vorgestellte Arbeit demonstriert neue Wege den Randeinfluss zu analysieren.

## Möglichkeiten und Einschränkungen der Strukturidentifikation

Strukturidentifikation, d. h. Bestimmung von Strukturgeometrien und Materialeigenschaften, mithilfe von Tracermessungen basiert auf der Tatsache, dass die Form einer Durchbruchskurve von der Verteilung von Strömungs- und Transportparametern im Gebiet abhängt. Die ideale Vorgehensweise ist in Abbildung 5 skizziert. Aus dem Bild geht her-

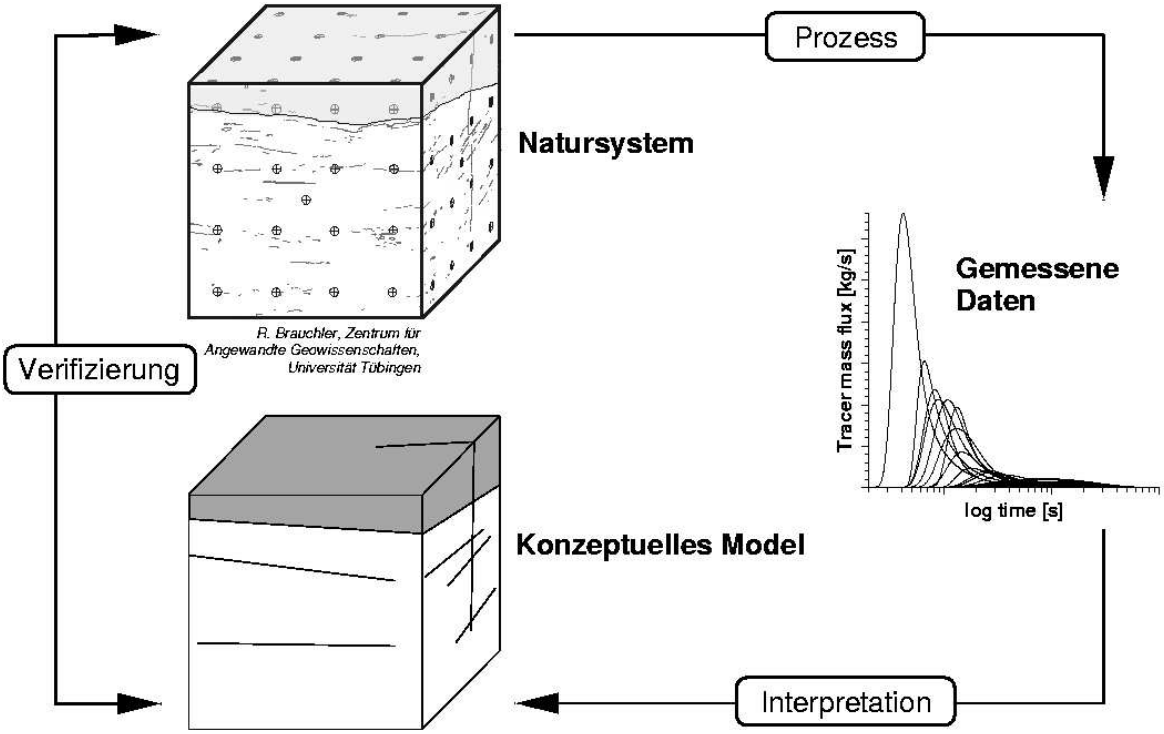


Abbildung 5: Ideale Vorgehensweise der Strukturidentifikation basierend auf Tracermessungen.

vor, dass die Schlüsselaufgabe hierbei die Interpretation der gemessenen Durchbruchskurven ist. Mithilfe von numerischer Simulation werden in dieser Arbeit Möglichkeiten und Einschränkungen der Strukturidentifikation basierend auf Durchbruchskurven untersucht (Chapter 4).

Zunächst wird eine Datenbasis für die Untersuchung geschaffen (Section 4.1). Zu diesem Zweck werden drei Gruppen von Testfällen definiert mit jeweils unterschiedlichen Struktureigenschaften (Abbildung 6). Die erste Gruppe (A) beinhaltet Gebiete mit blockförmigen Strukturen. Die zweite Gruppe (B) repräsentiert Gebiete mit wenigen Einzelklüften die sich auch schneiden können. Systeme mit regelmäßig verteilten Klüften gehören zur dritten Gruppe (C). Die gewählten Geometrien sind bewusst relativ einfach gestaltet um klar definierte Problemstellungen zu erhalten.

Die für diese Gebiete simulierten Durchbruchskurven werden zunächst im Hinblick auf Mechanismen, die zu bestimmten Formen einer Kurve führen, diskutiert. Hierbei wird das Problem der Mehrdeutigkeit von Durchbruchskurven deutlich (Section 4.2).

Anschließend wird ein Ansatz zur (1) Strukturlokalisierung sowie zur (2) Bestimmung

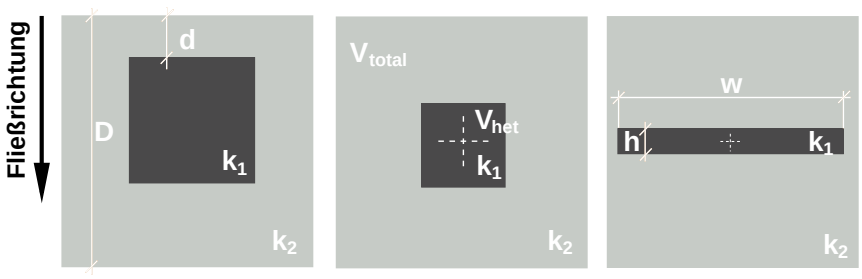


(a) Gruppe A: Blockförmige Strukturen.

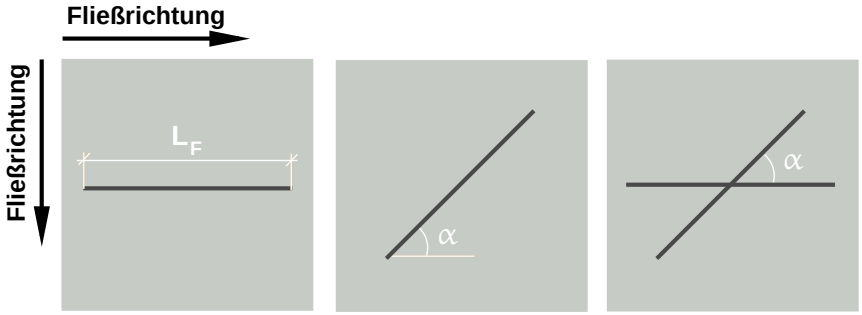


(b) Gruppe B: Wenige Klüfte.

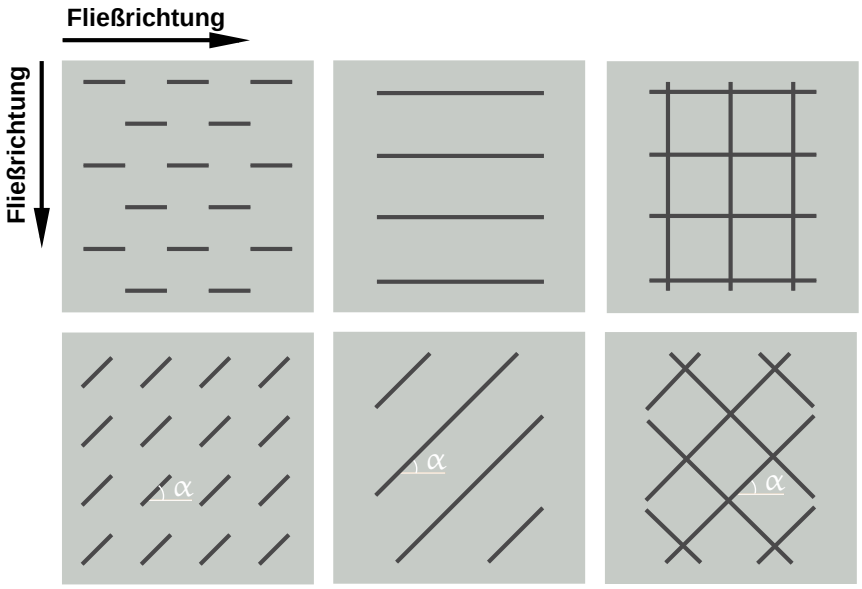


(c) Gruppe C: Systematisch verteilte Klüfte.

Abbildung 6: Übersicht der Testfälle in den drei Gruppen.

der Permeabilität von Struktur- und Hintergrundmaterial vorgestellt (Section 4.3 – 4.4). Dazu wird der bereits vorgestellte Modellaufbau mit periodischen Randbedingungen benutzt. Basierend auf der Form und vor allem auf der Erstankunftszeit der 26 Durchbruchskurven eines Gebietes wird die Lage der Strukturen sowie die Permeabilitäten approximiert. Hierbei kann gezeigt werden, dass vor allem für Gebiete der Gruppe A (blockförmige Strukturen) zuverlässige Ergebnisse erwartet werden können. Bei Gebieten der zwei anderen Gruppen liegt die größte Schwierigkeit in der Approximation der Kluftpermeabilitäten. Die Lage der Klüfte kann dagegen relativ gut bestimmt werden. Generell gilt, dass die Zuverlässigkeit der Approximation durch hinzuziehen zusätzlicher Information, z. B. lokaler geologische Kenntnisse oder Daten anderer Messungen, erhöht werden kann.

Die Anwendbarkeit des Identifikationsansatzes wird in zwei Schritten getestet. Als erstes werden Datensätze von zwei verschiedenen künstlichen Gebieten als Identifikationsgrundlage benutzt (Section 4.5). Die beiden Datensätze bestehen aus Durchbruchskurven, die von einer Person mit genauer Kenntnis der Gebiete simuliert wurden. Eine andere Person, die ausschließlich diese „gemessenen“ Daten sowie den „experimentellen“ Aufbau kennt, wertet die beiden Datensätze aus. Die Approximationsergebnisse werden anschließend überprüft und bewertet. Der erste Datensatz stammt von einem Gebiet mit blockförmigen Strukturen (Section 4.5.1). Entsprechend der Erfahrungen mit den Testfällen können die Strukturverteilung und die Permeabilitäten exakt identifiziert werden. Das zweite Gebiet beinhaltet wenige Einzelklüfte die sich möglicherweise schneiden (Section 4.5.2). Wie zu erwarten ist, ist die Approximation hier weniger genau. Es können allerdings die prinzipiellen Eigenschaften der Verteilung identifiziert werden. Es ist hauptsächlich die fehlende Möglichkeit die Permeabilität der Klüfte zu bestimmen die die Identifikation erschwert. Insgesamt sind die Testanwendungen erfolgreich. Das erzielte Ergebnis muss jedoch als eine Approximation der Strukturgeometrie und der Materialeigenschaften betrachtet werden und nicht als eine exakte Lösung.

Schließlich wird der Identifikationsansatz an einem realen Gebiet getestet (Section 4.6). Es handelt sich hierbei um den Sandsteinblock, der im Rahmen des Verbundprojektes „Festgesteins-Aquiferanalog“ untersucht wurde (Abbildung 1). Von den Projektpartnern der Universität Tübingen liegt bereits ein erstes Identifikationsergebnis vor. Hierfür wurden die gemessenen Kurven zunächst nach Messkonfiguration in drei Gruppen aufgeteilt, d. h. Portkonfigurationen die den gleichen Abstand zum Gebietsrand haben werden zusammen ausgewertet. Wie bereits in dieser Arbeit gezeigt, ist diese Aufteilung notwendig, da der Einfluss der undurchlässigen Gebietsränder eine wichtige Rolle spielt. Innerhalb jeder dieser Gruppen wurde weiter eine Klassifizierung der Durchbruchskurven nach Form und Ankunftszeit vorgenommen. So ergaben sich innerhalb jeder Gruppe drei „Cluster“ von Kurven mit ähnlichen Eigenschaften. Durch Interpretation dieser Clustereigenschaften konnten Rückschlüsse auf die Blockstruktur gezogen werden. Dieses Identifikationsergebnis wird hier durch numerischer Nachbildung des Gebietes verifiziert. Die Approximation der Lage von Strukturen und der Gebietspermeabilitäten wird basierend auf die durch arithmetische Mittelung entstehenden Durchbruchskurven durchgeführt. Das Ergebnis deutet auf eine Geometrie mit zwei horizontalen Schichten mit leicht geneigter Schichtgrenze hin. Die Permeabilität der oberen Schicht ist knapp eine Größenordnung höher als die der unteren Schicht. Es wird eine Anisotropie zwischen der horizontalen und vertikalen Richtung festgestellt. Mithilfe dieser Ergebnisse wird ein numerisches Modell aufgebaut und die gemes-

senen Kurven nachgebildet. Nach wenigen Anpassungen der ursprünglich approximierten Permeabilitäten wird eine gute Übereinstimmung der gemessenen und simulierten Durchbruchskurven erzielt wie in Abbildung 7 zu sehen ist.

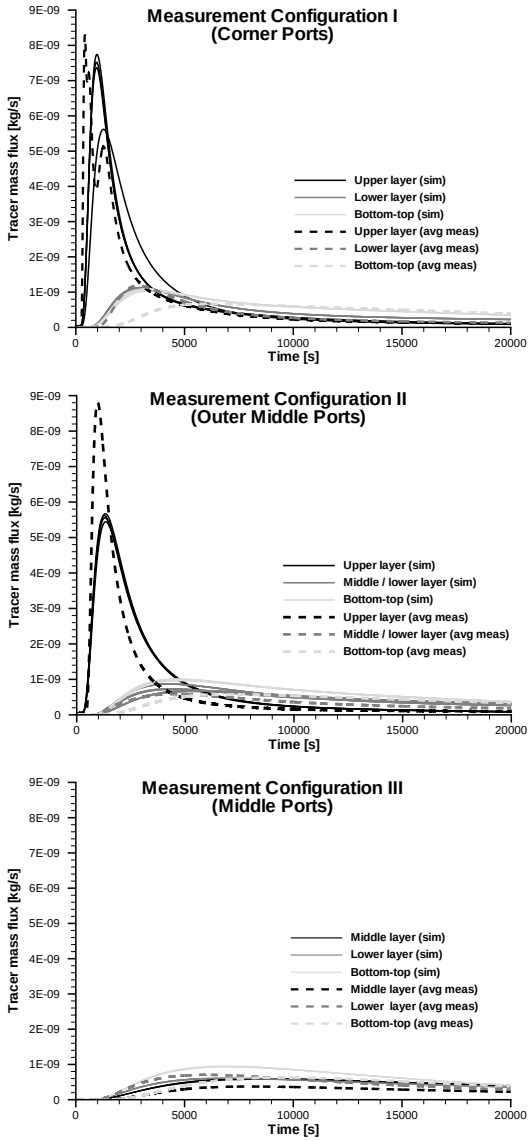


Abbildung 7: Vergleich der gemittelten gemessenen Durchbruchskurven und der einzelnen simulierten Kurven aufgeteilt nach Messkonfiguration.

Der in dieser Arbeit vorgestellte Identifikationsansatz, erweist sich hiermit als ein hilfreiches Werkzeug für die Approximation der Strukturgeometrie und der Materialeigenschaften. An dieser Stelle wird jedoch nochmals darauf hingewiesen, dass die Strukturidentifikation grundsätzlich auf alle zur Verfügung stehenden Daten und Informationen basiert werden sollte um ein möglichst zuverlässiges Ergebnis zu erhalten.

## Schlussbemerkungen und Ausblick

In dieser Arbeit wird, zum einen, der Randeinfluss auf Strömungs- und Transportmessungen und, zum anderen, Möglichkeiten und Einschränkungen der Strukturidentifikation untersucht.

Die Untersuchungen zeigen, dass allgemeingültige Aussagen bezüglich des *Randeinflusses* nur für sehr einfache Gebiete möglich sind. Komplexere Gebiete verlangen eine besondere Beachtung des Randeinflusses um einen ungünstigen experimentellen oder numerische Aufbau zu vermeiden und um gemessene und simulierte Daten korrekt zu interpretieren. Die vorgestellte Arbeit demonstriert neue Wege den Randeinfluss systematisch zu analysieren.

Aufgrund des Randeinflusses sind Messungen, die in unterschiedlichen Abständen von den Gebietsrändern ausgeführt werden, nicht direkt vergleichbar. Dies kann von bedeutendem Nachteil sein, besonders dann wenn die Daten statistisch ausgewertet werden sollen und ein möglichst großer Datensatz erwünscht ist. In einer solchen Situation wäre ein Verfahren zur Eliminierung des Randeinflusses bei gleichzeitiger Beibehaltung von Variationen aufgrund von Gebietseigenschaften sehr vorteilhaft. Im Rahmen des Forschungsprojektes „Festgesteins-Aquiferanalog“ wurden schon erste Schritte in dieser Richtung getan. Eine weitere Entwicklung eines solchen Normalisierungskonzeptes wäre eine wichtige Unterstützung bei der Auswertung von gemessenen Daten.

Die hier geführten Diskussionen der Möglichkeiten und Einschränkungen der *Strukturidentifikation* zeigen, dass der in dieser Arbeit neu entwickelten Ansatz einen wichtigen Beitrag zur Approximation der Strukturgeometrie und der Materialeigenschaften leistet. Es muss jedoch betont werden, dass ein möglichst genaues Ergebnis nur unter Berücksichtigung aller zur Verfügung stehenden Informationen erzielt werden kann.

Die vorgestellten Untersuchungen basieren hauptsächlich auf Strömungs- und Transportsimulationen künstlicher, klar definierter Gebiete. Die Bedingungen sind demzufolge vereinfacht im Vergleich zu einem natürlichen Gebiet. Um die Zuverlässigkeit des Identifikationsverfahrens weiter zu testen, sollte analysiert werden wie sich natürliche, kleinskalige Variationen auf das Approximationsergebnis auswirken. Zusätzliche Applikationen auf natürliche Gebiete sind erforderlich um die praktische Anwendbarkeit zu untersuchen.

**Institut für Wasserbau**
**Universität Stuttgart**

Pfaffenwaldring 61
70569 Stuttgart (Vaihingen)
Telefon (0711) 685 - 4717/41/52 o. - 4679
Telefax (0711) 685 - 7020 o. 4746 o. 4681
email: iws@iws.uni-stuttgart.de
http://www.iws.uni-stuttgart.de



# Verzeichnis der Mitteilungshefte

1 Röhnisch, Arthur: *Die Bemühungen um eine Wasserbauliche Versuchsanstalt an der Technischen Hochschule Stuttgart*, und
Fattah Abouleid, Abdel: *Beitrag zur Berechnung einer in lockeren Sand gerammten, zweifach verankerten Spundwand*, 1963

2 Marotz, Günter: *Beitrag zur Frage der Standfestigkeit von dichten Asphaltbelägen im Großwasserbau*, 1964

3 Gurr, Siegfried: *Beitrag zur Berechnung zusammengesetzter ebener Flächentragwerke unter besonderer Berücksichtigung ebener Stauwände, mit Hilfe von Randwert- und Lastwertmatrizen*, 1965

4 Plica, Peter: *Ein Beitrag zur Anwendung von Schalenkonstruktionen im Stahlwasserbau*, und Petrikat, Kurt: *Möglichkeiten und Grenzen des wasserbaulichen Versuchswesens*, 1966

5 Plate, Erich: *Beitrag zur Bestimmung der Windgeschwindigkeitsverteilung in der durch eine Wand gestörten bodennahen Luftschicht*, und
Röhnisch, Arthur; Marotz, Günter: *Neue Baustoffe und Bauausführungen für den Schutz der Böschungen und der Sohle von Kanälen, Flüssen und Häfen; Gestehungskosten und jeweilige Vorteile*, sowie Unny, T.E.: *Schwingungsuntersuchungen am Kegelstrahlschieber*, 1967

6 Seiler, Erich: *Die Ermittlung des Anlagenwertes der bundeseigenen Binnenschiffahrtsstraßen und Talsperren und des Anteils der Binnenschiffahrt an diesem Wert*, 1967

7 *Sonderheft anläßlich des 65. Geburtstages von Prof. Arthur Röhnisch mit Beiträgen von* Benk, Dieter; Breitling, J.; Gurr, Siegfried; Haberhauer, Robert; Honekamp, Hermann; Kuz, Klaus Dieter; Marotz, Günter; Mayer-Vorfelder, Hans-Jörg; Miller, Rudolf; Plate, Erich J.; Radomski, Helge; Schwarz, Helmut; Vollmer, Ernst; Wildenhahn, Eberhard; 1967

8 Jumikis, Alfred: *Beitrag zur experimentellen Untersuchung des Wassernachschubs in einem gefrierenden Boden und die Beurteilung der Ergebnisse*, 1968

9 Marotz, Günter: *Technische Grundlagen einer Wasserspeicherung im natürlichen Untergrund*, 1968

10 Radomski, Helge: *Untersuchungen über den Einfluß der Querschnittsform wellenförmiger Spundwände auf die statischen und rammtechnischen Eigenschaften*, 1968

11 Schwarz, Helmut: *Die Grenztragfähigkeit des Baugrundes bei Einwirkung vertikal gezogener Ankerplatten als zweidimensionales Bruchproblem*, 1969

12 Erbel, Klaus: *Ein Beitrag zur Untersuchung der Metamorphose von Mittelgebirgsschneedecken unter besonderer Berücksichtigung eines Verfahrens zur Bestimmung der thermischen Schneequalität*, 1969

13 Westhaus, Karl-Heinz: *Der Strukturwandel in der Binnenschiffahrt und sein Einfluß auf den Ausbau der Binnenschiffskanäle*, 1969

14 Mayer-Vorfelder, Hans-Jörg: *Ein Beitrag zur Berechnung des Erdwiderstandes unter Ansatz der logarithmischen Spirale als Gleitflächenfunktion*, 1970

15 Schulz, Manfred: *Berechnung des räumlichen Erddruckes auf die Wandung kreiszylindrischer Körper*, 1970

16 Mobasseri, Manoutschehr: *Die Rippenstützmauer. Konstruktion und Grenzen ihrer Standsicherheit*, 1970

17 Benk, Dieter: *Ein Beitrag zum Betrieb und zur Bemessung von Hochwasserrückhaltebecken*, 1970

18 Gàl, Attila: *Bestimmung der mitschwingenden Wassermasse bei überströmten Fischbauchklappen mit kreiszylindrischem Staublech*, 1971, vergriffen

19 Kuz, Klaus Dieter: *Ein Beitrag zur Frage des Einsetzens von Kavitationserscheinungen in einer Düsenströmung bei Berücksichtigung der im Wasser gelösten Gase*, 1971, vergriffen

20 Schaak, Hartmut: *Verteilleitungen von Wasserkraftanlagen*, 1971

21 *Sonderheft zur Eröffnung der neuen Versuchsanstalt des Instituts für Wasserbau der Universität Stuttgart mit Beiträgen von*
Brombach, Hansjörg; Dirksen, Wolfram; Gàl, Attila; Gerlach, Reinhard; Giesecke, Jürgen; Holthoff, Franz-Josef; Kuz, Klaus Dieter; Marotz, Günter; Minor, Hans-Erwin; Petrikat, Kurt; Röhnisch, Arthur; Rueff, Helge; Schwarz, Helmut; Vollmer, Ernst; Wildenhahn, Eberhard; 1972

22 Wang, Chung-su: *Ein Beitrag zur Berechnung der Schwingungen an Kegelstrahlschiebern*, 1972

23 Mayer-Vorfelder, Hans-Jörg: *Erdwiderstandsbeiwerte nach dem Ohde-Variationsverfahren*, 1972

24 Minor, Hans-Erwin: *Beitrag zur Bestimmung der Schwingungsanfachungsfunktionen überströmter Stauklappen*, 1972, vergriffen

25 Brombach, Hansjörg: *Untersuchung strömungsmechanischer Elemente (Fluidik) und die Möglichkeit der Anwendung von Wirbelkammerelementen im Wasserbau*, 1972, vergriffen

26 Wildenhahn, Eberhard: *Beitrag zur Berechnung von Horizontalfilterbrunnen*, 1972

27 Steinlein, Helmut: *Die Eliminierung der Schwebstoffe aus Flußwasser zum Zweck der unterirdischen Wasserspeicherung, gezeigt am Beispiel der Iller*, 1972

28 Holthoff, Franz Josef: *Die Überwindung großer Hubhöhen in der Binnenschiffahrt durch Schwimmerhebewerke*, 1973

29 Röder, Karl: *Einwirkungen aus Baugrundbewegungen auf trog- und kastenförmige Konstruktionen des Wasser- und Tunnelbaues*, 1973

30 Kretschmer, Heinz: *Die Bemessung von Bogenstaumauern in Abhängigkeit von der Talform*, 1973

31 Honekamp, Hermann: *Beitrag zur Berechnung der Montage von Unterwasserpipelines*, 1973

32 Giesecke, Jürgen: *Die Wirbelkammertriode als neuartiges Steuerorgan im Wasserbau*, und
Brombach, Hansjörg: *Entwicklung, Bauformen, Wirkungsweise und Steuereigenschaften von Wirbelkammerverstärkern*, 1974

33 Rueff, Helge: *Untersuchung der schwingungserregenden Kräfte an zwei hintereinander angeordneten Tiefschützen unter besonderer Berücksichtigung von Kavitation*, 1974

34 Röhnisch, Arthur: *Einpreßversuche mit Zementmörtel für Spannbeton - Vergleich der Ergebnisse von Modellversuchen mit Ausführungen in Hüllwellrohren*, 1975

35 *Sonderheft anläßlich des 65. Geburtstages von Prof. Dr.-Ing. Kurt Petrikat mit Beiträgen von*: Brombach, Hansjörg; Erbel, Klaus; Flinspach, Dieter; Fischer jr., Richard; Gàl, Attila; Gerlach, Reinhard; Giesecke, Jürgen; Haberhauer, Robert; Hafner Edzard; Hausenblas, Bernhard; Horlacher, Hans-Burkhard; Hutarew, Andreas; Knoll, Manfred; Krummet, Ralph; Marotz, Günter; Merkle, Theodor; Miller, Christoph; Minor, Hans-Erwin; Neumayer, Hans; Rao, Syamala; Rath, Paul; Rueff, Helge; Ruppert, Jürgen; Schwarz, Wolfgang; Topal-Gökceli, Mehmet; Vollmer, Ernst; Wang, Chung-su; Weber, Hans-Georg; 1975

36 Berger, Jochum: *Beitrag zur Berechnung des Spannungszustandes in rotationssymmetrisch belasteten Kugelschalen veränderlicher Wandstärke unter Gas- und Flüssigkeitsdruck durch Integration schwach singulärer Differentialgleichungen*, 1975

37 Dirksen, Wolfram: *Berechnung instationärer Abflußvorgänge in gestauten Gerinnen mittels Differenzenverfahren und die Anwendung auf Hochwasserrückhaltebecken*, 1976

38 Horlacher, Hans-Burkhard: *Berechnung instationärer Temperatur- und Wärmespannungsfelder in langen mehrschichtigen Hohlzylindern*, 1976

39 Hafner, Edzard: *Untersuchung der hydrodynamischen Kräfte auf Baukörper im Tiefwasserbereich des Meeres*, 1977, ISBN 3-921694-39-6

40 Ruppert, Jürgen: *Über den Axialwirbelkammerverstärker für den Einsatz im Wasserbau*, 1977, ISBN 3-921694-40-X

41 Hutarew, Andreas: *Beitrag zur Beeinflußbarkeit des Sauerstoffgehalts in Fließgewässern an Abstürzen und Wehren*, 1977, ISBN 3-921694-41-8, vergriffen

42 Miller, Christoph: *Ein Beitrag zur Bestimmung der schwingungserregenden Kräfte an unterströmten Wehren*, 1977, ISBN 3-921694-42-6

43 Schwarz, Wolfgang: *Druckstoßberechnung unter Berücksichtigung der Radial- und Längsverschiebungen der Rohrwandung*, 1978, ISBN 3-921694-43-4

44 Kinzelbach, Wolfgang: *Numerische Untersuchungen über den optimalen Einsatz variabler Kühlsysteme einer Kraftwerkskette am Beispiel Oberrhein*, 1978, ISBN 3-921694-44-2

45 Barczewski, Baldur: *Neue Meßmethoden für Wasser-Luftgemische und deren Anwendung auf zweiphasige Auftriebsstrahlen*, 1979, ISBN 3-921694-45-0

46 Neumayer, Hans: *Untersuchung der Strömungsvorgänge in radialen Wirbelkammerverstärkern*, 1979, ISBN 3-921694-46-9

47 Elalfy, Youssef-Elhassan: *Untersuchung der Strömungsvorgänge in Wirbelkammerdioden und -drosseln*, 1979, ISBN 3-921694-47-7

48 Brombach, Hansjörg: *Automatisierung der Bewirtschaftung von Wasserspeichern*, 1981, ISBN 3-921694-48-5

49 Geldner, Peter: *Deterministische und stochastische Methoden zur Bestimmung der Selbstdichtung von Gewässern*, 1981, ISBN 3-921694-49-3, vergriffen

50 Mehlhorn, Hans: *Temperaturveränderungen im Grundwasser durch Brauchwassereinleitungen*, 1982, ISBN 3-921694-50-7, vergriffen

51 Hafner, Edzard: *Rohrleitungen und Behälter im Meer*, 1983, ISBN 3-921694-51-5

52 Rinnert, Bernd: *Hydrodynamische Dispersion in porösen Medien: Einfluß von Dichteunterschieden auf die Vertikalvermischung in horizontaler Strömung*, 1983, ISBN 3-921694-52-3, vergriffen

53 Lindner, Wulf: *Steuerung von Grundwasserentnahmen unter Einhaltung ökologischer Kriterien*, 1983, ISBN 3-921694-53-1, vergriffen

54 Herr, Michael; Herzer, Jörg; Kinzelbach, Wolfgang; Kobus, Helmut; Rinnert, Bernd: *Methoden zur rechnerischen Erfassung und hydraulischen Sanierung von Grundwasserkontaminationen*, 1983, ISBN 3-921694-54-X

55 Schmitt, Paul: *Wege zur Automatisierung der Niederschlagsermittlung*, 1984, ISBN 3-921694-55-8, vergriffen

56 Müller, Peter: *Transport und selektive Sedimentation von Schwebstoffen bei gestau tem Abfluß*, 1985, ISBN 3-921694-56-6

57 El-Qawasmeh, Fuad: *Möglichkeiten und Grenzen der Tropfbewässerung unter besonderer Berücksichtigung der Verstopfungsanfälligkeit der Tropfelemente*, 1985, ISBN 3-921694-57-4, vergriffen

58 Kirchenbaur, Klaus: *Mikroprozessorgesteuerte Erfassung instationärer Druckfelder am Beispiel seegangsbelasteter Baukörper*, 1985, ISBN 3-921694-58-2

59 Kobus, Helmut (Hrsg.): *Modellierung des großräumigen Wärme- und Schadstofftransports im Grundwasser*, Tätigkeitsbericht 1984/85 (DFG-Forschergruppe an den Universitäten Hohenheim, Karlsruhe und Stuttgart), 1985, ISBN 3-921694-59-0, vergriffen

60 Spitz, Karlheinz: *Dispersion in porösen Medien: Einfluß von Inhomogenitäten und Dichteunterschieden*, 1985, ISBN 3-921694-60-4, vergriffen

61 Kobus, Helmut: *An Introduction to Air-Water Flows in Hydraulics*, 1985, ISBN 3-921694-61-2

62 Kaleris, Vassilios: *Erfassung des Austausches von Oberflächen- und Grundwasser in horizontalebenen Grundwassermodellen*, 1986, ISBN 3-921694-62-0

63 Herr, Michael: *Grundlagen der hydraulischen Sanierung verunreinigter Porengrundwasserleiter*, 1987, ISBN 3-921694-63-9

64 Marx, Walter: *Berechnung von Temperatur und Spannung in Massenbeton infolge Hydratation*, 1987, ISBN 3-921694-64-7

65 Koschitzky, Hans-Peter: *Dimensionierungskonzept für Sohlbelüfter in Schußrinnen zur Vermeidung von Kavitationsschäden*, 1987, ISBN 3-921694-65-5

66 Kobus, Helmut (Hrsg.): *Modellierung des großräumigen Wärme- und Schadstofftransports im Grundwasser*, Tätigkeitsbericht 1986/87 (DFG-Forschergruppe an den Universitäten Hohenheim, Karlsruhe und Stuttgart) 1987, ISBN 3-921694-66-3

67 Söll, Thomas: *Berechnungsverfahren zur Abschätzung anthropogener Temperaturanomalien im Grundwasser*, 1988, ISBN 3-921694-67-1

68 Dittrich, Andreas; Westrich, Bernd: *Bodenseeufererosion, Bestandsaufnahme und Bewertung*, 1988, ISBN 3-921694-68-X, vergriffen

69 Huwe, Bernd; van der Ploeg, Rienk R.: *Modelle zur Simulation des Stickstoffhaushaltes von Standorten mit unterschiedlicher landwirtschaftlicher Nutzung*, 1988, ISBN 3-921694-69-8, vergriffen

70 Stephan, Karl: *Integration elliptischer Funktionen*, 1988, ISBN 3-921694-70-1

71 Kobus, Helmut; Zilliox, Lothaire (Hrsg.): *Nitratbelastung des Grundwassers, Auswirkungen der Landwirtschaft auf die Grundwasser- und Rohwasserbeschaffenheit und Maßnahmen zum Schutz des Grundwassers*. Vorträge des deutsch-französischen Kolloquiums am 6. Oktober 1988, Universitäten Stuttgart und Louis Pasteur Strasbourg (Vorträge in deutsch oder französisch, Kurzfassungen zweisprachig), 1988, ISBN 3-921694-71-X

72 Soyeaux, Renald: *Unterströmung von Stauanlagen auf klüftigem Untergrund unter Berücksichtigung laminarer und turbulenter Fließzustände*,1991,ISBN 3-921694-72-8

73 Kohane, Roberto: *Berechnungsmethoden für Hochwasserabfluß in Fließgewässern mit überströmten Vorländern*, 1991, ISBN 3-921694-73-6

74 Hassinger, Reinhard: *Beitrag zur Hydraulik und Bemessung von Blocksteinrampen in flexibler Bauweise*, 1991, ISBN 3-921694-74-4, vergriffen

75 Schäfer, Gerhard: *Einfluß von Schichtenstrukturen und lokalen Einlagerungen auf die Längsdispersion in Porengrundwasserleitern*, 1991, ISBN 3-921694-75-2

76 Giesecke, Jürgen: *Vorträge, Wasserwirtschaft in stark besiedelten Regionen; Umweltforschung mit Schwerpunkt Wasserwirtschaft*, 1991, ISBN 3-921694-76-0

77 Huwe, Bernd: *Deterministische und stochastische Ansätze zur Modellierung des Stickstoffhaushalts landwirtschaftlich genutzter Flächen auf unterschiedlichem Skalenniveau*, 1992, ISBN 3-921694-77-9, vergriffen

78 Rommel, Michael: *Verwendung von Kluftdaten zur realitätsnahen Generierung von Kluftnetzen mit anschließender laminar-turbulenter Strömungsberechnung*, 1993, ISBN 3-92 1694-78-7

79 Marschall, Paul: *Die Ermittlung lokaler Stofffrachten im Grundwasser mit Hilfe von Einbohrloch-Meßverfahren*, 1993, ISBN 3-921694-79-5, vergriffen

80 Ptak, Thomas: *Stofftransport in heterogenen Porenaquiferen: Felduntersuchungen und stochastische Modellierung*, 1993, ISBN 3-921694-80-9, vergriffen

81 Haakh, Frieder: *Transientes Strömungsverhalten in Wirbelkammern,* 1993, ISBN 3-921694-81-7

82 Kobus, Helmut; Cirpka, Olaf; Barczewski, Baldur; Koschitzky, Hans-Peter: *Versuchseinrichtung zur Grundwasser und Altlastensanierung VEGAS, Konzeption und Programmrahmen*, 1993, ISBN 3-921694-82-5

83 Zang, Weidong: *Optimaler Echtzeit-Betrieb eines Speichers mit aktueller Abflußregenerierung*, 1994, ISBN 3-921694-83-3, vergriffen

84 Franke, Hans-Jörg: *Stochastische Modellierung eines flächenhaften Stoffeintrages und Transports in Grundwasser am Beispiel der Pflanzenschutzmittelproblematik*, 1995, ISBN 3-921694-84-1

85 Lang, Ulrich: *Simulation regionaler Strömungs- und Transportvorgänge in Karstaquiferen mit Hilfe des Doppelkontinuum-Ansatzes: Methodenentwicklung und Parameteridentifikation*, 1995, ISBN 3-921694-85-X, vergriffen

86 Helmig, Rainer: *Einführung in die Numerischen Methoden der Hydromechanik*, 1996, ISBN 3-921694-86-8, vergriffen

87 Cirpka, Olaf: *CONTRACT: A Numerical Tool for Contaminant Transport and Chemical Transformations - Theory and Program Documentation* -, 1996, ISBN 3-921694-87-6

88 Haberlandt, Uwe: *Stochastische Synthese und Regionalisierung des Niederschlages für Schmutzfrachtberechnungen*, 1996, ISBN 3-921694-88-4

89 Croisé, Jean: *Extraktion von flüchtigen Chemikalien aus natürlichen Lockergesteinen mittels erzwungener Luftströmung*, 1996, ISBN 3-921694-89-2

90 Jorde, Klaus: *Ökologisch begründete, dynamische Mindestwasserregelungen bei Ausleitungskraftwerken*, 1997, ISBN 3-921694-90-6

91 Helmig, Rainer: *Gekoppelte Strömungs- und Transportprozesse im Untergrund - Ein Beitrag zur Hydrosystemmodellierung-*, 1998, ISBN 3-921694-91-4

92 Emmert, Martin: *Numerische Modellierung nichtisothermer Gas-Wasser Systeme in porösen Medien*, 1997, ISBN 3-921694-92-2

93 Kern, Ulrich: *Transport von Schweb- und Schadstoffen in staugeregelten Fließgewässern am Beispiel des Neckars*, 1997, ISBN 3-921694-93-0

94 Förster, Georg: *Druckstoßdämpfung durch große Luftblasen in Hochpunkten von Rohrleitungen 1997*, ISBN 3-921694-94-9

95 Cirpka, Olaf: *Numerische Methoden zur Simulation des reaktiven Mehrkomponententransports im Grundwasser*, 1997, ISBN 3-921694-95-7

96 Färber, Arne: *Wärmetransport in der ungesättigten Bodenzone: Entwicklung einer thermischen In-situ-Sanierungstechnologie*, 1997, ISBN 3-921694-96-5

97 Betz, Christoph: *Wasserdampfdestillation von Schadstoffen im porösen Medium: Entwicklung einer thermischen In-situ-Sanierungstechnologie*, 1998, ISBN 3-921694-97-3

98 Xu, Yichun: *Numerical Modeling of Suspended Sediment Transport in Rivers*, 1998, ISBN 3-921694-98-1, vergriffen

99 Wüst, Wolfgang: *Geochemische Untersuchungen zur Sanierung CKW-kontaminierter Aquifere mit Fe(0)-Reaktionswänden,* 2000, ISBN 3-933761-02-2

100 Sheta, Hussam: *Simulation von Mehrphasenvorgängen in porösen Medien unter Einbeziehung von Hysterese-Effekten*, 2000, ISBN 3-933761-03-4

101 Ayros, Edwin: *Regionalisierung extremer Abflüsse auf der Grundlage statistischer Verfahren*, 2000, ISBN 3-933761-04-2, vergriffen

102 Huber, Ralf: *Compositional Multiphase Flow and Transport in Heterogeneous Porous Media*, 2000, ISBN 3-933761-05-0

103 Braun, Christopherus: *Ein Upscaling-Verfahren für Mehrphasenströmungen in porösen Medien*, 2000, ISBN 3-933761-06-9

104 Hofmann, Bernd: *Entwicklung eines rechnergestützten Managementsystems zur Beurteilung von Grundwasserschadensfällen*, 2000, ISBN 3-933761-07-7

105 Class, Holger: *Theorie und numerische Modellierung nichtisothermer Mehrphasenprozesse in NAPL-kontaminierten porösen Medien,* 2001, ISBN 3-933761-08-5

106 Schmidt, Reinhard: *Wasserdampf- und Heißluftinjektion zur thermischen Sanierung kontaminierter Standorte*, 2001, ISBN 3-933761-09-3

107 Reinhold Josef:, *Schadstoffextraktion mit hydraulischen Sanierungsverfahren unter Anwendung von grenzflächenaktiven Stoffen*, 2001, ISBN 3-933761-10-7

108 Schneider, Matthias: *Habitat- und Abflussmodellierung für Fließgewässer mit unscharfen Berechnungsansätzen*, 2001, ISBN 3-933761-11-5

109 Rathgeb, Andreas: *Hydrodynamische Bemessungsgrundlagen für Lockerdeckwerke an überströmbaren Erddämmen*, 2001, ISBN 3-933761-12-3

110 Lang, Stefan: *Parallele numerische Simulation instätionärer Probleme mit adaptiven Methoden auf unstrukturierten Gittern*, 2001, ISBN 3-933761-13-1

111 Appt, Jochen; Stumpp Simone: *Die Bodensee-Messkampagne 2001, IWS/CWR Lake Constance Measurement Program 2001*, 2002, ISBN 3-933761-14-X

112 Heimerl, Stephan: *Systematische Beurteilung von Wasserkraftprojekten,* 2002, ISBN 3-933761-15-8

113 Iqbal, Amin: *On the Management and Salinity Control of Drip Irrigation,* 2002, ISBN 3-933761-16-6

114 Silberhorn-Hemminger, Annette: *Modellierung von Kluftaquifersystemen: Geostatistische Analyse und deterministisch-stochastische Kluftgenerierung,* 2002, ISBN 3-933761-17-4

115 Winkler, Angela: *Prozesse des Wärme- und Stofftransports bei der In-situ-Sanierung mit festen Wärmequellen,* 2003, ISBN 3-933761-18-2

116 Marx, Walter: *Wasserkraft, Bewässerung, Umwelt - Planungs- und Bewertungsschwerpunkte der Wasserbewirtschaftung,* 2003, ISBN 3-933761-19-0

117 Hinkelmann, Reinhard: *Efficient Numerical Methods and Information-Processing Techniques in Environment Water,* 2003, ISBN 3-933761-20-4

118 Samaniego-Eguiguren, Luis Eduardo: *Hydrological Consequences of Land Use / Land Cover and Climatic Changes in Mesoscale Catchments*, 2003, ISBN 3-933761-21-2

119 Neunhäuserer, Lina: *Diskretisierungsansätze zur Modellierung von Strömungs- und Transportprozessen in geklüftet-porösen Medien*, 2003, ISBN 3-933761-22-0

120 Paul, Maren: *Simulation of Two-Phase Flow in Heterogeneous Poros Media with Adaptive Methods*, 2003, ISBN 3-933761-23-9

121 Ehret, Uwe: *Rainfall and Flood Nowcasting in Small Catchments using Weather Radar*, 2003, ISBN 3-933761-24-7

122 Haag, Ingo: *Der Sauerstoffhaushalt staugeregelter Flüsse am Beispiel des Neckars - Analysen, Experimente, Simulationen -,* 2003, ISBN 3-933761-25-5

123 Appt, Jochen: *Analysis of Basin-Scale Internal Waves in Upper Lake Constance,* 2003, ISBN 3-933761-26-3

124 Hrsg.: Schrenk, Volker; Batereau, Katrin; Barczewski, Baldur; Weber, Karolin und Koschitzky, Hans-Peter: *Symposium Ressource Fläche und VEGAS - Statuskolloquium 2003, 30. September und 1. Oktober 2003,* 2003, ISBN 3-933761-27-1

125 Omar Khalil Ouda: *Optimisation of Agricultural Water Use: A Decision Support System for the Gaza Strip,* 2003, ISBN 3-933761-28-0

126 Batereau, Katrin: *Sensorbasierte Bodenluftmessung zur Vor-Ort-Erkundung von Schadensherden im Untergrund*, 2004, ISBN 3-933761-29-8

127 Witt, Oliver: *Erosionsstabilität von Gewässersedimenten mit Auswirkung auf den Stofftransport bei Hochwasser am Beispiel ausgewählter Stauhaltungen des Oberrheins*, 2004, ISBN 3-933761-30-1

128 Jakobs, Hartmut: *Simulation nicht-isothermer Gas-Wasser-Prozesse in komplexen Kluft-Matrix-Systemen*, 2004, ISBN 3-933761-31-X

129 Li, Chen-Chien: *Deterministisch stochastisches Berechnungskonzept zur Beurteilung der Auswirkungen erosiver Hochwasserereignisse in Flussstauhaltungen,* 2004, ISBN 3-933761-32-8

130 Reichenberger, Volker; Helmig, Rainer; Jakobs, Hartmut; Bastian, Peter; Niessner, Jennifer: *Complex Gas-Water Processes in Discrete Fracture-Matrix Systems Upscaling, Mass-Conservative Discretization and Efficient Multilevel Solution,* 2004, ISBN 3-933761-33-6

131 Hrsg.: Barczewski, Baldur; Koschitzky, Hans-Peter; Weber, Karolin; Wege, Ralf: *VEGAS - Statuskolloquium 2004,* 5. Oktober 2004, 2004, ISBN 3-933761-34-4

132 Asie, Kemal Jabir: *Finite Volume Models for Multiphase Multicomponent Flow through Porous Media*. 2005, ISBN 3-933761-35-2

133 Jacoub, George: *Development of a 2-D Numerical Module for Particulate Contaminant Transport in Flood Retention Reservoirs and Impounded Rivers,* 2004, ISBN 3-933761-36-0

134 Nowak, Wolfgang: *Geostatistical Methods for the Identification of Flow and Transport Parameters in the Subsurface,* 2005, ISBN 3-933761-37-9

135 Süß, Mia: *Analysis of the influence of structures and boundaries on flow and transport processes in fractured porous media*, 2005, ISBN 3-933761-38-7